



Fiducial and differential cross-section measurements of electroweak $W\gamma jj$ production in pp collisions at $\sqrt{s} = 13$ TeV with the ATLAS detector

The ATLAS Collaboration

The observation of the electroweak production of a W boson and a photon in association with two jets, using pp collision data at the Large Hadron Collider at a centre of mass energy of $\sqrt{s} = 13$ TeV, is reported. The data were recorded by the ATLAS experiment from 2015 to 2018 and correspond to an integrated luminosity of 140 fb^{-1} . This process is sensitive to the quartic gauge boson couplings via the vector boson scattering mechanism and provides a stringent test of the electroweak sector of the Standard Model. Events are selected if they contain one electron or muon, missing transverse momentum, at least one photon, and two jets. Multivariate techniques are used to distinguish the electroweak $W\gamma jj$ process from irreducible background processes. The observed significance of the electroweak $W\gamma jj$ process is well above six standard deviations, compared to an expected significance of 6.3 standard deviations. Fiducial and differential cross sections are measured in a fiducial phase space close to the detector acceptance, which are in reasonable agreement with leading order Standard Model predictions from MADGRAPH5+PYTHIA8 and SHERPA. The results are used to constrain new physics effects in the context of an effective field theory.

Contents

1	Introduction	2
2	ATLAS detector	4
3	Monte Carlo event simulation	5
4	Object reconstruction and event selection	6
5	Background estimation	9
6	Signal extraction	11
6.1	Signal extraction for observation	11
6.2	Signal extraction for the differential cross-section measurement	12
7	Correction for detector effects	15
8	Systematic uncertainties	16
9	Results	18
9.1	Observation and fiducial cross-section for EW $W\gamma jj$ process	18
9.2	Differential cross-section for EW $W\gamma jj$ process	20
10	EFT interpretation	20
11	Conclusion	24

1 Introduction

The scattering of two vector bosons, e.g. $WZ \rightarrow W\gamma$, is sensitive to both the triple and quartic electroweak-boson self-interactions [1, 2]. In proton–proton (pp) collisions, the $W\gamma jj$ final state can be produced via many different mechanisms, as shown in Figure 1. Electroweak (EW) $W\gamma jj$ production concerns exclusively electroweak interactions of order α_{EW}^4 at tree level [3], where α_{EW} is the electroweak coupling constant. Although the contributions of interest are vector boson scattering (VBS) interactions involving quartic gauge couplings (QGCs), these cannot be distinguished from other electroweak contributions in a gauge-invariant manner. Thus, the signal process studied in this paper is the combination of all processes of order α_{EW}^4 shown in Figures 1(a)-1(c). The dominant background for EW $W\gamma jj$ production concerns processes of order $\alpha_S^2\alpha_{\text{EW}}^2$ at tree level in Figure 1(d), where α_S is the strong coupling constant and the jets are produced via strong interaction vertices; these processes are collectively referred to as strong $W\gamma jj$ production in this paper. Triboson diagrams, such as the one shown in Figure 1(b), do contribute to EW $W\gamma jj$ production. However, due to their distinct topology they require separate signal selection and background estimation methods and are thus generally the subject of separate studies.

The large cross-section of EW $W\gamma jj$ production predicted by the SM allows differential cross-sections to be measured with higher precision than other VBS processes. The differential measurements further enhance our sensitivity to potential anomalous quartic couplings of $WW\gamma\gamma$ and $WW\gamma Z$. In addition to the

VBS topology characterised by the two energetic jets in the forward and backward region, the leptonic decay channel of the EW $W\gamma jj$ production has a clean signature in the detector with exactly one charged lepton, missing transverse momentum, and at least one photon. This paper reports fiducial and differential cross-section measurements in the EW $W\gamma jj$ final state using 140 fb^{-1} of data recorded between 2015 and 2018 with the ATLAS detector.

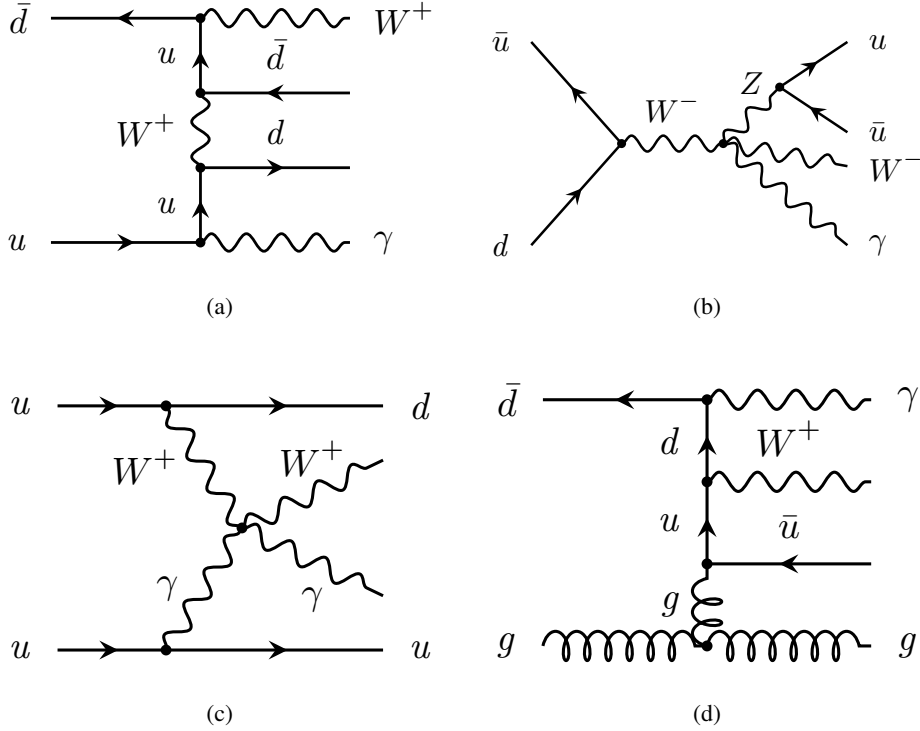


Figure 1: Representative Feynman diagrams for the $W\gamma jj$ final state: (a) EW $W\gamma jj$ production involving no gauge boson self-interactions, (b) Bremsstrahlung EW $W\gamma jj$ non-VBS production involving quartic gauge boson interactions, (c) $W\gamma$ VBS involving quartic gauge boson interactions, and (d) Strong $W\gamma jj$ production.

The CMS Collaboration reported the observation of the EW $W\gamma jj$ process [4] and measured EW $W\gamma jj$ differential cross-sections [5]. This analysis exploits two innovations compared to the CMS publication. First, multivariate techniques involving a neural network are used to isolate the EW $W\gamma jj$ signal from the strong $W\gamma jj$ background in a VBS-enhanced phase space; the resulting observed yield is corrected for detector effects and a fiducial cross-section is reported in a fiducial phase space at particle level as close as possible to the reconstruction level. Secondly, observables sensitive to the charge conjugation (C) and parity (P) structure of $WW\gamma\gamma$ and $WW\gamma Z$ couplings are measured. These measurements can be used to explore new sources of CP violation (CPV) in the gauge-boson sector that may partly explain the predominance of matter over anti-matter in the universe. The differential cross-sections for EW $W\gamma jj$ production are measured as functions of two types of observables: *VBS observables* and *charge conjugation and parity observables*.

- The VBS observables are those that are used to characterise specifically the VBS nature of events; they are additionally sensitive to anomalous QGCs (aQGCs) via dimension-8 operators of an effective field theory (EFT), which can be parameterised in the Éboli basis [2]. These observables include the invariant mass of the dijet system, m_{jj} , the transverse momentum of the two jets, p_T^{jj} , the lepton

transverse momentum, p_T^l , and the invariant mass of the lepton and the photon, $m_{l\gamma}$.

- The charge conjugation and parity observables probe the CP structure of $WW\gamma\gamma$ and $WW\gamma Z$ couplings. Two observables are studied: the signed azimuthal angle difference between the two jets, $\Delta\phi_{jj} = \phi_f^j - \phi_b^j$, where the two highest transverse-momentum jets are ordered by rapidity y such that $y_f^j > y_b^j$, and the signed azimuthal angle difference between the lepton and the photon, $\Delta\phi_{l\gamma} = \phi_f - \phi_b$, where the lepton and the photon are ordered such that $y_f > y_b$. Measurements of $\Delta\phi_{jj}$ have previously been proposed to constrain the CP-odd component involving Higgs boson couplings in Vector Boson Fusion (VBF) processes [6] and the $t\bar{t}H$ process [7].

The paper is organised as follows. Section 2 briefly describes the ATLAS detector. Section 3 documents the simulated signal and background samples used in this analysis. The object reconstruction and event selection is presented in Section 4. The background estimate is detailed in Section 5. The methodologies used for the fiducial and differential cross-section measurements are discussed in Section 6. Corrections for detector effects are described in Section 7, followed by a description of the systematic uncertainties in Section 8. The fiducial and differential EW $W\gamma jj$ cross-sections are presented in Section 9. Section 10 presents constraints on the Wilson coefficients of dimension-8 EFT.

2 ATLAS detector

The ATLAS detector [8] at the LHC covers nearly the entire solid angle around the collision point.¹ It consists of an inner tracking detector surrounded by a thin superconducting solenoid, electromagnetic and hadronic calorimeters, and a muon spectrometer incorporating three large superconducting air-core toroidal magnets.

The inner-detector system (ID) is immersed in a 2 T axial magnetic field and provides charged-particle tracking in the range $|\eta| < 2.5$. The high-granularity silicon pixel detector covers the vertex region and typically provides four measurements per track, the first hit generally being in the insertable B-layer (IBL) installed before Run 2 [9, 10]. It is followed by the SemiConductor Tracker (SCT), which usually provides eight measurements per track. These silicon detectors are complemented by the transition radiation tracker (TRT), which enables radially extended track reconstruction up to $|\eta| = 2.0$. The TRT also provides electron identification information based on the fraction of hits (typically 30 in total) above a higher energy-deposit threshold corresponding to transition radiation.

The calorimeter system covers the pseudorapidity range $|\eta| < 4.9$. Within the region $|\eta| < 3.2$, electromagnetic calorimetry is provided by barrel and endcap high-granularity lead/liquid-argon (LAr) calorimeters, with an additional thin LAr presampler covering $|\eta| < 1.8$ to correct for energy loss in material upstream of the calorimeters. Hadronic calorimetry is provided by the steel/scintillator-tile calorimeter, segmented into three barrel structures within $|\eta| < 1.7$, and two copper/LAr hadronic endcap calorimeters. The solid angle coverage is completed with forward copper/LAr and tungsten/LAr calorimeter modules optimised for electromagnetic and hadronic energy measurements respectively.

¹ ATLAS uses a right-handed coordinate system with its origin at the nominal interaction point (IP) in the centre of the detector and the z -axis along the beam pipe. The x -axis points from the IP to the centre of the LHC ring, and the y -axis points upwards. Polar coordinates (r, ϕ) are used in the transverse plane, ϕ being the azimuthal angle around the z -axis. The pseudorapidity is defined in terms of the polar angle θ as $\eta = -\ln \tan(\theta/2)$ and is equal to the rapidity $y = \frac{1}{2} \ln \left(\frac{E+p_z c}{E-p_z c} \right)$ in the relativistic limit. Angular distance is measured in units of $\Delta R \equiv \sqrt{(\Delta y)^2 + (\Delta\phi)^2}$.

The muon spectrometer (MS) comprises separate trigger and high-precision tracking chambers measuring the deflection of muons in a magnetic field generated by the superconducting air-core toroidal magnets. The field integral of the toroids ranges between 2.0 and 6.0 T m across most of the detector. Three layers of precision chambers, each consisting of layers of monitored drift tubes, cover the region $|\eta| < 2.7$, complemented by cathode-strip chambers in the forward region, where the background is highest. The muon trigger system covers the range $|\eta| < 2.4$ with resistive-plate chambers in the barrel, and thin-gap chambers in the endcap regions.

The luminosity is measured mainly by the LUCID-2 [11] detector that records Cherenkov light produced in the quartz windows of photomultipliers located close to the beam pipe.

Events are selected by the first-level trigger system implemented in custom hardware, followed by selections made by algorithms implemented in software in the high-level trigger [12]. The first-level trigger accepts events from the 40 MHz bunch crossings at a rate below 100 kHz, which the high-level trigger further reduces in order to record complete events to disk at about 1 kHz.

A software suite [13] is used in data simulation, in the reconstruction and analysis of real and simulated data, in detector operations, and in the trigger and data acquisition systems of the experiment.

3 Monte Carlo event simulation

Monte Carlo (MC) event generators are used in the analysis to simulate signal and background events produced in pp collisions. These simulated samples are used to design and optimise the analysis, evaluate systematic uncertainties, and characterise the effects of detector inefficiency and resolution.

Electroweak $W\gamma jj$ production is simulated with the SHERPA 2.2.12 [14] generator. Matrix elements at leading order (LO) in QCD with up to one additional emission are matched to a parton shower based on Catani–Seymour dipole factorisation [15, 16] using the MEPS@LO prescription [17–20]. Samples are simulated using the NNPDF3.0_{NNLO} parton distribution function (PDF) set [21], along with the dedicated set of tuned parton-shower parameters developed by the SHERPA authors. An alternative EW $W\gamma jj$ signal sample is produced using MADGRAPH5_AMC@NLO [22] at LO accuracy with the default dynamical scale choice and the NNPDF3.1_{LO} PDF set. PYTHIA 8.240 with the dipole recoil option turned on is used to add parton showering, hadronisation, and underlying-event activity. The A14 [23] set of tuned parton-shower parameters is used for PYTHIA 8.240, and EVTGEN [24] is used for the properties of bottom and charmed hadron decays. This alternative EW $W\gamma jj$ sample is used to evaluate a systematic uncertainty of the signal production due to the choice of event generator.

The dominant background process, strong $W\gamma jj$, is simulated using SHERPA 2.2.11 [14]. Matrix elements at next-to leading order (NLO) QCD accuracy for up to one additional parton and LO accuracy for up to three additional parton emissions are matched and merged with the SHERPA parton shower based on Catani–Seymour dipole factorisation [15, 16] using the MEPS@NLO prescription [17–20]. This sample uses NNPDF3.0_{NNLO} for the matrix element calculation with default parameters for parton showering, hadronisation, and underlying-event activity. An alternative strong $W\gamma jj$ sample is produced using MADGRAPH5_AMC@NLO at NLO accuracy for events with up to three partons in the final state with the NNPDF3.0_{NLO} PDF set and is interfaced with PYTHIA 8.240 with A14 parameters to provide parton showering, hadronisation, and underlying-event activity. This alternative strong $W\gamma jj$ sample is used to evaluate a systematic uncertainty of the strong $W\gamma jj$ background estimate due to the choice of event generator.

Prompt background events are those that contain at least one prompt photon, exactly one prompt charged lepton, and two jets. `SHERPA 2.2.12`, with the same settings as EW and strong $W\gamma jj$, is also used to simulate EW and strong $Z\gamma jj$ production. The remaining prompt backgrounds can arise from $tW\gamma$, $tq\gamma$, and $t\bar{t}\gamma$ processes, which are simulated using `MADGRAPH5_AMC@NLO` [22] with `NNPDF2.3NLO` for $tW\gamma$ and $t\bar{t}\gamma$ at LO, and $tq\gamma$ at NLO. To provide parton showering, hadronisation, and underlying-event activity these samples are interfaced `PYTHIA 8.235`, `PYTHIA 8.212`, and `PYTHIA 8.240`, respectively, with A14 parameters.

Contributions from background events arising from jets misidentified as leptons or photons, non-prompt leptons or photons from decays of hadrons, electrons reconstructed as photons, and photons arising from a separate pp interaction (“pile-up photons”) are estimated by using the data-driven methods that are outlined in Section 5. The term *fake leptons* is used to collectively refer to either non-prompt leptons or hadronic jets misreconstructed as leptons. MC simulated samples including W +jets, Z +jets, tW , $t\bar{t}$, diboson, and multijet events are used in the validation of data-driven methods and the evaluation of systematic uncertainties of the background estimations. In particular, simulated W +jets and Z +jets events, which are used in the validation of the non-prompt photon estimate, are produced at NLO accuracy using `SHERPA 2.2.11` with `NNPDF3.0NNLO` and default parameter tunes for parton showering, hadronisation, and underlying-event activity. Background events from electrons misreconstructed as photons can arise from tW , $t\bar{t}$, and Z +jets processes. The tW and $t\bar{t}$ processes are simulated using `POWHEG` at NLO accuracy with `NNPDF3.0NNLO` and `PYTHIA 8.230` with A14 parameters to provide parton showering, hadronisation, and underlying-event activity. Diboson and multijet events are used in the data-driven estimate of fake leptons. The diboson sample is simulated with `SHERPA 2.2.2` at NLO with `NNPDF3.0NLO` and default parameter tunes for parton showering, hadronisation, and underlying-event activity. The multijet sample is simulated using `PYTHIA 8.235` at LO accuracy with `NNPDF2.3LO` and A14 tunes for parton showering.

All simulated signal and background events are processed through the full ATLAS detector simulation using `GEANT4` [25] and then reconstructed using the same algorithms as the recorded data events. Differences between reconstructed leptons, photons, jets and missing transverse momentum in simulations and data are corrected using event-by-event scale factors with p_T and η dependence. The effect of multiple interactions in the same and neighbouring bunch crossings (pile-up) is modelled by overlaying the simulated hard-scattering event with inelastic pp events simulated with `PYTHIA 8.186` [26] using the `NNPDF2.3LO` set of PDFs [27] and the A3 set of tuned parton-shower parameters [28].

4 Object reconstruction and event selection

This analysis is performed using pp collision data collected between 2015 and 2018 at a centre-of-mass energy of $\sqrt{s} = 13$ TeV, corresponding to an integrated luminosity of 140 fb^{-1} [29].

Events are required to satisfy the unrescaled single-lepton triggers that have transverse momentum thresholds of 20–26 GeV, depending on the charged lepton flavour and data-taking periods [30, 31]; this is complemented by triggers with higher p_T thresholds and no isolation requirements to increase the overall trigger efficiency. Events are also required to satisfy detector and data quality requirements during stable beam conditions [32]. Candidate pp interaction vertices are reconstructed using charged-particle tracks; each candidate vertex must have at least two tracks with $p_T > 500$ MeV [33]. The vertex with the highest scalar sum of track p_T^2 is selected as the primary vertex. Events must contain at least one electron or muon, missing transverse momentum, at least one photon, and at least two jets.

Muons are reconstructed by matching tracks in the MS to a corresponding track in the ID. Each muon must satisfy the *tight* identification criteria and *tight* isolation working point [34]. Muons are constrained to originate from the primary vertex by requiring $|d_0/\sigma_{d_0}| < 3$ and $|z_0 \sin \theta| < 0.5$ mm, where d_0 is the distance of closest approach to the primary vertex in the transverse plane, with an uncertainty σ_{d_0} , and z_0 is the longitudinal difference between the point at which d_0 is defined and the primary vertex. Selected muons are required to have $p_T > 30$ GeV and $|\eta| < 2.5$.

Electrons are reconstructed from clusters of energy deposits in the ECAL and matched to a track reconstructed in the ID. Each electron must satisfy the *tight* identification and *tight* isolation working points [35]. Electrons are required to have $p_T > 30$ GeV and $|\eta| < 2.47$, excluding the calorimeter transition region $1.37 < |\eta| < 1.52$, $|d_0/\sigma_{d_0}| < 5$ and $|z_0 \sin \theta| < 0.5$ mm.

Photons are also reconstructed from clusters of energy deposits in the ECAL. Both converted and unconverted photons are used in the analysis. Converted photons are defined as photon clusters that are matched to one or two ID tracks consistent with a conversion vertex, while unconverted photons are defined as photon clusters that are matched to neither an ID electron track nor a conversion vertex. Each photon is required to satisfy *tight* identification and *tight* isolation working points [35]. Photons passing a *loose* identification requirement are retained in the analysis to define control regions for the data-driven background estimation method used to determine the background from jets misidentified as photons, which is described in Section 5. The *tight* isolation requirement is defined as $E_T^{\text{cone40}} < 0.022 \times p_T + 2.45$ GeV, where E_T^{cone40} is computed as the sum of transverse energies of positive-energy topological clusters in the calorimeter within a distance of $\Delta R = 0.4$ around the photon candidate [35]. Photons are required to have $p_T > 22$ GeV and $|\eta| < 2.37$, excluding the calorimeter transition region $1.37 < |\eta| < 1.52$.

Jets are reconstructed using a particle-flow method [36] that combines charged-particle tracks in the ID with topo-clusters formed from energy deposits in the calorimeters. The anti- k_t algorithm [37] with radius parameter $R = 0.4$ is used to define the jet. Each jet is required to have $p_T > 25$ GeV and $|\eta| < 4.4$. Jets with $p_T < 60$ GeV and $|\eta| < 2.4$ are required to originate from the primary vertex by using the *tight* working point of the jet vertex tagger (JVT) [38]. Jets that originate from noise bursts in the calorimeters are removed [39]. Events must have at least two jets with $p_T > 50$ GeV. Jets with $|\eta| < 2.5$ that contain *b*-hadrons are identified by a multivariate algorithm (DL1r) [40] with 85% tagging efficiency working point. Events identified as containing a *b*-jet by the DL1r algorithm are excluded to suppress backgrounds from processes involving top quarks.

The magnitude of the missing transverse momentum, E_T^{miss} , and its direction are calculated from the negative vector sum of a track-based soft term and all reconstructed electrons, muons, photons, and jets [41]. The soft term is calculated from tracks from the primary vertex that are not matched to any hard physics objects. Events are required to satisfy $E_T^{\text{miss}} > 30$ GeV.

To resolve ambiguities in the object reconstruction, an overlap removal procedure is applied. Jet candidates are removed if $\Delta R(j, l) < 0.2$ ($l = e, \mu$). Then, leptons are removed if $\Delta R(l, j) < 0.4$, and photons are removed if $\Delta R(\gamma, l) < 0.4$ or $\Delta R(\gamma, j) < 0.4$. Finally, electron candidates are removed if shared ID tracks exist between a muon and an electron.

Events are required to satisfy $m_T^W > 30$ GeV, where $m_T^W = \sqrt{2p_T^l E_T^{\text{miss}}(1 - \cos \Delta\phi)}$ and $\Delta\phi$ is the azimuthal angle difference between the lepton and missing transverse momentum in the transverse plane, relative to the beam axis. In addition, to reject events that have topologies consistent with leptonic *Z* decays in which one charged lepton is reconstructed as a photon, the invariant mass of the lepton and the photon must satisfy $|m_{l\gamma} - m_Z| > 10$ GeV. To further remove events containing two prompt charged leptons

consistent with a Z boson or two W bosons, events are rejected if a second lepton satisfying the following requirements is present: $p_T > 7$ GeV, the lepton-specific pseudorapidity requirements, both track impact parameter requirements, and *loose* identification [34, 35]. Finally, the two leading jets must have a rapidity difference $|\Delta y_{jj}| > 2$ and invariant mass $m_{jj} > 500$ GeV, which ensures a topology consistent with EW $W\gamma jj$ production.

The preceding selection criteria comprise the baseline selection. Baseline selected events are further divided into different signal and control regions, which differ depending on the purpose. The selection for the fiducial cross-section measurement of EW $W\gamma jj$ production divides the baseline region into a signal region, SR^{fid} , and a control region, CR^{fid} , by counting jets in the rapidity interval between the two leading jets, $N_{\text{jets}}^{\text{gap}}$. In EW $W\gamma jj$ events, the two leading jets are produced via an electroweak interaction and there is thus little hadronic activity between them; hence each event in SR^{fid} is required to satisfy $N_{\text{jets}}^{\text{gap}} = 0$, and CR^{fid} is defined by $N_{\text{jets}}^{\text{gap}} > 0$.

For the differential cross-section measurement, it is additionally required that events have $m_{jj} > 1$ TeV to enhance the EW $W\gamma jj$ signal purity; these events are then divided into three control regions (CR_A , CR_B , and CR_C) and one signal region (SR). The centrality of the lepton-photon system relative to the VBS tagged jets, j_1 and j_2 , is defined as $\xi_{l\gamma} = |(y_{l\gamma} - (y_{j_1} + y_{j_2})/2)/(y_{j_1} - y_{j_2})|$ and is used to form three control regions (CR_A , CR_B , and CR_C) and one signal region (SR), where $y_{l\gamma}$ is the rapidity of the lepton-photon system. In EW $W\gamma jj$ events, the W boson and photon are generally produced centrally, between the two leading jets, and thus these events have low $\xi_{l\gamma}$. The variables $\xi_{l\gamma}$ and $N_{\text{jets}}^{\text{gap}}$ are chosen to define the four regions because they are uncorrelated. The SR is defined by requiring that there must be little hadronic activity in the region between the two leading jets and that the reconstructed $l\gamma$ system is produced centrally ($N_{\text{jets}}^{\text{gap}} = 0$, $\xi_{l\gamma} < 0.35$). The remaining three regions are control regions with small EW $W\gamma jj$ contribution, and are used to constrain the dominant background from strong $W\gamma jj$ production: CR_A ($N_{\text{jets}}^{\text{gap}} > 0$, $\xi_{l\gamma} < 0.35$), CR_B ($N_{\text{jets}}^{\text{gap}} > 0$, $0.35 < \xi_{l\gamma} < 1$), and CR_C ($N_{\text{jets}}^{\text{gap}} = 0$, $0.35 < \xi_{l\gamma} < 1$).

The signal and control region selection requirements for both the fiducial and differential cross-section measurements are summarised in Table 1.

Table 1: Summary table for signal and control regions for the fiducial and differential cross-section measurements.

Fiducial cross-section	SR^{fid}		CR^{fid}	
	$N_{\text{jets}}^{\text{gap}} = 0$		$N_{\text{jets}}^{\text{gap}} > 0$	
Differential cross-section	SR	CR_A	CR_B	CR_C
$m_{jj} > 1$ TeV	$N_{\text{jets}}^{\text{gap}} = 0$ $\xi_{l\gamma} < 0.35$	$N_{\text{jets}}^{\text{gap}} > 0$ $\xi_{l\gamma} < 0.35$	$N_{\text{jets}}^{\text{gap}} > 0$ $0.35 < \xi_{l\gamma} < 1$	$N_{\text{jets}}^{\text{gap}} = 0$ $0.35 < \xi_{l\gamma} < 1$

Table 2 shows the number of signal and background events in SR^{fid} and CR^{fid} , after computing the data-driven backgrounds, as described in Section 5. The strong $W\gamma jj$ process accounts for 63% of the event yield in CR^{fid} and 52% in the SR^{fid} . The remaining prompt backgrounds, including top quark processes and EW and strong $Z\gamma jj$ processes, contribute 11% in CR^{fid} and 8% in SR^{fid} , while the non-prompt background fraction is 22% in CR^{fid} and 23% in SR^{fid} .

Table 2: Expected number of events in the signal and control regions used for the fiducial cross-section measurement and observation of EW $W\gamma jj$ production. Statistical and systematic uncertainties estimated in Section 8 are included for each component. The number of observed events in each region are included for comparison. The “non-prompt” background category includes non-prompt photons and fake leptons.

	$\text{SR}^{\text{fid}} \left(N_{\text{jets}}^{\text{gap}} = 0 \right)$	$\text{CR}^{\text{fid}} \left(N_{\text{jets}}^{\text{gap}} > 0 \right)$
EW $W\gamma jj$	520 ± 141	120 ± 49
Strong $W\gamma jj$	1550 ± 830	1970 ± 950
Non-prompt	692 ± 57	698 ± 58
Top quark processes	109 ± 18	183 ± 37
EW + strong $Z\gamma jj$	128 ± 34	163 ± 77
Total	3000 ± 830	3140 ± 960
Data	3341	3143

5 Background estimation

The main source of background arises from strong $W\gamma jj$ production. This background is estimated by using MC simulation and constrained using data in the control regions defined in Table 1; a detailed description of this procedure is provided in Section 6. Additional prompt backgrounds arise from $Z\gamma jj$ production and the production of one or more top quarks in association with photons. These prompt backgrounds are estimated by using MC simulations described in Section 3.

The largest non-prompt background arises primarily from W +jet production, where a jet is misidentified as a photon. This non-prompt photon background is estimated by using a data-driven template fit to the p_T -corrected photon isolation energy ($E_T^{\text{iso},\gamma} = E_T^{\text{cone40}} - 0.022 \times p_T$) distributions of prompt and non-prompt photons. The prompt photon template is determined from prompt photons in $W\gamma jj$ MC simulation. A control region enriched with non-prompt photons is defined by requiring photons to satisfy the *loose* identification criteria but fail to satisfy the selection criteria for at least one of four variables in the *tight* identification that define the photon shower shape. This selection is referred to as *LoosePrime4* [35]. The shape of the non-prompt photon template is extracted by parameterising the $E_T^{\text{iso},\gamma}$ distribution in this control region. Contributions from processes with prompt photons in the non-prompt photon control region are minimal but are accounted for with a systematic uncertainty of the background estimate. The fractions of prompt and non-prompt photons are extracted for each bin of each distribution using an unbinned, maximum-likelihood fit of the prompt and non-prompt templates to data. The extracted yields are verified using an “ABCD sideband method” [42] with the two dimensional plane defined by photon identification and isolation requirements. The dominant uncertainty in the non-prompt photon background is due to the choice of photon identification criteria used to define the non-prompt template regions. This non-prompt photon definition is varied by requiring photons to fail to satisfy at least one of two, three, or five shower shape selection variables used to define the tight identification [35], and the systematic uncertainty due to this identification choice varies from 4% to 16%. Other sources of systematic uncertainty arise from statistical uncertainties of the samples in the template and fit regions; prompt photon leakage into the non-prompt template regions, estimated from signal MC simulation; and the effect of photon isolation energy modelling uncertainties on the prompt photon templates.

A “fake factor” method is used to estimate the background from fake leptons: charged leptons arising from misreconstructed jets or in-flight decays of hadrons. The method defines *tight* leptons as those satisfying

all selection criteria described in Section 4 and *non-tight* leptons as those failing to satisfy either the *tight* identification or *tight* isolation criteria. *Non-tight* leptons must still satisfy *loose* identification in addition to the identification and isolation requirements associated with the single lepton triggers. The fake factor is defined as the ratio of events with one *tight* lepton to those events with one *non-tight* lepton. It is calculated differentially in lepton p_T and η in a non-prompt control region defined by exactly one lepton and at least one jet. Contributions from processes with prompt leptons are subtracted from the data prior to calculating the fake factor. The non-prompt lepton background is then determined in each bin of each measured distribution by applying the fake factor to prompt, background-subtracted data events that satisfy all the selection criteria except the *tight* lepton criteria. Sources of uncertainty arise from data and MC sample size in the control regions, relative fractions between heavy flavour decays and photon conversions, control region definitions for fake factor calculation, theoretical uncertainties of the prompt background, and the binning in p_T^l and η .

An electron can be misreconstructed as a converted photon ($e \rightarrow \gamma$) if the track reconstruction algorithm either fails to associate a B-layer hit to the track or associates a spurious conversion track to the electron. This background arises predominantly from Z +jets and $t\bar{t}$ processes, and the fake rate is determined using data by selecting candidate ee and $e\gamma$ events in a range of ± 20 GeV around the Z boson mass. The object selections for the electron and photon candidates satisfies the same criteria specified in Section 4. Compared with the analysis region selections described in Section 4, events must satisfy the following criteria: $E_T^{\text{miss}} < 20$ GeV, $m_T^W < 20$ GeV, and there are no jet requirements. The ee and $e\gamma$ event yields are obtained by fitting a double-sided Crystal Ball function [43] to m_{ee} or $m_{e\gamma}$ to model the Z boson decay along with an exponential function to account for backgrounds. The ratio of $N_{e\gamma}/N_{ee}$ is parameterised as functions of electron p_T and η and applied to data events with $eejj$ and $e\mu jj$ final states, where one electron replaces the photon in the event selection, to estimate the $e \rightarrow \gamma$ background in electron and muon channels, respectively. Sources of systematic uncertainties for the $e \rightarrow \gamma$ fake rate arise from variations in the invariant mass fit range, varying the binning in p_T and η , and replacing the exponential background parameterisation with a fourth-order Bernstein polynomial [44].

No explicit requirement is imposed on the longitudinal position of the photon relative to the primary vertex, Δz_γ , as it is not well-measured for unconverted photons. As a result, a combinatorial background arises whereby a photon originating from one pp interaction is selected alongside a Wjj event from another pp interaction from the same bunch crossing. This pile-up photon background is estimated by using a data-driven method [45] that exploits the difference in Δz_γ between hard scatter and pile-up photons. Because the pile-up photon fraction, f_{PU} , is independent of the photon conversion status, events are selected if they contain a converted photon with two tracks and a conversion vertex with radius < 125 mm such that the conversion occurs within the pixel detector, allowing for an accurate measurement of Δz_γ . The sidebands of the Δz_γ distribution in background-subtracted data and $W\gamma jj$ simulation are used to estimate the fraction of events in each analysis region that have photons originating from a pile-up interaction. A control region dominated by pile-up photon background is defined by $|\Delta z_\gamma| > 50$ mm. Due to the limited number of events in this data control region, the statistical precision of f_{PU} is almost 90% while the systematic uncertainty is negligible compared with the statistical uncertainty. The pile-up background contains a component where a pile-up jet can be misidentified as a photon. The fraction of prompt photons is estimated by using inclusive prompt photon events obtained from data recorded using single photon triggers, and f_{PU} is then multiplied by this fraction. The estimated f_{PU} is $(1.7 \pm 1.6)\%$ in SR^{fid} and $(0.45 \pm 0.39)\%$ in CR^{fid} ; it is neglected for the differential cross-section measurement due to the limited number of events in the control region of pile-up photons arising from the additional requirement of $m_{jj} > 1$ TeV. The procedure to extract the EW $W\gamma jj$ fiducial cross-section is repeated without the pile-up photon background, and the uncertainty on the fiducial cross-section is unchanged.

6 Signal extraction

6.1 Signal extraction for observation

A neural network (NN) is used to classify signal and background processes. The NN is trained on the EW $W\gamma jj$ process as the signal model and the sum of strong $W\gamma jj$, $Z\gamma jj$, and top quark processes as the background model, which are weighted according to their cross-sections. All events used in the training satisfy the signal region SR^{fid} selection described in Section 4. Two NN classifiers are created after training on two statistically independent but otherwise identical samples. A binary cross-entropy loss function is used during the training and the loss for each event is weighted by its weight. The NN consists of a batch normalisation layer followed by three densely connected hidden layers of 512 nodes each. Each hidden node uses a LeakyRelu activation function [46]. The last hidden layer is densely connected with the output layer that uses a sigmoid activation function. The model is trained with the Adam learning rate optimiser [47] with an initial learning rate of 3×10^{-5} . The NN is trained to discriminate signal from background using 13 kinematic observables. These 13 observables, ranked according to importance, consist of the lepton-photon centrality, $\xi_{l\gamma}$; pseudorapidity difference between the two jets, $\Delta\eta_{jj}$; angular distance between the lepton-photon system and the dijet system, $\Delta R(l\gamma, jj)$; p_{T}^{γ} ; p_{T}^l ; photon centrality, ξ_{γ} ; angular distance between leading jet and photon, $\Delta R(j_{\text{lead}}, \gamma)$; angular distance between lepton and photon, $\Delta R(l, \gamma)$; transverse momentum of the lepton-photon system, $p_{\text{T}}^{l\gamma}$; azimuthal angle difference between the lepton-photon and the dijet system, $\Delta\phi(l\gamma, jj)$; m_{T}^W ; leading jet transverse momentum, $p_{\text{T}}^{j_{\text{lead}}}$; and $\eta_{j_{\text{lead}}}$. The optimal hyperparameters are determined using a grid search by repeating the training with different combinations of the number of hidden layers, number of nodes, and learning rate; the model architecture with the lowest loss on test data is chosen. The NN trained on one statistically independent sample is applied to the other for evaluation. No significant differences between the two NNs are found, and thus the average value of the two NN output scores is used for data and data-driven background events.

A profile likelihood fit to the NN score in the SR^{fid} and CR^{fid} region is performed simultaneously to maximise the likelihood for observing n^{data} events given the number of predicted events. The expected number of events depends on two floating normalisation factors: μ_{strong} for strong $W\gamma jj$ and μ_{EW} as the EW $W\gamma jj$ signal strength. The likelihood function \mathcal{L} can be written in a simplified form as the product of Poisson distributions multiplied by the product of Gaussian constraints,

$$\mathcal{L} = \prod_r \prod_i P(n_{r,i}^{\text{data}} | \mu_{\text{EW}} S_{r,i}(\boldsymbol{\theta}) + B_{r,i}(\mu_{\text{strong}}, \boldsymbol{\theta})) \times \prod_j G(\theta_j), \quad (1)$$

where r is either SR^{fid} or CR^{fid} , i represents the bin number of the NN score in region r , $\boldsymbol{\theta}$ refers to nuisance parameters constrained by the Gaussian term $G(\theta_j)$ for each systematic uncertainty source j , $S_{r,i}(\boldsymbol{\theta})$ is the number of predicted events from EW $W\gamma jj$ simulation, and $B_{r,i}(\boldsymbol{\theta})$ is the number of background events.

The shape of the NN score for EW $W\gamma jj$ and strong $W\gamma jj$ is taken from the corresponding MC while the normalisation for each process is floated, namely, μ_{EW} and μ_{strong} , respectively. The other backgrounds are allowed to vary within their respective uncertainties. The EW $W\gamma jj$ measurement depends on a set of nuisance parameters that represent the impact of uncertainties on the fit; these uncertainties are discussed in Section 8. The observed significance is evaluated by performing a background-only simultaneous fit to data in SR^{fid} and CR^{fid} to estimate the probability of rejecting the background-only hypothesis. The signal region was blinded when analysis decisions and optimisations were made to avoid biasing the measurement.

Figure 2 shows the top three ranked observables of the NN in the signal region with the values of nuisance parameters and normalisation factors obtained from the fit of the NN score distributions to templates in different variables results and Figure 3 shows the output NN score in SR^{fid} and CR^{fid} after performing the profile likelihood fit in the corresponding observables. Good agreement with the observed data is seen in both the regions except for the slight shape difference in $\xi_{l\gamma}$ between MC and data. Instead of injecting the nuisance parameter from the fit to the NN score, the maximum-likelihood fit was performed to $\xi_{l\gamma}$ directly to obtain the nuisance parameters, resulting in excellent agreement between MC and data after the fit. Therefore the maximum-likelihood fit has sufficient flexibility to give reliable results despite mismodelling between MC and data before the fit.

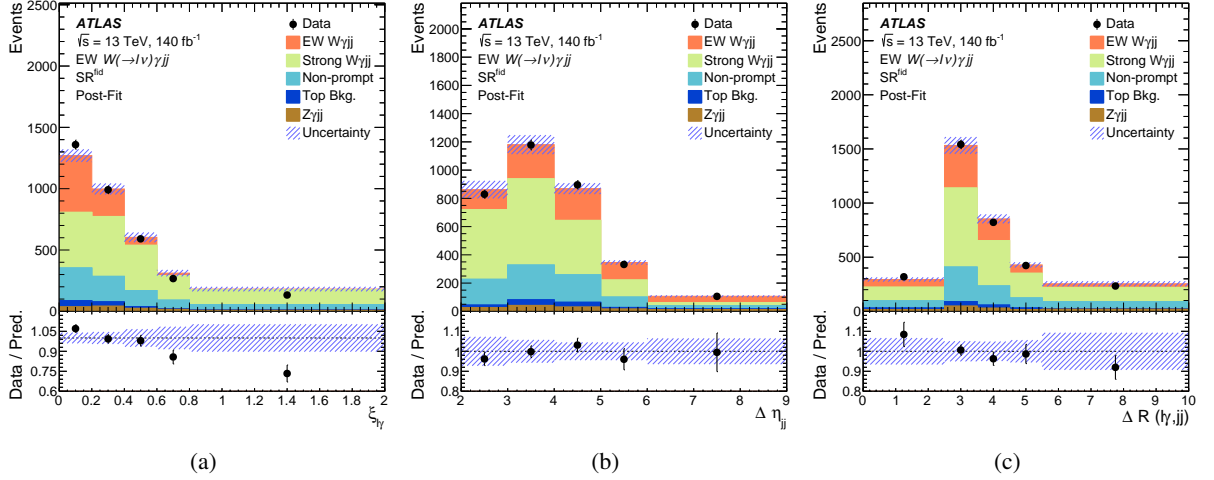


Figure 2: Distributions of the predicted and observed yields for the three highest ranked variables in the NN after performing the profile likelihood fit, as functions of (a) $\xi_{l\gamma}$, (b) $\Delta\eta_{jj}$, and (c) $\Delta R(l\gamma, jj)$. The observed data is represented by solid circles and the associated vertical error bar represents the statistical uncertainty of the data. The predicted yields comprise simulated EW $W\gamma jj$ signal, backgrounds from non-prompt photons and leptons that are estimated by using data-driven methods, and backgrounds that are estimated with simulation. The hashed band represents the quadrature sum of the statistical and systematic uncertainties.

6.2 Signal extraction for the differential cross-section measurement

The EW $W\gamma jj$ event yields are also extracted differentially as functions of m_{jj} , p_T^{jj} , $\Delta\phi_{jj}$, p_T^l , $m_{l\gamma}$, and $\Delta\phi_{l\gamma}$ using the methodology documented in Ref. [48]. This method exploits signal and control regions in a binned log-likelihood fit [49, 50], which are used to constrain both the shape and normalisation of the strong $W\gamma jj$ background. The data are split into four regions (SR, CR_A, CR_B, and CR_C) by imposing the selection criteria for $\xi_{l\gamma}$ and $N_{\text{jets}}^{\text{gap}}$ defined in Table 1 in Section 4. The variables $\xi_{l\gamma}$ and $N_{\text{jets}}^{\text{gap}}$ are uncorrelated, and are thus chosen to define these four regions. The EW $W\gamma jj$ event is produced centrally and has little hadronic activity in between the forward and backward jets, hence each event in the SR is required to satisfy $N_{\text{jets}}^{\text{gap}} = 0$ and $\xi_{l\gamma} < 0.35$. The control regions are deficient in EW $W\gamma jj$, and are defined by inverting the requirement on either $\xi_{l\gamma}$ or $N_{\text{jets}}^{\text{gap}}$.

The binned log likelihood is defined as:

$$\ln \mathcal{L} = - \sum_{r,i} \nu_{ri}^s + \sum_{r,i} N_{ri}^{\text{data}} \ln \nu_{ri}^s,$$

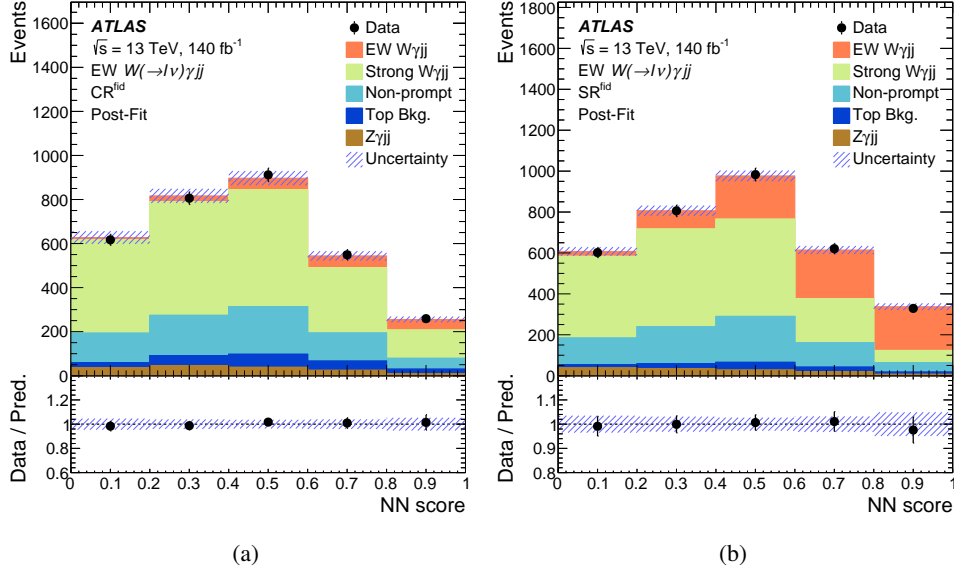


Figure 3: Distribution of the predicted and observed yields as a function of the NN score in the CR^{fid} (a) and SR^{fid} (b) regions after performing the profile likelihood fit. Data is represented by solid circles, and the associated vertical error bar represents the statistical uncertainty on the data. The predicted yields comprise simulated EW $W\gamma jj$ signal, backgrounds from non-prompt photons and leptons that are estimated by using data-driven methods, and backgrounds that are estimated with simulation. The hashed band represents the quadrature sum of the statistical and systematic uncertainties.

where r corresponds to one of the four regions SR , CR_A , CR_B , and CR_C , i corresponds to the bin of the kinematic observable, N_{ri}^{data} corresponds to the data yield in bin i of region r , and v_{ri}^s corresponds to the prediction that relies on the s sources of experimental systematic uncertainty.

The fitted number of events in region r and bin i is expressed as

$$v_{ri} = \mu_{\text{EW},i} v_{ri}^{\text{EW,MC}} + v_{ri}^{\text{strong}} + v_{ri}^{\text{other,bkg}}, \quad (2)$$

where $\mu_{\text{EW},i}$ is the signal strength of EW $W\gamma jj$ in bin i , and $v_{ri}^{\text{EW,MC}}$ and $v_{ri}^{\text{other,bkg}}$ correspond to the EW $W\gamma jj$ prediction and contributions from reducible background processes, respectively. The strong $W\gamma jj$ prediction is constrained using the signal-suppressed control regions based on the following four relations:

$$\begin{aligned} v_{\text{CR}_A,i}^{\text{strong}} &= b_{L,i} v_{\text{CR}_A,i}^{\text{strong,MC}}, & v_{\text{CR}_B,i}^{\text{strong}} &= b_{H,i} v_{\text{CR}_B,i}^{\text{strong,MC}}, \\ v_{\text{SR},i}^{\text{strong}} &= b_{L,i} c v_{\text{SR},i}^{\text{strong,MC}}, & v_{\text{CR}_C,i}^{\text{strong}} &= b_{H,i} c v_{\text{CR}_C,i}^{\text{strong,MC}}. \end{aligned} \quad (3)$$

The parameters $b_{L,i}$ and $b_{H,i}$ are sets of bin-dependent free parameters that correspond to the $\xi_{l\gamma} < 0.35$ and $\xi_{l\gamma} > 0.35$ regions, respectively. The low- $\xi_{l\gamma}$ parameter, $b_{L,i}$, is primarily constrained by CR_A , while $b_{H,i}$ is primarily constrained by CR_B . These two sets of parameters introduce additional degrees of freedom to the predicted strong $W\gamma jj$ event yield to allow the fitted number of strong $W\gamma jj$ events to be more consistent with the observed data. A floating parameter c is used to provide a residual correction that can

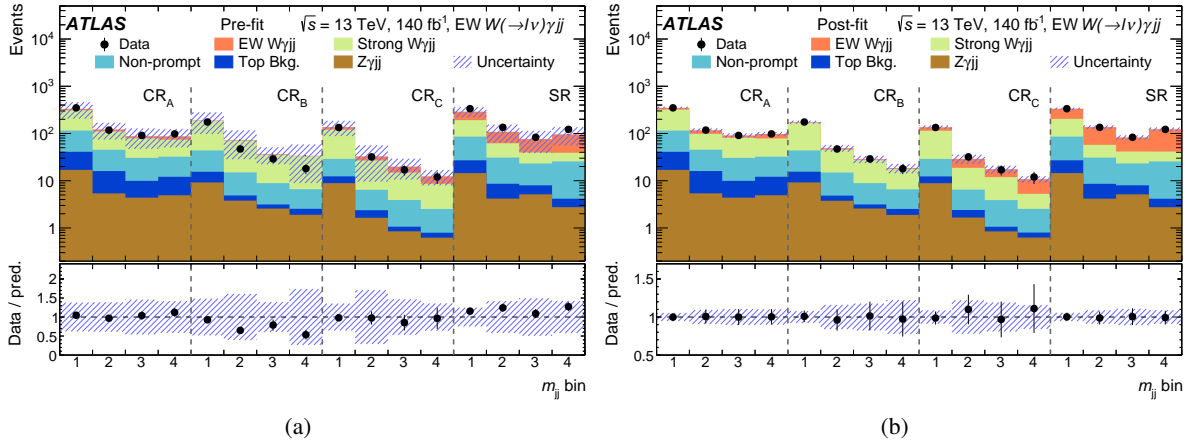


Figure 4: Distribution of the observed and predicted yields as a function of m_{jj} in the SR, CR_A, CR_B, and CR_C regions, both (a) pre-fit and (b) post-fit. Data is represented by solid circles, and the associated vertical error bar represents the statistical uncertainty of the data. The predicted yields comprise simulated EW $W\gamma jj$ signal, backgrounds from non-prompt photons and leptons that are estimated by using data-driven methods, and backgrounds that are estimated with simulation. The hashed band represents the quadrature sum of the statistical and systematic uncertainties, which are constrained in the fit. The bin edges are (1, 1.4, 1.7, 2.1, 5.3) TeV.

account for any mismodelling across $N_{\text{jets}}^{\text{gap}}$. This configuration is less prone to fit instabilities coming from the limited number of observed events than is the two-parameter linear fit of Ref. [48].

For each bin i , the binned maximum-likelihood fit consists of the following free parameters: the signal strength $\mu_{\text{EW},i}$, the free parameter c , and the $b_{L,i}$ and $b_{H,i}$ corrections to the strong $W\gamma jj$ process. This constitutes an overall number of $3 \times N_{\text{bins}} + 1$ parameters that are constrained by the $4 \times N_{\text{bins}}$ measurements in data, where N_{bins} corresponds to the number of bins in the measurement of the differential observable.

The alternative predictions for EW $W\gamma jj$ and strong $W\gamma jj$ introduced in Section 3 are used to assess the systematic uncertainties discussed in Section 8. The statistical uncertainty arising from the limited size of the data and simulated MC samples is evaluated using the bootstrap method [51], each with 10 000 toy experiments. The signal extraction is repeated for each toy experiment, where the event yields in each bin of the signal and control regions are sampled according to a Poisson distribution. The mean and RMS of the extracted event yields among these toy experiments are used to define the extracted EW $W\gamma jj$ yield and associated statistical uncertainty. Each source of systematic uncertainty is varied and applied to the templates coherently in each region and propagated through the fit. The theory uncertainties due to QCD scales, PDFs, and α_S are evaluated following the procedures discussed in Section 8.

Figure 4 shows the pre- and post-fit agreement between data and predicted yields as functions of m_{jj} in SR, CR_A, CR_B, and CR_C. The floating parameter c ranges from 1.06 to 1.22 depending on the observable while the overall scaling factor for strong $W\gamma jj$ ($b_{L,i} c$) ranges between 1.07 and 1.39. Good post-fit agreement between the predicted yields and data is observed in all four regions. The pre-fit systematic uncertainties presented on the figures are estimated as documented in Section 8. The three control regions allow for a constraint of the systematic uncertainties, in particular the strong $W\gamma jj$ modelling uncertainties.

The differential EW $W\gamma jj$ signal extraction method is validated with two procedures. In the first cross-check, a different choice of control regions for the strong $W\gamma jj$ process is assigned in Equation 3, where $b_{L,i}$ and $b_{H,i}$ instead link the strong background yields at same $N_{\text{jets}}^{\text{gap}}$ values, and are thus constrained at

high $\xi_{l\gamma}$, and the free parameter c provides residual corrections considering the mismodelling across $\xi_{l\gamma}$. In the second method, the data-driven corrections to the strong $W\gamma jj$ contributions are derived only in either CR_A or CR_C . The extracted EW $W\gamma jj$ event yields obtained using each of these two methods are consistent with the nominal results.

7 Correction for detector effects

The fiducial and differential cross-sections at particle level are obtained by correcting the reconstruction-level EW $W\gamma jj$ event yield for the detector effects of inefficiency and resolution.

The particle-level regions are defined using all final-state stable particles with a mean lifetime of $c\tau > 10$ mm. To reduce model-dependence associated with extrapolations across phase space, the particle-level selection is defined to mimic the detector-level event selection described in Section 4. Particle-level dressed leptons are formed by combining the four momenta of each prompt electron or muon with the prompt photons that lie within $\Delta R = 0.1$ of the prompt lepton excluding electrons or muons from tau decays. Events must contain exactly one dressed lepton with $p_T > 30$ GeV. Leptons are required to fall within the same detector acceptance as the reconstruction level, with muons satisfying $|\eta| < 2.5$ and electrons satisfying $|\eta| < 2.47$ excluding the region $1.37 < |\eta| < 1.52$. Events must contain at least one prompt photon with $p_T > 22$ GeV and $|\eta| < 2.37$, excluding the region $1.37 < |\eta| < 1.52$. At particle level, the photon isolation energy, E_T^{iso} is defined as the sum of the transverse energy of stable particles within a cone of $\Delta R = 0.4$ around the prompt photon, excluding the photon itself and neutrinos. To minimise the model dependence, SHERPA EW $W\gamma jj$ simulation is used to determine a particle-level photon isolation requirement that best mimics the detector-level behaviour; particle-level photons must satisfy $E_T^{\text{iso}} < 0.2E_T^\gamma$. Jets are reconstructed with the anti- k_t algorithm using all final-state particles as input except the dressed lepton and prompt neutrinos. Events are required to contain zero jets that fall within $\Delta R = 0.4$ around a b -hadron, and must contain at least two jets with $p_T > 50$ GeV and $|\eta| < 4.4$. The particle-level missing transverse momentum, defined as the vector sum of the transverse momenta of all non-interacting, final-state stable particles, must satisfy $E_T^{\text{miss}} > 30$ GeV. These leptons, jets, and photons are then selected in a VBS topology by using the same requirements as the reconstruction-level selection, which are listed in Table 3. The particle-level phase space definition is slightly different for the fiducial and differential cross-section measurements to ensure the definitions are as close as possible to the signal extraction method at reconstruction level.

The integrated fiducial cross-section, $\sigma_{EW\ W\gamma jj}^{\text{fid}}$, is defined as :

$$\sigma_{EW\ W\gamma jj}^{\text{fid}} = \frac{N_{EW\ W\gamma jj}}{L \cdot C_{EW\ W\gamma jj}}, \quad (4)$$

where $N_{EW\ W\gamma jj}$ is the number of extracted EW $W\gamma jj$ events after performing the fit described in Section 6.1, L is the integrated luminosity, and $C_{EW\ W\gamma jj}$ is the correction factor estimated by using the EW $W\gamma jj$ MC. The statistical uncertainty due to the limited size of data and simulation samples are propagated through Equation 4, along with each source of systematic uncertainty affecting $N_{EW\ W\gamma jj}$ and $C_{EW\ W\gamma jj}$, which are treated as fully correlated.

For the differential cross-section measurement each distribution is unfolded using an iterative Bayesian method with two iterations [52, 53]. The binnings of the observables are optimised to ensure the relative statistical precision of the extracted EW $W\gamma jj$ event yield is similar across bins using an Asimov dataset [54] formed by the $W\gamma$ and non- $W\gamma$ simulation samples. The binning for each observable is optimised using

Table 3: Particle-level definition for the fiducial and differential EW $W\gamma jj$ measurement.

Object	Selection requirements
Dressed muons	$p_T > 30$ GeV and $ \eta < 2.5$
Dressed electrons	$p_T > 30$ GeV and $ \eta < 2.47$ (excluding $1.37 < \eta < 1.52$)
Isolated photons	$E_T^\gamma > 22$ GeV and $ \eta < 2.37$ (excluding $1.37 < \eta < 1.52$) and $E_T^{\text{iso}} < 0.2E_T^\gamma$
Jets	At least two jets with $p_T > 50$ GeV and $ y < 4.4$, b -jet veto
Missing transverse momentum	$E_T^{\text{miss}} > 30$ GeV and $m_T^W > 30$ GeV
VBS topology	$N_\ell = 1, N_\gamma \geq 1, m_{\ell\gamma} - m_Z > 10$ GeV $\Delta R_{\min}(\ell, j) > 0.4, \Delta R_{\min}(\gamma, j) > 0.4, \Delta R_{\min}(\ell, \gamma) > 0.4$ $\Delta R_{\min}(j_1, j_2) > 0.4, \Delta\phi_{\min}(E_T^{\text{miss}}, j) > 0.4$ $N_{\text{jets}} \geq 2, p_T^{j_1}, p_T^{j_2} > 50$ GeV $m_{jj} > 500$ GeV, $ \Delta y_{jj} > 2$
Fiducial measurement	VBS topology
Differential measurement	VBS topology $\oplus (m_{jj} > 1000$ GeV, $N_{\text{jets}}^{\text{gap}} = 0$, and $\xi_{W\gamma} < 0.35$)

the EW $W\gamma jj$ and strong $W\gamma jj$ simulation samples, such that a similar statistical precision is obtained for each bin of the extracted yield. An additional requirement that the bin width is not smaller than twice the resolution of the observable is enforced. The number of iterations are determined by minimising the quadrature sum of the bias and the statistical uncertainty due to unfolding, where the bias is estimated by comparing the unfolded distribution after a certain number of iterations to the true distribution in the EW $W\gamma jj$ simulation. The value and statistical uncertainty on the fiducial EW $W\gamma jj$ cross-section are derived from the mean and root mean square (RMS) of the 10 000 toy experiments described in Section 6.2, propagated through the unfolding. These modified distributions and response matrices are then used to repeat the unfolding procedure for each toy experiment. The statistical uncertainty in each bin corresponds to the standard deviation of the unfolded results from the ensemble of 10 000 toy experiments. Systematic uncertainties that affect both the signal extraction and the unfolding are treated as correlated and propagated through the unfolding to the final results.

8 Systematic uncertainties

Experimental sources of systematic uncertainty arise from the reconstruction and energy calibration of objects including charged leptons, photons, jets, heavy-flavour tagging of jets, and missing transverse momentum. These uncertainties affect both the normalisation and shape of the simulated background processes, the shape of the simulated EW $W\gamma jj$ process in the signal extraction, and the normalisation and shape of simulations used to unfold the inclusive and differential cross-sections of the EW $W\gamma jj$ process.

The lepton trigger efficiencies and lepton and photon reconstruction, identification, and isolation efficiencies in simulations are corrected using scale factors derived from data, as described in Section 4. Systematic uncertainties due to this procedure are evaluated by varying the scale factors based on their associated uncertainties [34, 35]. Uncertainties arising from differences between simulation and data in the

reconstructed lepton (photon) momentum are evaluated by scaling and smearing the lepton (photon) transverse momentum.

Jets are calibrated using a combination of MC-based and data-driven corrections [55]. Uncertainties in the measurements due to uncertainties in the jet energy scale and resolution corrections are evaluated by scaling and smearing the jet four-momentum in the simulation by the uncertainties associated with each of these corrections. Uncertainties arising from the imperfect modelling of the JVT in the simulation are estimated by varying the JVT requirement. Furthermore, uncertainties arising from differences between simulation and data in b -jet tagging efficiencies are estimated by varying the associated scale factors [40].

Uncertainties from the E_T^{miss} measurement are estimated by propagating the uncertainties in the transverse momenta of hard physics objects and by applying uncertainties associated with momentum scale and resolution to the track-based term [41].

Additional sources of experimental uncertainty arise due to the modelling of pile-up and the luminosity determination. The uncertainty in the combined 2015–2018 integrated luminosity is 0.83% [29], obtained using the LUCID-2 detector [11] for the primary luminosity measurements, complemented by measurements using the inner detector and calorimeters.

For the EW $W\gamma jj$ fiducial cross-section measurement, each source of experimental systematic uncertainty is introduced as a nuisance parameter using a Gaussian constraint in the likelihood, as described in Section 6.1. For the differential signal extraction, 10 000 pseudo-experiments are constructed for simulated MC samples, where each pseudo-experiment samples each simulated MC event with a unit-mean Poisson distribution. For data, in each experiment the number of data events in each bin is determined by sampling a Poisson distribution of mean equal to the nominal bin content. When evaluating the statistical significance of the systematic uncertainties, the distribution of Poisson fluctuations is the same in the nominal as that in the systematic variations. The EW $W\gamma jj$ yield is extracted for each pseudo-experiment, and the effect of the systematic uncertainty on the yield is calculated as the mean of the distribution of differences between the varied and nominal for each pseudo-experiment. The statistical significance of each experimental systematic uncertainty is evaluated by computing the RMS of the distribution of differences between the varied and nominal pseudo-experiments. A smoothing procedure is applied to reduce bin-to-bin statistical fluctuations such that the difference between uncertainties with or without smoothing is statistically insignificant. All experimental systematic uncertainties are treated as correlated among processes and regions. For both the inclusive and differential cross-sections, the dominant experimental systematic uncertainties arise from the calibration of jets and modelling of pile-up conditions, resulting in approximately 4% uncertainty in the inclusive cross-section and 5%–9% uncertainty in the differential measurements.

Theoretical uncertainties are accounted for from all simulated signal and background processes that affect the EW $W\gamma jj$ signal extraction. Each source of theoretical uncertainty is estimated by repeating the signal extraction and unfolding procedure with an uncertainty variation applied and propagating this through the unfolded measurements. Theoretical uncertainties arise due to higher-order QCD corrections, the PDFs used in the simulations, the accuracy of the strong coupling constant α_S , and the choice of event generators. The effects of higher-order QCD corrections are estimated by varying each of the renormalisation (μ_R) and factorisation (μ_F) scales by a factor of two with $0.5 \leq \mu_F/\mu_R \leq 2.0$. Uncertainties due to the PDFs are evaluated by varying each Hessian eigenvector of the nominal NNPDF3.0_{NNLO} set and comparing results obtained from nominal PDFs to alternative PDFs such as NNPDF3.1_{NNLO} [56], CT18_{NNLO} [57], MSHT2020_{NNLO} [58], and PDF4LHC15_{NNLO} [59]. If the difference between the nominal PDF and alternative PDF is not covered by the quadrature sum of the eigenvector changes in NNPDF3.0_{NNLO}, an additional uncertainty is assigned. The uncertainty due to α_S is evaluated with the nominal PDF by varying

the nominal $\alpha_S = 0.118$ by ± 0.001 . For the EW $W\gamma jj$ signal extraction, the systematic uncertainty arising from the choice of event generator for the strong $W\gamma jj$ and EW $W\gamma jj$ processes is estimated using the symmetrised envelope formed by the difference between the extracted event yield between the nominal generator, SHERPA, and the alternative generator, MADGRAPH5+PYTHIA8. For the differential cross-section measurement, the choice of event generator is extracted using the same method as with the experimental systematic uncertainties.

Treatment of the theory uncertainties is briefly discussed here. For the fiducial cross-section measurement, the QCD scale uncertainties are treated as uncorrelated between signal and control regions, because it is a conservative approach in this case as the QCD scales are varied separately instead of simultaneously in these two regions. The PDF and α_S uncertainties are treated as correlated between regions but kept uncorrelated between different processes. Unlike the decorrelation of theory uncertainties across regions for the fiducial cross-section measurement of EW $W\gamma jj$, this treatment of theory uncertainties is not necessary for the differential cross-section measurement for two reasons: first, the differential cross-section is measured in each bin of the observable using the fit described above, hence the theory uncertainties are decorrelated between bins of observables; and second, correlations of QCD scale variations across $N_{\text{jets}}^{\text{gap}}$ are taken into account by the floating parameter c in Equation 3 in Section 6.2 such that only the uncertainties in c are required.

Systematic uncertainties related to the unfolding procedure in the differential cross-section measurements are evaluated as follows. First, the EW $W\gamma jj$ process simulated with the alternative generator, MADGRAPH, is used to extract the EW $W\gamma jj$ signal and unfold the data. The difference from the nominal result is applied as a systematic uncertainty on the unfolded EW $W\gamma jj$ distributions. Second, 10 000 truth toy experiments are generated for the particle-level distribution according to a Gaussian distribution with mean equal to the value of the corresponding bin and RMS equal to the statistical uncertainty of the bin. The nominal response matrix is then applied to the particle-level distribution from each toy experiment to create a reconstruction-level pseudo-dataset, which is then unfolded with the nominal response matrix to produce an unfolded pseudo-dataset. The difference in the observable distribution between the truth toy experiment and the unfolded pseudo-dataset constitutes a systematic uncertainty on the unfolded result.

Table 4 shows the impact of the statistical and systematic uncertainties on the fiducial and differential cross-section measurement. The precision of the fiducial cross-section is limited by the statistical precision of the sample followed by the modelling uncertainties, and the largest experimental uncertainties arise from uncertainties in the jet energy scale and jet energy resolution of reconstructed jets. Figure 5 shows the fractional systematic uncertainties as functions of m_{jj} and p_T^l . The uncertainties in the differential measurement are mostly dominated by the systematic variations arising from strong $W\gamma jj$ and EW $W\gamma jj$ modelling and the impact of the jet energy scale and resolution uncertainties, for distributions including jets.

9 Results

9.1 Observation and fiducial cross-section for EW $W\gamma jj$ process

The measured signal strength, μ_{EW} , is 1.5 ± 0.5 . This includes a significant modelling uncertainty on the prediction of the fiducial cross-section due to the difference in cross-section prediction between SHERPA and MADGRAPH5+PYTHIA8, which can be seen in Figure 6. The observed significance is determined using a likelihood ratio test, and is calculated to be above six standard deviations, compared with an expected

Table 4: Impact of uncertainties on the measured fiducial cross-section. Squared values of impacts are obtained by fixing a set of nuisance parameters of the uncertainty sources corresponding to the category to the best-fit values, then calculating the difference between the squares of the resulting uncertainty from the total uncertainty of the nominal fit.

Uncertainty Source	Fractional Uncertainty [%]
MC Statistics	11
Jets	8
Lepton, photon, pile-up	8
EW $W\gamma jj$ modelling	7
Data Statistics	6
Strong $W\gamma jj$ modelling	6
Non-prompt background	2
Luminosity	2
Other Background modelling	2
E_T^{miss}	1

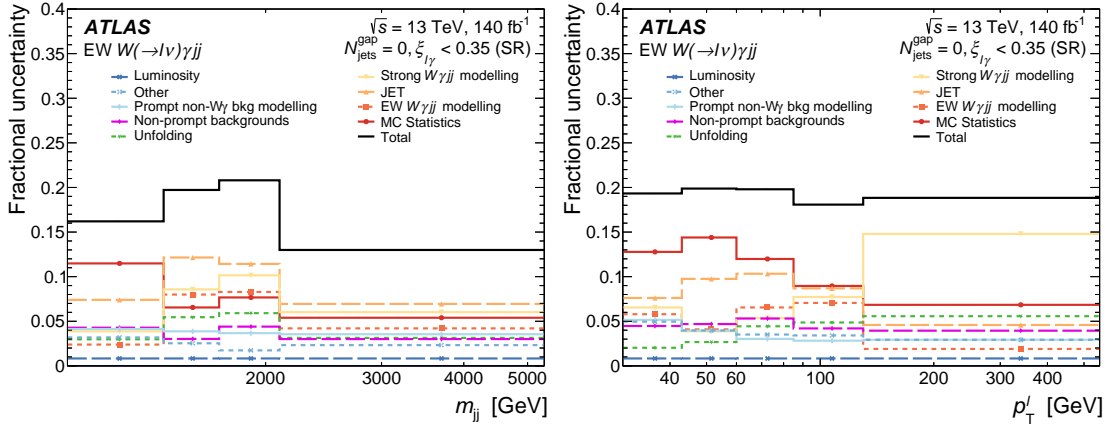


Figure 5: Fractional uncertainty in the EW $W\gamma jj$ measurement as functions of m_{jj} and p_T^l . Uncertainties are grouped in categories that are added in quadrature to give total uncertainties. Systematic uncertainties due to reconstruction of leptons, photons, pile-up, and heavy-flavour jets are grouped in the category “Other”.

significance of 6.3σ . The significance is obtained using the central value of the SHERPA prediction for the SM EW $W\gamma jj$ signal. The large normalisation uncertainty on the predicted cross-section does not impact the calculation of the signal significance.

The measured EW $W\gamma jj$ fiducial cross-section in the phase space defined in Section 7 is determined to be $\sigma_{\text{EW}} = 13.2 \pm 2.5$ fb. The difference in fractional uncertainty between μ_{EW} and σ_{EW} is due to a large normalisation component of the signal modelling uncertainty from the choice of event generator. These predictions from SHERPA and MADGRAPH5+PYTHIA8 are compared with the measured fiducial cross-section in Figure 6. The MADGRAPH5+PYTHIA8 prediction is in agreement with the data within uncertainties while SHERPA underestimates the data within two standard deviations. The theoretical uncertainties in the predicted cross-sections include systematic uncertainties from the QCD scales, PDFs, and α_S variations. The difference between the predicted cross-section between MADGRAPH5+PYTHIA8 and SHERPA arises due to the third parton included in the matrix element of SHERPA [60].

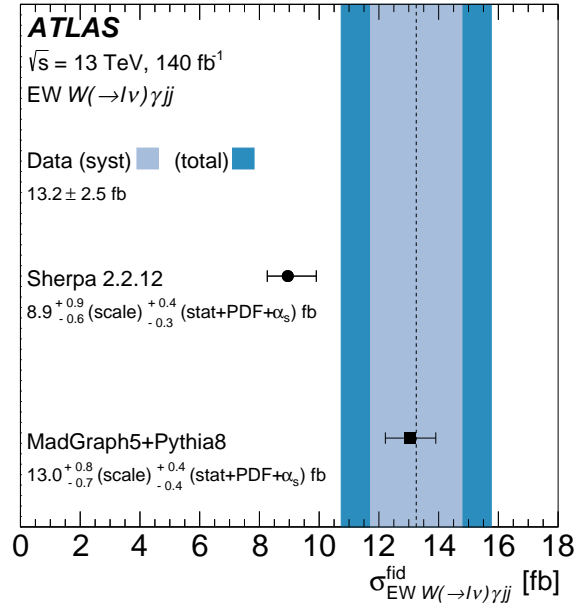


Figure 6: The measured EW $W\gamma jj$ fiducial cross-section compared with the predictions of SHERPA and MADGRAPH5+PYTHIA8. The central value of the measured fiducial cross-section is represented by a dashed vertical line. The light shaded band represents the total uncertainty on the measured fiducial cross-section, while the darker shaded band represents the systematic uncertainty. Each MC prediction is represented with a solid circle, and the associated horizontal error bars correspond to the quadrature sum of statistical uncertainties and theoretical uncertainties. The impacts of various sources of systematic and theoretical modelling uncertainties in the fiducial cross-section are shown in Table 4.

9.2 Differential cross-section for EW $W\gamma jj$ process

Figure 7 shows the differential cross-sections for EW $W\gamma jj$ production as functions of m_{jj} , p_T^{jj} , $\Delta\phi_{jj}$, p_T^l , $m_{l\gamma}$, and $\Delta\phi_{l\gamma}$. The predictions from both MADGRAPH5+PYTHIA8 and SHERPA are in agreement with the data within uncertainties.

The presence of anomalous quartic gauge coupling can modify the distributions of these observables at the tails of m_{jj} , p_T^{jj} , p_T^l or $m_{l\gamma}$. This is investigated further in Section 10. Enhancement of CP violation of Higgs and gauge boson couplings in the diboson sector may distort the shape of $\Delta\phi_{jj}$ and $\Delta\phi_{l\gamma}$, thus the measurements of these two observables can be used to constrain the presence of CP-odd contributions to the EW $W\gamma jj$ process.

10 EFT interpretation

The differential cross-section measurements presented in Section 9 are used to constrain dimension-8 (D-8) operators [2]. These operators are implemented in the Éboli model including twenty independent, charge-conjugation and parity conserving D-8 operators that can change the QGCs. The measured distributions for the six observables are sensitive to sixteen D-8 operators and the most stringent limits from interpretations of these distributions are reported.

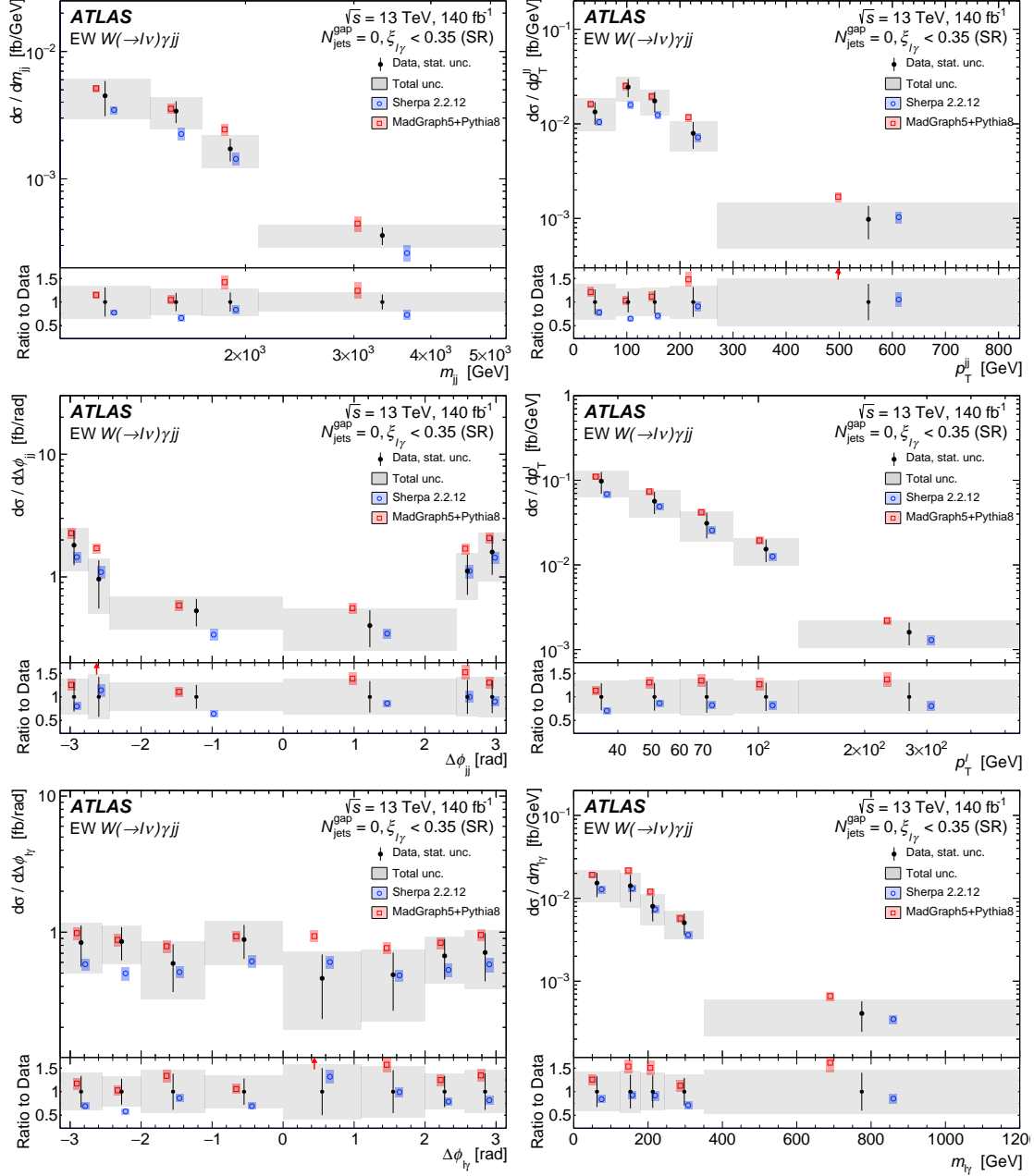


Figure 7: EW $W\gamma jj$ measured differential cross-section (solid circles) as functions of m_{jj} , p_T^{jj} , $\Delta\phi_{jj}$, $p_T^{l\gamma}$, and $\Delta\phi_{l\gamma}$ in comparison to SHERPA (open circles) and MADGRAPH5+PYTHIA8 (open squares) predictions. The vertical error bars on the predictions are determined by varying QCD scales, PDFs, α_S (for SHERPA), and MC statistical uncertainties. The vertical (shaded) error bars on the data correspond to the data statistical (total) uncertainties.

The effective Lagrangian, \mathcal{L}_{eff} , including aQGCs represented by the higher dimension operators and the corresponding Wilson coefficients, is given by:

$$\mathcal{L}_{\text{eff}} = \mathcal{L}_{\text{SM}} + \sum_j \frac{f_j^{(8)}}{\Lambda^4} O_j^{(8)}, \quad (5)$$

where \mathcal{L}_{SM} is the SM Lagrangian, $O_i^{(8)}$ correspond to D-8 operators with dimensionless couplings $f_j^{(8)}$ (Wilson coefficients), and Λ is the energy scale of new physics. The D-8 operators are the lowest-order operators that can change QGCs without affecting the triple gauge couplings². It is assumed that the D-6 operators do not affect the EW $W\gamma jj$ or strong $W\gamma jj$ processes. These D-8 operators can be classified into two groups: mixed-scalar operators ($O_{M0,1,2,3,4,5,7}$), consisting of two covariant derivatives of the Higgs field and two field strength tensors, and tensor-type operators, consisting of four field strength tensors ($O_{T0,1,2,3,4,5,6,7}$).

Theoretical predictions for the EW $W\gamma jj$ process are constructed based on the effective Lagrangian in Equation 5. The amplitude for the EW $W\gamma jj$ process, \mathcal{M} , consists of the SM contribution, \mathcal{M}_{SM} , and the pure D-8 part including the aQGCs, $\mathcal{M}_{\text{D-8}}$.

The differential cross-section can be decomposed into the following three terms:

$$|\mathcal{M}|^2 = |\mathcal{M}_{\text{SM}}|^2 + 2\text{Re}(\mathcal{M}_{\text{SM}}^* \mathcal{M}_{\text{D-8}}) + |\mathcal{M}_{\text{D-8}}|^2, \quad (6)$$

where the pure SM term is $|\mathcal{M}_{\text{SM}}|^2$, $|\mathcal{M}_{\text{D-8}}|^2$ is the pure D-8 term that scales quadratically with $f_j^{(8)}$, and the interference term between the SM and D-8 amplitudes is $2\text{Re}(\mathcal{M}_{\text{SM}}^* \mathcal{M}_{\text{D-8}})$, which scales linearly with $f_j^{(8)}$. It was found that the pure D-8 term affects the differential cross-section measurements significantly more than the interference term. The pure SM part in Equation 6 is taken to be the LO prediction from MADGRAPH5+PYTHIA8, described in Section 3. The D-8 and interference terms are generated at LO using MADGRAPH5+PYTHIA8, with the same PDF and parameter tunes for modelling as the SM term. QCD scale uncertainties for the EFT contributions are taken directly from the corresponding uncertainty estimate in the SM EW $W\gamma jj$ process using MADGRAPH5+PYTHIA8.

Limits on the D-8 operator coefficients are determined using test statistics based on the profile likelihood ratio. The profile likelihood ratio is constructed in terms of the measured cross-section as functions of each of the six observables and the corresponding theoretical prediction parameterised in terms of Wilson coefficients. The profile-likelihood test statistics, which are assumed to follow a χ^2 distribution with one degree of freedom according to Wilks' theorem [61], allows the 95% confidence level (CL) bounds on Wilson coefficients. The expected 95% coverage is further validated using 1000 pseudo experiments.

The most stringent expected limit on each coefficient is obtained from either the p_T^{jj} or p_T^l distribution. Observed and expected limits on the Wilson coefficients at 95% CL are presented in Table 5 and Table 6 with or without unitarity preservation by introducing the clipping technique described in Ref. [62]. The observed limits are tighter than the expected limits because MADGRAPH5+PYTHIA8 overshoots the differential measurement shown in Figure 7.

The limits on the D-8 Wilson coefficients using the clipping technique are estimated as functions of a cut-off scale, and for values of $M_{W\gamma}$ greater than the cut-off scale the anomalous interaction contribution is

² Triple gauge couplings are represented by dimension-6 operators that affect both strong and EW production of VBS processes. These are strongly constrained by vector boson fusion processes.

set to zero. Figure 8 shows a scan of the cut-off scale for the $T3$ operator when fitting the p_T^{jj} distribution. p_T^{jj} is found to be the most sensitive observable to the tensor-type operators while p_T^l is found to be the most sensitive observable to the mixed scalar operators. The constraints on the f_{T3} and f_{T4} operators represent the first such limits at the LHC.

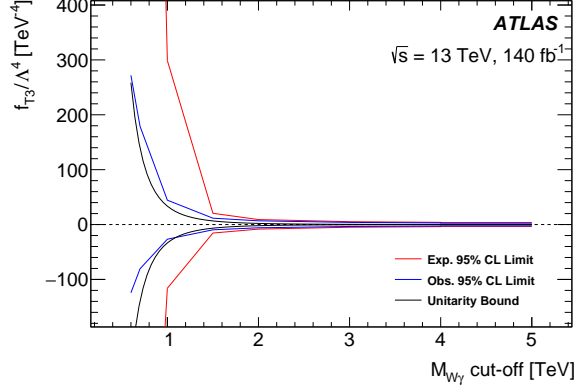


Figure 8: Expected and observed 95% CL limits of the tensor-type operator coupling f_{T3} from the fit to p_T^{jj} at different values of $m_{W\gamma}$. Bounds from partial wave unitarity constraints are also shown.

Table 5: Expected and observed limits on dimension-8 operators modifying the $WW\gamma\gamma$ coupling when fitting either the p_T^{jj} or p_T^l distribution.

Coefficients [TeV ⁻⁴]	Observable	Expected [TeV ⁻⁴]	Observed [TeV ⁻⁴]
f_{T0}/Λ^4	p_T^{jj}	[-2.4, 2.4]	[-1.8, 1.8]
f_{T1}/Λ^4	p_T^{jj}	[-1.5, 1.6]	[-1.1, 1.2]
f_{T2}/Λ^4	p_T^{jj}	[-4.4, 4.7]	[-3.1, 3.5]
f_{T3}/Λ^4	p_T^{jj}	[-3.3, 3.5]	[-2.4, 2.6]
f_{T4}/Λ^4	p_T^{jj}	[-3.0, 3.0]	[-2.2, 2.2]
f_{T5}/Λ^4	p_T^{jj}	[-1.7, 1.7]	[-1.2, 1.3]
f_{T6}/Λ^4	p_T^{jj}	[-1.5, 1.5]	[-1.0, 1.1]
f_{T7}/Λ^4	p_T^{jj}	[-3.8, 3.9]	[-2.7, 2.8]
f_{M0}/Λ^4	p_T^l	[-28, 28]	[-24, 24]
f_{M1}/Λ^4	p_T^l	[-43, 44]	[-37, 38]
f_{M2}/Λ^4	p_T^l	[-10, 10]	[-8.6, 8.5]
f_{M3}/Λ^4	p_T^l	[-16, 16]	[-13, 14]
f_{M4}/Λ^4	p_T^l	[-18, 18]	[-15, 15]
f_{M5}/Λ^4	p_T^l	[-17, 14]	[-14, 12]
f_{M7}/Λ^4	p_T^l	[-78, 77]	[-66, 65]

Table 6: Expected and observed 95% CL limits for specified $M_{W\gamma}$ cut-off values, where the expected limit for some operators intersects with the unitarity bounds derived from partial wave unitarity constraints. Entries with an $M_{W\gamma}$ cut-off scale of “-” indicate that the contribution from the operators do not cross the unitarity bound over the range of the clipping scan. The fit to either the p_T^{jj} or p_T^l distribution is used to extract the limits.

Coefficients [TeV ⁻⁴]	Observable	$M_{W\gamma}$ cut-off [TeV]	Expected [TeV ⁻⁴]	Observed [TeV ⁻⁴]
f_{T0}/Λ^4	p_T^{jj}	-	[-2.4,2.4]	[-1.7,1.8]
f_{T1}/Λ^4	p_T^{jj}	-	[-1.5,1.6]	[-1.1,1.2]
f_{T2}/Λ^4	p_T^{jj}	-	[-4.4,4.7]	[-3.1,3.5]
f_{T3}/Λ^4	p_T^{jj}	-	[-3.3,3.5]	[-2.4,2.6]
f_{T4}/Λ^4	p_T^{jj}	-	[-3.0,3.0]	[-2.2,2.2]
f_{T5}/Λ^4	p_T^{jj}	1.1	[-9.9,9.9]	[-7.5,7.5]
f_{T6}/Λ^4	p_T^{jj}	1.3	[-7.4,7.6]	[-5.2,5.4]
f_{T7}/Λ^4	p_T^{jj}	-	[-3.8,3.9]	[-2.7,2.8]
f_{M0}/Λ^4	p_T^l	-	[-38,37]	[-38,37]
f_{M1}/Λ^4	p_T^l	-	[-57,58]	[-41,42]
f_{M2}/Λ^4	p_T^l	0.8	[-110,110]	[-88,82]
f_{M3}/Λ^4	p_T^l	1.1	[-100,110]	[-73,77]
f_{M4}/Λ^4	p_T^l	1.0	[-118,111]	[-89,83]
f_{M5}/Λ^4	p_T^l	1.3	[-57,80]	[-32,77]
f_{M7}/Λ^4	p_T^l	-	[-96,95]	[-69,68]

11 Conclusion

An observation of the electroweak production of $W\gamma jj$ and measurements of its fiducial and differential cross-section are reported, using pp collision data collected with the ATLAS detector at a centre-of-mass energy of $\sqrt{s} = 13$ TeV that correspond to an integrated luminosity of 140 fb^{-1} . This process provides a unique probe of the quartic gauge coupling via the vector boson scattering production mechanism, and measurements of EW $W\gamma jj$ production are therefore sensitive to the $WW\gamma Z$ and $WW\gamma\gamma$ quartic gauge boson couplings.

Advanced machine learning techniques are used to establish the observation of the EW $W\gamma jj$ process with a significance of well above six standard deviations. The measured fiducial cross-section for the EW $W\gamma jj$ process is determined to be $13.2 \pm 2.5 \text{ fb}$, consistent with LO predictions from MADGRAPH5+PYTHIA8, whereas SHERPA underestimates the measured cross-section. Differential cross-sections are measured as functions of six kinematic observables in a stricter fiducial phase space. These observables are either sensitive to the quartic gauge couplings or the CP violation structure of $WW\gamma Z$ and $WW\gamma\gamma$ couplings. The data are corrected for detector effects of inefficiency and resolution using an iterative Bayesian unfolding method and are compared with theoretical predictions from MADGRAPH5+PYTHIA8 and SHERPA 2.2.12. These unfolded distributions are described by LO predictions within uncertainties, in which MADGRAPH5+PYTHIA8 tends to overshoot the measurement at high m_{jj} and p_T^{jj} while SHERPA 2.2.12 shows reasonable agreement but tends to underestimate the data across the six observables. The shape of these distributions are described reasonably well by both predictions. These differential measurements are used to search for anomalous quartic boson interactions using dimension-8 operators in the context of an effective field theory. The transverse momentum of the dijet system is found to be the most sensitive

observable to the tensor-type operators while the charged lepton transverse momentum is found to be the most sensitive observable to the mixed scalar operators. The first LHC constraints on f_{T3} and f_{T4} are presented.

Acknowledgements

We thank CERN for the very successful operation of the LHC and its injectors, as well as the support staff at CERN and at our institutions worldwide without whom ATLAS could not be operated efficiently.

The crucial computing support from all WLCG partners is acknowledged gratefully, in particular from CERN, the ATLAS Tier-1 facilities at TRIUMF/SFU (Canada), NDGF (Denmark, Norway, Sweden), CC-IN2P3 (France), KIT/GridKA (Germany), INFN-CNAF (Italy), NL-T1 (Netherlands), PIC (Spain), RAL (UK) and BNL (USA), the Tier-2 facilities worldwide and large non-WLCG resource providers. Major contributors of computing resources are listed in Ref. [63].

We gratefully acknowledge the support of ANPCyT, Argentina; YerPhI, Armenia; ARC, Australia; BMWFW and FWF, Austria; ANAS, Azerbaijan; CNPq and FAPESP, Brazil; NSERC, NRC and CFI, Canada; CERN; ANID, Chile; CAS, MOST and NSFC, China; Minciencias, Colombia; MEYS CR, Czech Republic; D NRF and DNSRC, Denmark; IN2P3-CNRS and CEA-DRF/IRFU, France; SRNSFG, Georgia; BMBF, HGF and MPG, Germany; GSRI, Greece; RGC and Hong Kong SAR, China; ISF and Benozio Center, Israel; INFN, Italy; MEXT and JSPS, Japan; CNRST, Morocco; NWO, Netherlands; RCN, Norway; MNiSW, Poland; FCT, Portugal; MNE/IFA, Romania; MESTD, Serbia; MSSR, Slovakia; ARRS and MIZŠ, Slovenia; DSI/NRF, South Africa; MICINN, Spain; SRC and Wallenberg Foundation, Sweden; SERI, SNSF and Cantons of Bern and Geneva, Switzerland; NSTC, Taipei; TENMAK, Türkiye; STFC, United Kingdom; DOE and NSF, United States of America.

Individual groups and members have received support from BCKDF, CANARIE, CRC and DRAC, Canada; CERN-CZ, PRIMUS 21/SCI/017 and UNCE SCI/013, Czech Republic; COST, ERC, ERDF, Horizon 2020, ICSC-NextGenerationEU and Marie Skłodowska-Curie Actions, European Union; Investissements d’Avenir Labex, Investissements d’Avenir Idex and ANR, France; DFG and AvH Foundation, Germany; Herakleitos, Thales and Aristeia programmes co-financed by EU-ESF and the Greek NSRF, Greece; BSF-NSF and MINERVA, Israel; Norwegian Financial Mechanism 2014-2021, Norway; NCN and NAWA, Poland; La Caixa Banking Foundation, CERCA Programme Generalitat de Catalunya and PROMETEO and GenT Programmes Generalitat Valenciana, Spain; Göran Gustafssons Stiftelse, Sweden; The Royal Society and Leverhulme Trust, United Kingdom.

In addition, individual members wish to acknowledge support from CERN: European Organization for Nuclear Research (CERN PJAS); Chile: Agencia Nacional de Investigación y Desarrollo (FONDECYT 1190886, FONDECYT 1210400, FONDECYT 1230812, FONDECYT 1230987); China: Chinese Ministry of Science and Technology (MOST-2023YFA1605700), National Natural Science Foundation of China (NSFC - 12175119, NSFC 12275265, NSFC-12075060); Czech Republic: PRIMUS Research Programme (PRIMUS/21/SCI/017); EU: H2020 European Research Council (ERC - 101002463); European Union: European Research Council (ERC - 948254, ERC 101089007), Horizon 2020 Framework Programme (MUCCA - CHIST-ERA-19-XAI-00), European Union, Future Artificial Intelligence Research (FAIR-NextGenerationEU PE00000013), Italian Center for High Performance Computing, Big Data and Quantum Computing (ICSC, NextGenerationEU); France: Agence Nationale de la Recherche (ANR-20-CE31-0013, ANR-21-CE31-0013, ANR-21-CE31-0022, ANR-22-EDIR-0002), Investissements

d'Avenir Labex (ANR-11-LABX-0012); Germany: Baden-Württemberg Stiftung (BW Stiftung-Postdoc Eliteprogramme), Deutsche Forschungsgemeinschaft (DFG - 469666862, DFG - CR 312/5-2); Italy: Istituto Nazionale di Fisica Nucleare (ICSC, NextGenerationEU), Ministero dell'Università e della Ricerca (PRIN - 20223N7F8K - PNRR M4.C2.1.1); Japan: Japan Society for the Promotion of Science (JSPS KAKENHI JP21H05085, JSPS KAKENHI JP22H01227, JSPS KAKENHI JP22H04944, JSPS KAKENHI JP22KK0227); Netherlands: Netherlands Organisation for Scientific Research (NWO Veni 2020 - VI.Veni.202.179); Norway: Research Council of Norway (RCN-314472); Poland: Polish National Agency for Academic Exchange (PPN/PPO/2020/1/00002/U/00001), Polish National Science Centre (NCN 2021/42/E/ST2/00350, NCN OPUS nr 2022/47/B/ST2/03059, NCN UMO-2019/34/E/ST2/00393, UMO-2020/37/B/ST2/01043, UMO-2021/40/C/ST2/00187, UMO-2022/47/O/ST2/00148); Slovenia: Slovenian Research Agency (ARIS grant J1-3010); Spain: BBVA Foundation (LEO22-1-603), Generalitat Valenciana (Artemisa, FEDER, IDIFEDER/2018/048), Ministry of Science and Innovation (MCIN & NextGenEU PCI2022-135018-2, MICIN & FEDER PID2021-125273NB, RYC2019-028510-I, RYC2020-030254-I, RYC2021-031273-I, RYC2022-038164-I), PROMETEO and GenT Programmes Generalitat Valenciana (CIDEAGENT/2019/023, CIDEAGENT/2019/027); Sweden: Swedish Research Council (VR 2018-00482, VR 2022-03845, VR 2022-04683, VR grant 2021-03651), Knut and Alice Wallenberg Foundation (KAW 2017.0100, KAW 2018.0157, KAW 2018.0458, KAW 2019.0447, KAW 2022.0358); Switzerland: Swiss National Science Foundation (SNSF - PCEFP2_194658); United Kingdom: Leverhulme Trust (Leverhulme Trust RPG-2020-004), Royal Society (NIF-R1-231091); United States of America: U.S. Department of Energy (ECA DE-AC02-76SF00515), Neubauer Family Foundation.

References

- [1] O. J. P. Éboli, M. C. Gonzalez-Garcia and S. M. Lietti, *Bosonic quartic couplings at CERN LHC*, *Phys. Rev. D* **69** (2004) 095005, arXiv: [hep-ph/0310141](#).
- [2] O. J. P. Éboli and M. C. Gonzalez-Garcia, *Classifying the bosonic quartic couplings*, *Phys. Rev. D* **93** (2016) 093013, arXiv: [1604.03555 \[hep-ph\]](#).
- [3] E. Accomando, A. Ballestrero, A. Belhouari and E. Maina, *Isolating vector boson scattering at the CERN LHC: Gauge cancellations and the equivalent vector boson approximation versus complete calculations*, *Phys. Rev. D* **74** (2006) 073010, arXiv: [hep-ph/0608019](#).
- [4] CMS Collaboration, *Observation of electroweak production of $W\gamma$ with two jets in proton–proton collisions at $\sqrt{s} = 13$ TeV*, *Phys. Lett. B* **811** (2020) 135988, arXiv: [2008.10521 \[hep-ex\]](#).
- [5] CMS Collaboration, *Measurement of the electroweak production of $W\gamma$ in association with two jets in proton–proton collisions at $\sqrt{s} = 13$ TeV*, *Phys. Rev. D* **108** (2023) 032017, arXiv: [2212.12592 \[hep-ex\]](#).
- [6] T. Plehn, D. Rainwater and D. Zeppenfeld, *Determining the Structure of Higgs Couplings at the LHC*, *Phys. Rev. Lett.* **88** (2002), arXiv: [hep-ph/0105325](#).
- [7] G. Klamke and D. Zeppenfeld, *Higgs plus two jet production via gluon fusion as a signal at the CERN LHC*, *JHEP* **0704** (2007), arXiv: [hep-ph/0703202](#).
- [8] ATLAS Collaboration, *The ATLAS Experiment at the CERN Large Hadron Collider*, *JINST* **3** (2008) S08003.
- [9] ATLAS Collaboration, *ATLAS Insertable B-Layer: Technical Design Report*, ATLAS-TDR-19; CERN-LHCC-2010-013, 2010, URL: <https://cds.cern.ch/record/1291633>, Addendum: ATLAS-TDR-19-ADD-1; CERN-LHCC-2012-009, 2012, URL: <https://cds.cern.ch/record/1451888>.
- [10] B. Abbott et al., *Production and integration of the ATLAS Insertable B-Layer*, *JINST* **13** (2018) T05008, arXiv: [1803.00844 \[physics.ins-det\]](#).
- [11] G. Avoni, *The new LUCID-2 detector for luminosity measurement and monitoring in ATLAS*, *JINST* **13** (2018) P07017.
- [12] ATLAS Collaboration, *Performance of the ATLAS trigger system in 2015*, *Eur. Phys. J. C* **77** (2017) 317, arXiv: [1611.09661 \[hep-ex\]](#).
- [13] ATLAS Collaboration, *The ATLAS Collaboration Software and Firmware*, ATL-SOFT-PUB-2021-001, 2021, URL: <https://cds.cern.ch/record/2767187>.
- [14] E. Bothmann et al., *Event generation with Sherpa 2.2*, *SciPost Phys.* **7** (2019) 034, arXiv: [1905.09127 \[hep-ph\]](#).
- [15] T. Gleisberg and S. Höche, *Comix, a new matrix element generator*, *JHEP* **12** (2008) 039, arXiv: [0808.3674 \[hep-ph\]](#).
- [16] S. Schumann and F. Krauss, *A parton shower algorithm based on Catani–Seymour dipole factorisation*, *JHEP* **03** (2008) 038, arXiv: [0709.1027 \[hep-ph\]](#).

- [17] S. Höche, F. Krauss, M. Schönherr and F. Siegert, *A critical appraisal of NLO+PS matching methods*, *JHEP* **09** (2012) 049, arXiv: [1111.1220 \[hep-ph\]](#).
- [18] S. Höche, F. Krauss, M. Schönherr and F. Siegert, *QCD matrix elements + parton showers. The NLO case*, *JHEP* **04** (2013) 027, arXiv: [1207.5030 \[hep-ph\]](#).
- [19] S. Catani, F. Krauss, B. R. Webber and R. Kuhn, *QCD Matrix Elements + Parton Showers*, *JHEP* **11** (2001) 063, arXiv: [hep-ph/0109231](#).
- [20] S. Höche, F. Krauss, S. Schumann and F. Siegert, *QCD matrix elements and truncated showers*, *JHEP* **05** (2009) 053, arXiv: [0903.1219 \[hep-ph\]](#).
- [21] NNPDF Collaboration, R. D. Ball et al., *Parton distributions for the LHC run II*, *JHEP* **04** (2015) 040, arXiv: [1410.8849 \[hep-ph\]](#).
- [22] J. Alwall et al., *The automated computation of tree-level and next-to-leading order differential cross sections, and their matching to parton shower simulations*, *JHEP* **07** (2014) 079, arXiv: [1405.0301 \[hep-ph\]](#).
- [23] ATLAS Collaboration, *ATLAS Pythia 8 tunes to 7 TeV data*, ATL-PHYS-PUB-2014-021, 2014, URL: <https://cds.cern.ch/record/1966419>.
- [24] D. J. Lange, *The EvtGen particle decay simulation package*, *Nucl. Instrum. Meth. A* **462** (2001) 152.
- [25] S. Agostinelli et al., *GEANT4 – a simulation toolkit*, *Nucl. Instrum. Meth. A* **506** (2003) 250.
- [26] T. Sjöstrand, S. Mrenna and P. Skands, *A brief introduction to PYTHIA 8.1*, *Comput. Phys. Commun.* **178** (2008) 852, arXiv: [0710.3820 \[hep-ph\]](#).
- [27] NNPDF Collaboration, R. D. Ball et al., *Parton distributions with LHC data*, *Nucl. Phys. B* **867** (2013) 244, arXiv: [1207.1303 \[hep-ph\]](#).
- [28] ATLAS Collaboration, *The Pythia 8 A3 tune description of ATLAS minimum bias and inelastic measurements incorporating the Donnachie–Landshoff diffractive model*, ATL-PHYS-PUB-2016-017, 2016, URL: <https://cds.cern.ch/record/2206965>.
- [29] ATLAS Collaboration, *Luminosity determination in pp collisions at $\sqrt{s} = 13$ TeV using the ATLAS detector at the LHC*, *Eur. Phys. J. C* **83** (2023), arXiv: [2212.09379 \[hep-ex\]](#).
- [30] ATLAS Collaboration, *Performance of the ATLAS muon triggers in Run 2*, *JINST* **15** (2020) P09015, arXiv: [2004.13447 \[physics.ins-det\]](#).
- [31] ATLAS Collaboration, *Performance of electron and photon triggers in ATLAS during LHC Run 2*, *Eur. Phys. J. C* **80** (2020) 47, arXiv: [1909.00761 \[hep-ex\]](#).
- [32] ATLAS Collaboration, *ATLAS data quality operations and performance for 2015–2018 data-taking*, *JINST* **15** (2020) P04003, arXiv: [1911.04632 \[physics.ins-det\]](#).
- [33] ATLAS Collaboration, *Vertex Reconstruction Performance of the ATLAS Detector at $\sqrt{s} = 13$ TeV*, ATL-PHYS-PUB-2015-026, 2015, URL: <https://cds.cern.ch/record/2037717>.
- [34] ATLAS Collaboration, *Muon reconstruction and identification efficiency in ATLAS using the full Run 2 pp collision data set at $\sqrt{s} = 13$ TeV*, *Eur. Phys. J. C* **81** (2021) 578, arXiv: [2012.00578 \[hep-ex\]](#).

- [35] ATLAS Collaboration, *Electron and photon performance measurements with the ATLAS detector using the 2015–2017 LHC proton–proton collision data*, *JINST* **14** (2019) P12006, arXiv: [1908.00005 \[hep-ex\]](#).
- [36] ATLAS Collaboration, *Jet reconstruction and performance using particle flow with the ATLAS Detector*, *Eur. Phys. J. C* **77** (2017) 466, arXiv: [1703.10485 \[hep-ex\]](#).
- [37] M. Cacciari, G. P. Salam and G. Soyez, *The anti- k_t jet clustering algorithm*, *JHEP* **04** (2008) 063, arXiv: [0802.1189 \[hep-ph\]](#).
- [38] ATLAS Collaboration, *Performance of pile-up mitigation techniques for jets in pp collisions at $\sqrt{s} = 8$ TeV using the ATLAS detector*, *Eur. Phys. J. C* **76** (2016) 581, arXiv: [1510.03823 \[hep-ex\]](#).
- [39] ATLAS Collaboration, *Selection of jets produced in 13 TeV proton–proton collisions with the ATLAS detector*, ATLAS-CONF-2015-029, 2015, URL: <https://cds.cern.ch/record/2037702>.
- [40] ATLAS Collaboration, *Optimisation and performance studies of the ATLAS b-tagging algorithms for the 2017-18 LHC run*, ATL-PHYS-PUB-2017-013, 2017, URL: <https://cds.cern.ch/record/2273281>.
- [41] ATLAS Collaboration, *Performance of missing transverse momentum reconstruction with the ATLAS detector using proton–proton collisions at $\sqrt{s} = 13$ TeV*, *Eur. Phys. J. C* **78** (2018) 903, arXiv: [1802.08168 \[hep-ex\]](#).
- [42] ATLAS Collaboration, *Measurement of the inclusive isolated prompt photon cross section in pp collisions at $\sqrt{s} = 7$ TeV with the ATLAS detector*, *Phys. Rev. D* **83** (2011) 052005, arXiv: [1012.4389 \[hep-ex\]](#).
- [43] Gaiser, J., *Charmonium spectroscopy from radiative decays of J/Ψ and Ψ'* , SLAC-R-255 (1982).
- [44] S., Bernstein, *Proof of theorem of Weierstrass based on the calculus of probabilities*, *Comm. Kharkov Math. Soc.* **13** (1912) 1.
- [45] ATLAS Collaboration, *Measurement of the $Z(\rightarrow \ell^+\ell^-)\gamma$ production cross-section in pp collisions at $\sqrt{s} = 13$ TeV with the ATLAS detector*, *JHEP* **03** (2020) 054, arXiv: [1911.04813 \[hep-ex\]](#).
- [46] A. L. Maas, ‘Rectifier Nonlinearities Improve Neural Network Acoustic Models’, *Proceedings of the 30th International Conference on Machine Learning*, vol. 28, 3, 2013.
- [47] D. P. Kingma and J. Ba, *Adam: A Method for Stochastic Optimization*, (2014), arXiv: [1412.6980 \[hep-ex\]](#).
- [48] ATLAS Collaboration, *Differential cross-section measurements for the electroweak production of dijets in association with a Z boson in proton–proton collisions at ATLAS*, *Eur. Phys. J. C* **81** (2021) 163, arXiv: [2006.15458 \[hep-ex\]](#).
- [49] R. Barlow, *Extended maximum likelihood*, *Nucl. Instrum. Meth. A* **297** (1990) 496.
- [50] M. Tanabashi and others (Particle Data Group), *Review of Particle Physics*, *Phys. Rev. D* **98** (2018) 030001.
- [51] ATLAS Collaboration, *Evaluating statistical uncertainties and correlations using the bootstrap method*, ATL-PHYS-PUB-2021-011, 2021, URL: <https://cds.cern.ch/record/2759945>.

- [52] G. D’Agostini, *A multidimensional unfolding method based on Bayes’ theorem*, [Nucl. Instrum. Meth. A **362** \(1995\) 487](#), ISSN: 0168-9002.
- [53] T. Adye, ‘Unfolding algorithms and tests using RooUnfold’, *Proceedings, 2011 Workshop on Statistical Issues Related to Discovery Claims in Search Experiments and Unfolding (PHYSTAT 2011)* (CERN, Geneva, Switzerland, 17th–20th Jan. 2011) 313, arXiv: [1105.1160 \[physics.data-an\]](#).
- [54] G. Cowan, K. Cranmer, E. Gross and O. Vitells, *Asymptotic formulae for likelihood-based tests of new physics*, [Eur. Phys. J. C **71** \(2011\) 1554](#), arXiv: [1007.1727 \[physics.data-an\]](#), Erratum: [Eur. Phys. J. C **73** \(2013\) 2501](#).
- [55] ATLAS Collaboration, *Jet energy scale and resolution measured in proton–proton collisions at $\sqrt{s} = 13$ TeV with the ATLAS detector*, [Eur. Phys. J. C **81** \(2021\) 689](#), arXiv: [2007.02645 \[hep-ex\]](#).
- [56] NNPDF Collaboration, *Parton distributions from high-precision collider data*, [Eur. Phys. J. C **77** \(2017\)](#), arXiv: [1706.00428 \[hep-ex\]](#).
- [57] T.-J. Hou et al., *Progress in the CTEQ-TEA NNLO global QCD analysis*, (2019), arXiv: [1908.11394 \[hep-ph\]](#).
- [58] S. Bailey, T. Cridge, L. A. Harland-Lang, A. D. Martin and R. Thorne, *Parton distributions from LHC, HERA, Tevatron and fixed target data: MSHT20 PDFs*, [Eur. Phys. J. C **81** \(2021\)](#), arXiv: [2012.04684](#).
- [59] J. Butterworth et al., *PDF4LHC recommendations for LHC Run II*, [J. Phys. G **43** \(2016\) 023001](#), arXiv: [1510.03865 \[hep-ph\]](#).
- [60] A. Ballestrero et al., *Precise predictions for same-sign W-boson scattering at the LHC*, [Eur. Phys. J. C **78** \(2018\)](#), arXiv: [1803.07943](#).
- [61] S. S. Wilks, *The Large-Sample Distribution of the Likelihood Ratio for Testing Composite Hypotheses*, [Ann. Math. Statist. **9** \(1938\) 60](#).
- [62] E. d. S. Almeida, O. J. P. Éboli and M. C. Gonzalez-Garcia, *Unitarity constraints on anomalous quartic couplings*, [Phys. Rev. D **101** \(2020\) 113003](#), arXiv: [2004.05174 \[hep-ph\]](#).
- [63] ATLAS Collaboration, *ATLAS Computing Acknowledgements*, ATL-SOFT-PUB-2023-001, 2023, URL: <https://cds.cern.ch/record/2869272>.

The ATLAS Collaboration

G. Aad ¹⁰³, E. Aakvaag ¹⁶, B. Abbott ¹²¹, K. Abeling ⁵⁵, N.J. Abicht ⁴⁹, S.H. Abidi ²⁹, M. Aboeela ⁴⁴, A. Aboulhorma ^{35e}, H. Abramowicz ¹⁵², H. Abreu ¹⁵¹, Y. Abulaiti ¹¹⁸, B.S. Acharya ^{69a,69b,1}, A. Ackermann ^{63a}, C. Adam Bourdarios ⁴, L. Adamczyk ^{86a}, S.V. Addepalli ²⁶, M.J. Addison ¹⁰², J. Adelman ¹¹⁶, A. Adiguzel ^{21c}, T. Adaye ¹³⁵, A.A. Affolder ¹³⁷, Y. Afik ³⁹, M.N. Agaras ¹³, J. Agarwala ^{73a,73b}, A. Aggarwal ¹⁰¹, C. Agheorghiesei ^{27c}, A. Ahmad ³⁶, F. Ahmadov ^{38,y}, W.S. Ahmed ¹⁰⁵, S. Ahuja ⁹⁶, X. Ai ^{62e}, G. Aielli ^{76a,76b}, A. Aikot ¹⁶⁴, M. Ait Tamlihat ^{35e}, B. Aitbenchikh ^{35a}, I. Aizenberg ¹⁷⁰, M. Akbiyik ¹⁰¹, T.P.A. Åkesson ⁹⁹, A.V. Akimov ³⁷, D. Akiyama ¹⁶⁹, N.N. Akolkar ²⁴, S. Aktas ^{21a}, K. Al Houry ⁴¹, G.L. Alberghi ^{23b}, J. Albert ¹⁶⁶, P. Albicocco ⁵³, G.L. Albouy ⁶⁰, S. Alderweireldt ⁵², Z.L. Alegria ¹²², M. Aleksa ³⁶, I.N. Aleksandrov ³⁸, C. Alexa ^{27b}, T. Alexopoulos ¹⁰, F. Alfonsi ^{23b}, M. Algren ⁵⁶, M. Alhroob ¹⁴², B. Ali ¹³³, H.M.J. Ali ⁹², S. Ali ¹⁴⁹, S.W. Alibocus ⁹³, M. Aliev ^{33c}, G. Alimonti ^{71a}, W. Alkakhri ⁵⁵, C. Allaire ⁶⁶, B.M.M. Allbrooke ¹⁴⁷, J.F. Allen ⁵², C.A. Allendes Flores ^{138f}, P.P. Allport ²⁰, A. Aloisio ^{72a,72b}, F. Alonso ⁹¹, C. Alpigiani ¹³⁹, M. Alvarez Estevez ¹⁰⁰, A. Alvarez Fernandez ¹⁰¹, M. Alves Cardoso ⁵⁶, M.G. Alviggi ^{72a,72b}, M. Aly ¹⁰², Y. Amaral Coutinho ^{83b}, A. Ambler ¹⁰⁵, C. Amelung ³⁶, M. Amerl ¹⁰², C.G. Ames ¹¹⁰, D. Amidei ¹⁰⁷, K.J. Amirie ¹⁵⁶, S.P. Amor Dos Santos ^{131a}, K.R. Amos ¹⁶⁴, S. An ⁸⁴, V. Ananiev ¹²⁶, C. Anastopoulos ¹⁴⁰, T. Andeen ¹¹, J.K. Anders ³⁶, S.Y. Andrean ^{47a,47b}, A. Andreazza ^{71a,71b}, S. Angelidakis ⁹, A. Angerami ^{41,aa}, A.V. Anisenkov ³⁷, A. Annovi ^{74a}, C. Antel ⁵⁶, M.T. Anthony ¹⁴⁰, E. Antipov ¹⁴⁶, M. Antonelli ⁵³, F. Anulli ^{75a}, M. Aoki ⁸⁴, T. Aoki ¹⁵⁴, J.A. Aparisi Pozo ¹⁶⁴, M.A. Aparo ¹⁴⁷, L. Aperio Bella ⁴⁸, C. Appelt ¹⁸, A. Apyan ²⁶, S.J. Arbiol Val ⁸⁷, C. Arcangeletti ⁵³, A.T.H. Arce ⁵¹, E. Arena ⁹³, J-F. Arguin ¹⁰⁹, S. Argyropoulos ⁵⁴, J.-H. Arling ⁴⁸, O. Arnaez ⁴, H. Arnold ¹¹⁵, G. Artoni ^{75a,75b}, H. Asada ¹¹², K. Asai ¹¹⁹, S. Asai ¹⁵⁴, N.A. Asbah ³⁶, K. Assamagan ²⁹, R. Astalos ^{28a}, K.S.V. Astrand ⁹⁹, S. Atashi ¹⁶⁰, R.J. Atkin ^{33a}, M. Atkinson ¹⁶³, H. Atmani ^{35f}, P.A. Atlasiddha ¹²⁹, K. Augsten ¹³³, S. Auricchio ^{72a,72b}, A.D. Auriol ²⁰, V.A. Austrup ¹⁰², G. Avolio ³⁶, K. Axiotis ⁵⁶, G. Azuelos ^{109,ae}, D. Babal ^{28b}, H. Bachacou ¹³⁶, K. Bachas ^{153,p}, A. Bachiu ³⁴, F. Backman ^{47a,47b}, A. Badea ³⁹, T.M. Baer ¹⁰⁷, P. Bagnaia ^{75a,75b}, M. Bahmani ¹⁸, D. Bahner ⁵⁴, K. Bai ¹²⁴, J.T. Baines ¹³⁵, L. Baines ⁹⁵, O.K. Baker ¹⁷³, E. Bakos ¹⁵, D. Bakshi Gupta ⁸, V. Balakrishnan ¹²¹, R. Balasubramanian ¹¹⁵, E.M. Baldin ³⁷, P. Balek ^{86a}, E. Ballabene ^{23b,23a}, F. Balli ¹³⁶, L.M. Baltos ^{63a}, W.K. Balunas ³², J. Balz ¹⁰¹, E. Banas ⁸⁷, M. Bandieramonte ¹³⁰, A. Bandyopadhyay ²⁴, S. Bansal ²⁴, L. Barak ¹⁵², M. Barakat ⁴⁸, E.L. Barberio ¹⁰⁶, D. Barberis ^{57b,57a}, M. Barbero ¹⁰³, M.Z. Barel ¹¹⁵, K.N. Barends ^{33a}, T. Barillari ¹¹¹, M-S. Barisits ³⁶, T. Barklow ¹⁴⁴, P. Baron ¹²³, D.A. Baron Moreno ¹⁰², A. Baroncelli ^{62a}, G. Barone ²⁹, A.J. Barr ¹²⁷, J.D. Barr ⁹⁷, F. Barreiro ¹⁰⁰, J. Barreiro Guimarães da Costa ^{14a}, U. Barron ¹⁵², M.G. Barros Teixeira ^{131a}, S. Barsov ³⁷, F. Bartels ^{63a}, R. Bartoldus ¹⁴⁴, A.E. Barton ⁹², P. Bartos ^{28a}, A. Basan ¹⁰¹, M. Baselga ⁴⁹, A. Bassalat ^{66,b}, M.J. Basso ^{157a}, R. Bate ¹⁶⁵, R.L. Bates ⁵⁹, S. Batlamous ¹⁰⁰, B. Batool ¹⁴², M. Battaglia ¹³⁷, D. Battulga ¹⁸, M. Baucé ^{75a,75b}, M. Bauer ³⁶, P. Bauer ²⁴, L.T. Bazzano Hurrell ³⁰, J.B. Beacham ⁵¹, T. Beau ¹²⁸, J.Y. Beaucamp ⁹¹, P.H. Beauchemin ¹⁵⁹, P. Bechtel ²⁴, H.P. Beck ^{19,o}, K. Becker ¹⁶⁸, A.J. Beddall ⁸², V.A. Bednyakov ³⁸, C.P. Bee ¹⁴⁶, L.J. Beemster ¹⁵, T.A. Beermann ³⁶, M. Begalli ^{83d}, M. Begel ²⁹, A. Behera ¹⁴⁶, J.K. Behr ⁴⁸, J.F. Beirer ³⁶, F. Beisiegel ²⁴, M. Belfkir ^{117b}, G. Bella ¹⁵², L. Bellagamba ^{23b}, A. Bellerive ³⁴, P. Bellos ²⁰, K. Beloborodov ³⁷, D. Bencheikroun ^{35a}, F. Bendebba ^{35a}, Y. Benhammou ¹⁵²,

K.C. Benkendorfer [ID⁶¹](#), L. Beresford [ID⁴⁸](#), M. Beretta [ID⁵³](#), E. Bergeaas Kuutmann [ID¹⁶²](#), N. Berger [ID⁴](#),
 B. Bergmann [ID¹³³](#), J. Beringer [ID^{17a}](#), G. Bernardi [ID⁵](#), C. Bernius [ID¹⁴⁴](#), F.U. Bernlochner [ID²⁴](#),
 F. Bernon [ID^{36,103}](#), A. Berrocal Guardia [ID¹³](#), T. Berry [ID⁹⁶](#), P. Berta [ID¹³⁴](#), A. Berthold [ID⁵⁰](#), S. Bethke [ID¹¹¹](#),
 A. Betti [ID^{75a,75b}](#), A.J. Bevan [ID⁹⁵](#), N.K. Bhalla [ID⁵⁴](#), M. Bhamjee [ID^{33c}](#), S. Bhatta [ID¹⁴⁶](#),
 D.S. Bhattacharya [ID¹⁶⁷](#), P. Bhattarai [ID¹⁴⁴](#), K.D. Bhide [ID⁵⁴](#), V.S. Bhopatkar [ID¹²²](#), R.M. Bianchi [ID¹³⁰](#),
 G. Bianco [ID^{23b,23a}](#), O. Biebel [ID¹¹⁰](#), R. Bielski [ID¹²⁴](#), M. Biglietti [ID^{77a}](#), C.S. Billingsley [ID⁴⁴](#), M. Bindi [ID⁵⁵](#),
 A. Bingul [ID^{21b}](#), C. Bini [ID^{75a,75b}](#), A. Biondini [ID⁹³](#), C.J. Birch-sykes [ID¹⁰²](#), G.A. Bird [ID³²](#), M. Birman [ID¹⁷⁰](#),
 M. Biros [ID¹³⁴](#), S. Biryukov [ID¹⁴⁷](#), T. Bisanz [ID⁴⁹](#), E. Bisceglie [ID^{43b,43a}](#), J.P. Biswal [ID¹³⁵](#), D. Biswas [ID¹⁴²](#),
 I. Bloch [ID⁴⁸](#), A. Blue [ID⁵⁹](#), U. Blumenschein [ID⁹⁵](#), J. Blumenthal [ID¹⁰¹](#), V.S. Bobrovnikov [ID³⁷](#),
 M. Boehler [ID⁵⁴](#), B. Boehm [ID¹⁶⁷](#), D. Bogavac [ID³⁶](#), A.G. Bogdanchikov [ID³⁷](#), C. Bohm [ID^{47a}](#),
 V. Boisvert [ID⁹⁶](#), P. Bokan [ID³⁶](#), T. Bold [ID^{86a}](#), M. Bomben [ID⁵](#), M. Bona [ID⁹⁵](#), M. Boonekamp [ID¹³⁶](#),
 C.D. Booth [ID⁹⁶](#), A.G. Borbély [ID⁵⁹](#), I.S. Bordulev [ID³⁷](#), H.M. Borecka-Bielska [ID¹⁰⁹](#), G. Borissov [ID⁹²](#),
 D. Bortoletto [ID¹²⁷](#), D. Boscherini [ID^{23b}](#), M. Bosman [ID¹³](#), J.D. Bossio Sola [ID³⁶](#), K. Bouaouda [ID^{35a}](#),
 N. Bouchhar [ID¹⁶⁴](#), J. Boudreau [ID¹³⁰](#), E.V. Bouhova-Thacker [ID⁹²](#), D. Boumediene [ID⁴⁰](#),
 R. Bouquet [ID^{57b,57a}](#), A. Boveia [ID¹²⁰](#), J. Boyd [ID³⁶](#), D. Boye [ID²⁹](#), I.R. Boyko [ID³⁸](#), J. Bracinik [ID²⁰](#),
 N. Brahimí [ID⁴](#), G. Brandt [ID¹⁷²](#), O. Brandt [ID³²](#), F. Braren [ID⁴⁸](#), B. Brau [ID¹⁰⁴](#), J.E. Brau [ID¹²⁴](#),
 R. Brenner [ID¹⁷⁰](#), L. Brenner [ID¹¹⁵](#), R. Brenner [ID¹⁶²](#), S. Bressler [ID¹⁷⁰](#), D. Britton [ID⁵⁹](#), D. Britzger [ID¹¹¹](#),
 I. Brock [ID²⁴](#), G. Brooijmans [ID⁴¹](#), E. Brost [ID²⁹](#), L.M. Brown [ID¹⁶⁶](#), L.E. Bruce [ID⁶¹](#), T.L. Bruckler [ID¹²⁷](#),
 P.A. Bruckman de Renstrom [ID⁸⁷](#), B. Brüers [ID⁴⁸](#), A. Bruni [ID^{23b}](#), G. Bruni [ID^{23b}](#), M. Bruschi [ID^{23b}](#),
 N. Brusino [ID^{75a,75b}](#), T. Buanes [ID¹⁶](#), Q. Buat [ID¹³⁹](#), D. Buchin [ID¹¹¹](#), A.G. Buckley [ID⁵⁹](#), O. Bulekov [ID³⁷](#),
 B.A. Bullard [ID¹⁴⁴](#), S. Burdin [ID⁹³](#), C.D. Burgard [ID⁴⁹](#), A.M. Burger [ID³⁶](#), B. Burghgrave [ID⁸](#),
 O. Burlayenko [ID⁵⁴](#), J.T.P. Burr [ID³²](#), C.D. Burton [ID¹¹](#), J.C. Burzynski [ID¹⁴³](#), E.L. Busch [ID⁴¹](#),
 V. Büscher [ID¹⁰¹](#), P.J. Bussey [ID⁵⁹](#), J.M. Butler [ID²⁵](#), C.M. Buttar [ID⁵⁹](#), J.M. Butterworth [ID⁹⁷](#),
 W. Buttinger [ID¹³⁵](#), C.J. Buxo Vazquez [ID¹⁰⁸](#), A.R. Buzykaev [ID³⁷](#), S. Cabrera Urbán [ID¹⁶⁴](#),
 L. Cadamuro [ID⁶⁶](#), D. Caforio [ID⁵⁸](#), H. Cai [ID¹³⁰](#), Y. Cai [ID^{14a,14e}](#), Y. Cai [ID^{14c}](#), V.M.M. Cairo [ID³⁶](#),
 O. Cakir [ID^{3a}](#), N. Calace [ID³⁶](#), P. Calafiura [ID^{17a}](#), G. Calderini [ID¹²⁸](#), P. Calfayan [ID⁶⁸](#), G. Callea [ID⁵⁹](#),
 L.P. Caloba [ID^{83b}](#), D. Calvet [ID⁴⁰](#), S. Calvet [ID⁴⁰](#), M. Calvetti [ID^{74a,74b}](#), R. Camacho Toro [ID¹²⁸](#),
 S. Camarda [ID³⁶](#), D. Camarero Munoz [ID²⁶](#), P. Camarri [ID^{76a,76b}](#), M.T. Camerlingo [ID^{72a,72b}](#),
 D. Cameron [ID³⁶](#), C. Camincher [ID¹⁶⁶](#), M. Campanelli [ID⁹⁷](#), A. Camplani [ID⁴²](#), V. Canale [ID^{72a,72b}](#),
 A.C. Canbay [ID^{3a}](#), E. Canonero [ID⁹⁶](#), J. Cantero [ID¹⁶⁴](#), Y. Cao [ID¹⁶³](#), F. Capocasa [ID²⁶](#), M. Capua [ID^{43b,43a}](#),
 A. Carbone [ID^{71a,71b}](#), R. Cardarelli [ID^{76a}](#), J.C.J. Cardenas [ID⁸](#), F. Cardillo [ID¹⁶⁴](#), G. Carducci [ID^{43b,43a}](#),
 T. Carli [ID³⁶](#), G. Carlino [ID^{72a}](#), J.I. Carlotto [ID¹³](#), B.T. Carlson [ID^{130,q}](#), E.M. Carlson [ID^{166,157a}](#),
 J. Carmignani [ID⁹³](#), L. Carminati [ID^{71a,71b}](#), A. Carnelli [ID¹³⁶](#), M. Carnesale [ID^{75a,75b}](#), S. Caron [ID¹¹⁴](#),
 E. Carquin [ID^{138f}](#), S. Carrá [ID^{71a}](#), G. Carratta [ID^{23b,23a}](#), A.M. Carroll [ID¹²⁴](#), T.M. Carter [ID⁵²](#),
 M.P. Casado [ID^{13,i}](#), M. Caspar [ID⁴⁸](#), F.L. Castillo [ID⁴](#), L. Castillo Garcia [ID¹³](#), V. Castillo Gimenez [ID¹⁶⁴](#),
 N.F. Castro [ID^{131a,131e}](#), A. Catinaccio [ID³⁶](#), J.R. Catmore [ID¹²⁶](#), T. Cavaliere [ID⁴](#), V. Cavaliere [ID²⁹](#),
 N. Cavalli [ID^{23b,23a}](#), Y.C. Cekmecelioglu [ID⁴⁸](#), E. Celebi [ID^{21a}](#), S. Cella [ID³⁶](#), F. Celli [ID¹²⁷](#),
 M.S. Centonze [ID^{70a,70b}](#), V. Cepaitis [ID⁵⁶](#), K. Cerny [ID¹²³](#), A.S. Cerqueira [ID^{83a}](#), A. Cerri [ID¹⁴⁷](#),
 L. Cerrito [ID^{76a,76b}](#), F. Cerutti [ID^{17a}](#), B. Cervato [ID¹⁴²](#), A. Cervelli [ID^{23b}](#), G. Cesarini [ID⁵³](#), S.A. Cetin [ID⁸²](#),
 D. Chakraborty [ID¹¹⁶](#), J. Chan [ID^{17a}](#), W.Y. Chan [ID¹⁵⁴](#), J.D. Chapman [ID³²](#), E. Chapon [ID¹³⁶](#),
 B. Chargeishvili [ID^{150b}](#), D.G. Charlton [ID²⁰](#), M. Chatterjee [ID¹⁹](#), C. Chauhan [ID¹³⁴](#), Y. Che [ID^{14c}](#),
 S. Chekanov [ID⁶](#), S.V. Chekulaev [ID^{157a}](#), G.A. Chelkov [ID^{38,a}](#), A. Chen [ID¹⁰⁷](#), B. Chen [ID¹⁵²](#), B. Chen [ID¹⁶⁶](#),
 H. Chen [ID^{14c}](#), H. Chen [ID²⁹](#), J. Chen [ID^{62c}](#), J. Chen [ID¹⁴³](#), M. Chen [ID¹²⁷](#), S. Chen [ID¹⁵⁴](#), S.J. Chen [ID^{14c}](#),
 X. Chen [ID^{62c,136}](#), X. Chen [ID^{14b,ad}](#), Y. Chen [ID^{62a}](#), C.L. Cheng [ID¹⁷¹](#), H.C. Cheng [ID^{64a}](#), S. Cheong [ID¹⁴⁴](#),
 A. Cheplakov [ID³⁸](#), E. Cheremushkina [ID⁴⁸](#), E. Cherepanova [ID¹¹⁵](#), R. Cherkaoui El Moursli [ID^{35e}](#),
 E. Cheu [ID⁷](#), K. Cheung [ID⁶⁵](#), L. Chevalier [ID¹³⁶](#), V. Chiarella [ID⁵³](#), G. Chiarelli [ID^{74a}](#), N. Chiedde [ID¹⁰³](#),
 G. Chiodini [ID^{70a}](#), A.S. Chisholm [ID²⁰](#), A. Chitan [ID^{27b}](#), M. Chitishvili [ID¹⁶⁴](#), M.V. Chizhov [ID³⁸](#),

K. Choi ¹¹, Y. Chou ¹³⁹, E.Y.S. Chow ¹¹⁴, K.L. Chu ¹⁷⁰, M.C. Chu ^{64a}, X. Chu ^{14a,14e},
 J. Chudoba ¹³², J.J. Chwastowski ⁸⁷, D. Cieri ¹¹¹, K.M. Ciesla ^{86a}, V. Cindro ⁹⁴, A. Ciocio ^{17a},
 F. Cirotto ^{72a,72b}, Z.H. Citron ¹⁷⁰, M. Citterio ^{71a}, D.A. Ciubotaru ^{27b}, A. Clark ⁵⁶, P.J. Clark ⁵²,
 C. Clarry ¹⁵⁶, J.M. Clavijo Columbie ⁴⁸, S.E. Clawson ⁴⁸, C. Clement ^{47a,47b}, J. Clercx ⁴⁸,
 Y. Coadou ¹⁰³, M. Cobal ^{69a,69c}, A. Coccaro ^{57b}, R.F. Coelho Barrue ^{131a},
 R. Coelho Lopes De Sa ¹⁰⁴, S. Coelli ^{71a}, B. Cole ⁴¹, J. Collot ⁶⁰, P. Conde Muiño ^{131a,131g},
 M.P. Connell ^{33c}, S.H. Connell ^{33c}, E.I. Conroy ¹²⁷, F. Conventi ^{72a,af}, H.G. Cooke ²⁰,
 A.M. Cooper-Sarkar ¹²⁷, F.A. Corchia ^{23b,23a}, A. Cordeiro Oudot Choi ¹²⁸, L.D. Corpe ⁴⁰,
 M. Corradi ^{75a,75b}, F. Corriveau ^{105,w}, A. Cortes-Gonzalez ¹⁸, M.J. Costa ¹⁶⁴, F. Costanza ⁴,
 D. Costanzo ¹⁴⁰, B.M. Cote ¹²⁰, G. Cowan ⁹⁶, K. Cranmer ¹⁷¹, D. Cremonini ^{23b,23a},
 S. Crépe-Renaudin ⁶⁰, F. Crescioli ¹²⁸, M. Cristinziani ¹⁴², M. Cristoforetti ^{78a,78b}, V. Croft ¹¹⁵,
 J.E. Crosby ¹²², G. Crosetti ^{43b,43a}, A. Cueto ¹⁰⁰, H. Cui ^{14a,14e}, Z. Cui ⁷, W.R. Cunningham ⁵⁹,
 F. Curcio ¹⁶⁴, J.R. Curran ⁵², P. Czodrowski ³⁶, M.M. Czurylo ³⁶,
 M.J. Da Cunha Sargedas De Sousa ^{57b,57a}, J.V. Da Fonseca Pinto ^{83b}, C. Da Via ¹⁰²,
 W. Dabrowski ^{86a}, T. Dado ⁴⁹, S. Dahbi ¹⁴⁹, T. Dai ¹⁰⁷, D. Dal Santo ¹⁹, C. Dallapiccola ¹⁰⁴,
 M. Dam ⁴², G. D'amen ²⁹, V. D'Amico ¹¹⁰, J. Damp ¹⁰¹, J.R. Dandoy ³⁴, M. Danninger ¹⁴³,
 V. Dao ³⁶, G. Darbo ^{57b}, S.J. Das ^{29,ag}, F. Dattola ⁴⁸, S. D'Auria ^{71a,71b}, A. D'Avanzo ^{72a,72b},
 C. David ^{33a}, T. Davidek ¹³⁴, B. Davis-Purcell ³⁴, I. Dawson ⁹⁵, H.A. Day-hall ¹³³, K. De ⁸,
 R. De Asmundis ^{72a}, N. De Biase ⁴⁸, S. De Castro ^{23b,23a}, N. De Groot ¹¹⁴, P. de Jong ¹¹⁵,
 H. De la Torre ¹¹⁶, A. De Maria ^{14c}, A. De Salvo ^{75a}, U. De Sanctis ^{76a,76b}, F. De Santis ^{70a,70b},
 A. De Santo ¹⁴⁷, J.B. De Vivie De Regie ⁶⁰, D.V. Dedovich ³⁸, J. Degens ⁹³, A.M. Deiana ⁴⁴,
 F. Del Corso ^{23b,23a}, J. Del Peso ¹⁰⁰, F. Del Rio ^{63a}, L. Delagrangé ¹²⁸, F. Deliot ¹³⁶,
 C.M. Delitzsch ⁴⁹, M. Della Pietra ^{72a,72b}, D. Della Volpe ⁵⁶, A. Dell'Acqua ³⁶,
 L. Dell'Asta ^{71a,71b}, M. Delmastro ⁴, P.A. Delsart ⁶⁰, S. Demers ¹⁷³, M. Demichev ³⁸,
 S.P. Denisov ³⁷, L. D'Eramo ⁴⁰, D. Derendarz ⁸⁷, F. Derue ¹²⁸, P. Dervan ⁹³, K. Desch ²⁴,
 C. Deutsch ²⁴, F.A. Di Bello ^{57b,57a}, A. Di Ciaccio ^{76a,76b}, L. Di Ciaccio ⁴,
 A. Di Domenico ^{75a,75b}, C. Di Donato ^{72a,72b}, A. Di Girolamo ³⁶, G. Di Gregorio ³⁶,
 A. Di Luca ^{78a,78b}, B. Di Micco ^{77a,77b}, R. Di Nardo ^{77a,77b}, M. Diamantopoulou ³⁴, F.A. Dias ¹¹⁵,
 T. Dias Do Vale ¹⁴³, M.A. Diaz ^{138a,138b}, F.G. Diaz Capriles ²⁴, M. Didenko ¹⁶⁴, E.B. Diehl ¹⁰⁷,
 S. Díez Cornell ⁴⁸, C. Díez Pardos ¹⁴², C. Dimitriadi ^{162,24}, A. Dimitrievska ²⁰, J. Dingfelder ²⁴,
 I-M. Dinu ^{27b}, S.J. Dittmeier ^{63b}, F. Dittus ³⁶, M. Divisek ¹³⁴, F. Djama ¹⁰³, T. Djobava ^{150b},
 C. Doglioni ^{102,99}, A. Dohnalova ^{28a}, J. Dolejsi ¹³⁴, Z. Dolezal ¹³⁴, K.M. Dona ³⁹,
 M. Donadelli ^{83c}, B. Dong ¹⁰⁸, J. Donini ⁴⁰, A. D'Onofrio ^{72a,72b}, M. D'Onofrio ⁹³,
 J. Dopke ¹³⁵, A. Doria ^{72a}, N. Dos Santos Fernandes ^{131a}, P. Dougan ¹⁰², M.T. Dova ⁹¹,
 A.T. Doyle ⁵⁹, M.A. Dragnet ¹²⁷, E. Dreyer ¹⁷⁰, I. Drivas-koulouris ¹⁰, M. Drnevich ¹¹⁸,
 M. Drozdova ⁵⁶, D. Du ^{62a}, T.A. du Pree ¹¹⁵, F. Dubinin ³⁷, M. Dubovsky ^{28a}, E. Duchovni ¹⁷⁰,
 G. Duckeck ¹¹⁰, O.A. Ducu ^{27b}, D. Duda ⁵², A. Dudarev ³⁶, E.R. Duden ²⁶, M. D'uffizi ¹⁰²,
 L. Duflost ⁶⁶, M. Dührssen ³⁶, I. Duminica ^{27g}, A.E. Dumitriu ^{27b}, M. Dunford ^{63a}, S. Dungs ⁴⁹,
 K. Dunne ^{47a,47b}, A. Duperrin ¹⁰³, H. Duran Yildiz ^{3a}, M. Düren ⁵⁸, A. Durglishvili ^{150b},
 B.L. Dwyer ¹¹⁶, G.I. Dyckes ^{17a}, M. Dyndal ^{86a}, B.S. Dziedzic ⁸⁷, Z.O. Earnshaw ¹⁴⁷,
 G.H. Eberwein ¹²⁷, B. Eckerova ^{28a}, S. Eggebrecht ⁵⁵, E. Egidio Purcino De Souza ¹²⁸,
 L.F. Ehrke ⁵⁶, G. Eigen ¹⁶, K. Einsweiler ^{17a}, T. Ekelof ¹⁶², P.A. Ekman ⁹⁹, S. El Farkh ^{35b},
 Y. El Ghazali ^{35b}, H. El Jarrari ³⁶, A. El Moussaouy ¹⁰⁹, V. Ellajosyula ¹⁶², M. Ellert ¹⁶²,
 F. Ellinghaus ¹⁷², N. Ellis ³⁶, J. Elmsheuser ²⁹, M. Elsayy ^{117a}, M. Elsing ³⁶,
 D. Emelianov ¹³⁵, Y. Enari ¹⁵⁴, I. Ene ^{17a}, S. Epari ¹³, P.A. Erland ⁸⁷, M. Errenst ¹⁷²,
 M. Escalier ⁶⁶, C. Escobar ¹⁶⁴, E. Etzion ¹⁵², G. Evans ^{131a}, H. Evans ⁶⁸, L.S. Evans ⁹⁶,
 A. Ezhilov ³⁷, S. Ezzarqtouni ^{35a}, F. Fabbri ^{23b,23a}, L. Fabbri ^{23b,23a}, G. Facini ⁹⁷,

V. Fadeyev ¹³⁷, R.M. Fakhruddinov ³⁷, D. Fakoudis ¹⁰¹, S. Falciano ^{75a},
L.F. Falda Ulhoa Coelho ³⁶, P.J. Falke ²⁴, F. Fallavollita ¹¹¹, J. Faltova ¹³⁴, C. Fan ¹⁶³,
Y. Fan ^{14a}, Y. Fang ^{14a,14e}, M. Fanti ^{71a,71b}, M. Faraj ^{69a,69b}, Z. Farazpay ⁹⁸, A. Farbin ⁸,
A. Farilla ^{77a}, T. Farooque ¹⁰⁸, S.M. Farrington ⁵², F. Fassi ^{35e}, D. Fassouliotis ⁹,
M. Faucci Giannelli ^{76a,76b}, W.J. Fawcett ³², L. Fayard ⁶⁶, P. Federic ¹³⁴, P. Federicova ¹³²,
O.L. Fedin ^{37,a}, M. Feickert ¹⁷¹, L. Feligioni ¹⁰³, D.E. Fellers ¹²⁴, C. Feng ^{62b}, M. Feng ^{14b},
Z. Feng ¹¹⁵, M.J. Fenton ¹⁶⁰, L. Ferencz ⁴⁸, R.A.M. Ferguson ⁹², S.I. Fernandez Luengo ^{138f},
P. Fernandez Martinez ¹³, M.J.V. Fernoux ¹⁰³, J. Ferrando ⁹², A. Ferrari ¹⁶², P. Ferrari ^{115,114},
R. Ferrari ^{73a}, D. Ferrere ⁵⁶, C. Ferretti ¹⁰⁷, F. Fiedler ¹⁰¹, P. Fiedler ¹³³, A. Filipčič ⁹⁴,
E.K. Filmer ¹, F. Filthaut ¹¹⁴, M.C.N. Fiolhais ^{131a,131c,c}, L. Fiorini ¹⁶⁴, W.C. Fisher ¹⁰⁸,
T. Fitschen ¹⁰², P.M. Fitzhugh ¹³⁶, I. Fleck ¹⁴², P. Fleischmann ¹⁰⁷, T. Flick ¹⁷², M. Flores ^{33d,ab},
L.R. Flores Castillo ^{64a}, L. Flores Sanz De Acedo ³⁶, F.M. Follega ^{78a,78b}, N. Fomin ¹⁶,
J.H. Foo ¹⁵⁶, A. Formica ¹³⁶, A.C. Forti ¹⁰², E. Fortin ³⁶, A.W. Fortman ^{17a}, M.G. Foti ^{17a},
L. Fountas ^{9j}, D. Fournier ⁶⁶, H. Fox ⁹², P. Francavilla ^{74a,74b}, S. Francescato ⁶¹,
S. Franchellucci ⁵⁶, M. Franchini ^{23b,23a}, S. Franchino ^{63a}, D. Francis ³⁶, L. Franco ¹¹⁴,
V. Franco Lima ³⁶, L. Franconi ⁴⁸, M. Franklin ⁶¹, G. Frattari ²⁶, W.S. Freund ^{83b}, Y.Y. Frid ¹⁵²,
J. Friend ⁵⁹, N. Fritzsche ⁵⁰, A. Froch ⁵⁴, D. Froidevaux ³⁶, J.A. Frost ¹²⁷, Y. Fu ^{62a},
S. Fuenzalida Garrido ^{138f}, M. Fujimoto ¹⁰³, K.Y. Fung ^{64a}, E. Furtado De Simas Filho ^{83e},
M. Furukawa ¹⁵⁴, J. Fuster ¹⁶⁴, A. Gabrielli ^{23b,23a}, A. Gabrielli ¹⁵⁶, P. Gadow ³⁶,
G. Gagliardi ^{57b,57a}, L.G. Gagnon ^{17a}, S. Gaid ¹⁶¹, S. Galantzan ¹⁵², E.J. Gallas ¹²⁷,
B.J. Gallop ¹³⁵, K.K. Gan ¹²⁰, S. Ganguly ¹⁵⁴, Y. Gao ⁵², F.M. Garay Walls ^{138a,138b}, B. Garcia ²⁹,
C. García ¹⁶⁴, A. Garcia Alonso ¹¹⁵, A.G. Garcia Caffaro ¹⁷³, J.E. García Navarro ¹⁶⁴,
M. Garcia-Sciveres ^{17a}, G.L. Gardner ¹²⁹, R.W. Gardner ³⁹, N. Garelli ¹⁵⁹, D. Garg ⁸⁰,
R.B. Garg ^{144,m}, J.M. Gargan ⁵², C.A. Garner ¹⁵⁶, C.M. Garvey ^{33a}, P. Gaspar ^{83b}, V.K. Gassmann ¹⁵⁹,
G. Gaudio ^{73a}, V. Gautam ¹³, P. Gauzzi ^{75a,75b}, I.L. Gavrilenko ³⁷, A. Gavrilyuk ³⁷, C. Gay ¹⁶⁵,
G. Gaycken ⁴⁸, E.N. Gazis ¹⁰, A.A. Geanta ^{27b}, C.M. Gee ¹³⁷, A. Gekow ¹²⁰, C. Gemme ^{57b},
M.H. Genest ⁶⁰, A.D. Gentry ¹¹³, S. George ⁹⁶, W.F. George ²⁰, T. Geralis ⁴⁶,
P. Gessinger-Befurt ³⁶, M.E. Geyik ¹⁷², M. Ghani ¹⁶⁸, K. Ghorbanian ⁹⁵, A. Ghosal ¹⁴²,
A. Ghosh ¹⁶⁰, A. Ghosh ⁷, B. Giacobbe ^{23b}, S. Giagu ^{75a,75b}, T. Giani ¹¹⁵, P. Giannetti ^{74a},
A. Giannini ^{62a}, S.M. Gibson ⁹⁶, M. Gignac ¹³⁷, D.T. Gil ^{86b}, A.K. Gilbert ^{86a}, B.J. Gilbert ⁴¹,
D. Gillberg ³⁴, G. Gilles ¹¹⁵, L. Ginabat ¹²⁸, D.M. Gingrich ^{2,ae}, M.P. Giordani ^{69a,69c},
P.F. Giraud ¹³⁶, G. Giugliarelli ^{69a,69c}, D. Giugni ^{71a}, F. Giuli ³⁶, I. Gkialas ^{9j}, L.K. Gladilin ³⁷,
C. Glasman ¹⁰⁰, G.R. Gledhill ¹²⁴, G. Glemža ⁴⁸, M. Glisic ¹²⁴, I. Gnesi ^{43b,f}, Y. Go ²⁹,
M. Goblirsch-Kolb ³⁶, B. Gocke ⁴⁹, D. Godin ¹⁰⁹, B. Gokturk ^{21a}, S. Goldfarb ¹⁰⁶, T. Golling ⁵⁶,
M.G.D. Gololo ^{33g}, D. Golubkov ³⁷, J.P. Gombas ¹⁰⁸, A. Gomes ^{131a,131b}, G. Gomes Da Silva ¹⁴²,
A.J. Gomez Delegido ¹⁶⁴, R. Gonçalo ^{131a,131c}, L. Gonella ²⁰, A. Gongadze ^{150c}, F. Gonnella ²⁰,
J.L. Gonski ¹⁴⁴, R.Y. González Andana ⁵², S. González de la Hoz ¹⁶⁴, R. Gonzalez Lopez ⁹³,
C. Gonzalez Renteria ^{17a}, M.V. Gonzalez Rodrigues ⁴⁸, R. Gonzalez Suarez ¹⁶²,
S. Gonzalez-Sevilla ⁵⁶, L. Goossens ³⁶, B. Gorini ³⁶, E. Gorini ^{70a,70b}, A. Gorišek ⁹⁴,
T.C. Gosart ¹²⁹, A.T. Goshaw ⁵¹, M.I. Gostkin ³⁸, S. Goswami ¹²², C.A. Gottardo ³⁶,
S.A. Gotz ¹¹⁰, M. Gouighri ^{35b}, V. Goumarre ⁴⁸, A.G. Goussiou ¹³⁹, N. Govender ^{33c},
I. Grabowska-Bold ^{86a}, K. Graham ³⁴, E. Gramstad ¹²⁶, S. Grancagnolo ^{70a,70b}, C.M. Grant ^{1,136},
P.M. Gravila ^{27f}, F.G. Gravili ^{70a,70b}, H.M. Gray ^{17a}, M. Greco ^{70a,70b}, C. Grefe ²⁴,
I.M. Gregor ⁴⁸, K.T. Greif ¹⁶⁰, P. Grenier ¹⁴⁴, S.G. Grewe ¹¹¹, A.A. Grillo ¹³⁷, K. Grimm ³¹,
S. Grinstein ^{13,s}, J.-F. Grivaz ⁶⁶, E. Gross ¹⁷⁰, J. Grosse-Knetter ⁵⁵, J.C. Grundy ¹²⁷,
L. Guan ¹⁰⁷, C. Gubbels ¹⁶⁵, J.G.R. Guerrero Rojas ¹⁶⁴, G. Guerrieri ^{69a,69c}, F. Guescini ¹¹¹,
R. Gugel ¹⁰¹, J.A.M. Guhit ¹⁰⁷, A. Guida ¹⁸, E. Guilloton ¹⁶⁸, S. Guindon ³⁶, F. Guo ^{14a,14e},

J. Guo ^{62c}, L. Guo ⁴⁸, Y. Guo ¹⁰⁷, R. Gupta ⁴⁸, R. Gupta ¹³⁰, S. Gurbuz ²⁴, S.S. Gurdasani ⁵⁴, G. Gustavino ³⁶, M. Guth ⁵⁶, P. Gutierrez ¹²¹, L.F. Gutierrez Zagazeta ¹²⁹, M. Gutsche ⁵⁰, C. Gutschow ⁹⁷, C. Gwenlan ¹²⁷, C.B. Gwilliam ⁹³, E.S. Haaland ¹²⁶, A. Haas ¹¹⁸, M. Habedank ⁴⁸, C. Haber ^{17a}, H.K. Hadavand ⁸, A. Hadeef ⁵⁰, S. Hadzic ¹¹¹, A.I. Hagan ⁹², J.J. Hahn ¹⁴², E.H. Haines ⁹⁷, M. Haleem ¹⁶⁷, J. Haley ¹²², J.J. Hall ¹⁴⁰, G.D. Hallewell ¹⁰³, L. Halser ¹⁹, K. Hamano ¹⁶⁶, M. Hamer ²⁴, G.N. Hamity ⁵², E.J. Hampshire ⁹⁶, J. Han ^{62b}, K. Han ^{62a}, L. Han ^{14c}, L. Han ^{62a}, S. Han ^{17a}, Y.F. Han ¹⁵⁶, K. Hanagaki ⁸⁴, M. Hance ¹³⁷, D.A. Hangal ⁴¹, H. Hanif ¹⁴³, M.D. Hank ¹²⁹, J.B. Hansen ⁴², P.H. Hansen ⁴², K. Hara ¹⁵⁸, D. Harada ⁵⁶, T. Harenberg ¹⁷², S. Harkusha ³⁷, M.L. Harris ¹⁰⁴, Y.T. Harris ¹²⁷, J. Harrison ¹³, N.M. Harrison ¹²⁰, P.F. Harrison ¹⁶⁸, N.M. Hartman ¹¹¹, N.M. Hartmann ¹¹⁰, R.Z. Hasan ^{96,135}, Y. Hasegawa ¹⁴¹, S. Hassan ¹⁶, R. Hauser ¹⁰⁸, C.M. Hawkes ²⁰, R.J. Hawkings ³⁶, Y. Hayashi ¹⁵⁴, S. Hayashida ¹¹², D. Hayden ¹⁰⁸, C. Hayes ¹⁰⁷, R.L. Hayes ¹¹⁵, C.P. Hays ¹²⁷, J.M. Hays ⁹⁵, H.S. Hayward ⁹³, F. He ^{62a}, M. He ^{14a,14e}, Y. He ¹⁵⁵, Y. He ⁴⁸, Y. He ⁹⁷, N.B. Heatley ⁹⁵, V. Hedberg ⁹⁹, A.L. Heggelund ¹²⁶, N.D. Hehir ^{95,*}, C. Heidegger ⁵⁴, K.K. Heidegger ⁵⁴, W.D. Heidorn ⁸¹, J. Heilman ³⁴, S. Heim ⁴⁸, T. Heim ^{17a}, J.G. Heinlein ¹²⁹, J.J. Heinrich ¹²⁴, L. Heinrich ^{111,ac}, J. Hejbal ¹³², A. Held ¹⁷¹, S. Hellesund ¹⁶, C.M. Helling ¹⁶⁵, S. Hellman ^{47a,47b}, R.C.W. Henderson ⁹², L. Henkelmann ³², A.M. Henriques Correia ³⁶, H. Herde ⁹⁹, Y. Hernández Jiménez ¹⁴⁶, L.M. Herrmann ²⁴, T. Herrmann ⁵⁰, G. Herten ⁵⁴, R. Hertenberger ¹¹⁰, L. Hervas ³⁶, M.E. Hesping ¹⁰¹, N.P. Hessey ^{157a}, M. Hidaoui ^{35b}, E. Hill ¹⁵⁶, S.J. Hillier ²⁰, J.R. Hinds ¹⁰⁸, F. Hinterkeuser ²⁴, M. Hirose ¹²⁵, S. Hirose ¹⁵⁸, D. Hirschbuehl ¹⁷², T.G. Hitchings ¹⁰², B. Hiti ⁹⁴, J. Hobbs ¹⁴⁶, R. Hobincu ^{27e}, N. Hod ¹⁷⁰, M.C. Hodgkinson ¹⁴⁰, B.H. Hodgkinson ¹²⁷, A. Hoecker ³⁶, D.D. Hofer ¹⁰⁷, J. Hofer ⁴⁸, T. Holm ²⁴, M. Holzbock ¹¹¹, L.B.A.H. Hommels ³², B.P. Honan ¹⁰², J. Hong ^{62c}, T.M. Hong ¹³⁰, B.H. Hooberman ¹⁶³, W.H. Hopkins ⁶, Y. Horii ¹¹², S. Hou ¹⁴⁹, A.S. Howard ⁹⁴, J. Howarth ⁵⁹, J. Hoya ⁶, M. Hrabovsky ¹²³, A. Hrynevich ⁴⁸, T. Hryn'ova ⁴, P.J. Hsu ⁶⁵, S.-C. Hsu ¹³⁹, T. Hsu ⁶⁶, M. Hu ^{17a}, Q. Hu ^{62a}, S. Huang ^{64b}, X. Huang ^{14a,14e}, Y. Huang ¹⁴⁰, Y. Huang ¹⁰¹, Y. Huang ^{14a}, Z. Huang ¹⁰², Z. Hubacek ¹³³, M. Huebner ²⁴, F. Hugging ²⁴, T.B. Huffman ¹²⁷, C.A. Hugli ⁴⁸, M. Huhtinen ³⁶, S.K. Huijberts ¹⁶, R. Hulsken ¹⁰⁵, N. Huseynov ¹², J. Huston ¹⁰⁸, J. Huth ⁶¹, R. Hyneman ¹⁴⁴, G. Iacobucci ⁵⁶, G. Iakovidis ²⁹, I. Ibragimov ¹⁴², L. Iconomidou-Fayard ⁶⁶, J.P. Iddon ³⁶, P. Iengo ^{72a,72b}, R. Iguchi ¹⁵⁴, T. Iizawa ¹²⁷, Y. Ikegami ⁸⁴, N. Ilic ¹⁵⁶, H. Imam ^{35a}, M. Ince Lezki ⁵⁶, T. Ingebretsen Carlson ^{47a,47b}, G. Introzzi ^{73a,73b}, M. Iodice ^{77a}, V. Ippolito ^{75a,75b}, R.K. Irwin ⁹³, M. Ishino ¹⁵⁴, W. Islam ¹⁷¹, C. Issever ^{18,48}, S. Istin ^{21a,ai}, H. Ito ¹⁶⁹, R. Iuppa ^{78a,78b}, A. Ivina ¹⁷⁰, J.M. Izen ⁴⁵, V. Izzo ^{72a}, P. Jacka ^{132,133}, P. Jackson ¹, B.P. Jaeger ¹⁴³, C.S. Jagfeld ¹¹⁰, G. Jain ^{157a}, P. Jain ⁵⁴, K. Jakobs ⁵⁴, T. Jakoubek ¹⁷⁰, J. Jamieson ⁵⁹, K.W. Janas ^{86a}, M. Javurkova ¹⁰⁴, L. Jeanty ¹²⁴, J. Jejelava ^{150a,z}, P. Jenni ^{54,g}, C.E. Jessiman ³⁴, C. Jia ^{62b}, J. Jia ¹⁴⁶, X. Jia ⁶¹, X. Jia ^{14a,14e}, Z. Jia ^{14c}, C. Jiang ⁵², S. Jiggins ⁴⁸, J. Jimenez Pena ¹³, S. Jin ^{14c}, A. Jinaru ^{27b}, O. Jinnouchi ¹⁵⁵, P. Johansson ¹⁴⁰, K.A. Johns ⁷, J.W. Johnson ¹³⁷, D.M. Jones ¹⁴⁷, E. Jones ⁴⁸, P. Jones ³², R.W.L. Jones ⁹², T.J. Jones ⁹³, H.L. Joos ^{55,36}, R. Joshi ¹²⁰, J. Jovicevic ¹⁵, X. Ju ^{17a}, J.J. Junggeburth ¹⁰⁴, T. Junkermann ^{63a}, A. Juste Rozas ^{13,s}, M.K. Juzek ⁸⁷, S. Kabana ^{138e}, A. Kaczmarzka ⁸⁷, M. Kado ¹¹¹, H. Kagan ¹²⁰, M. Kagan ¹⁴⁴, A. Kahn ⁴¹, A. Kahn ¹²⁹, C. Kahra ¹⁰¹, T. Kaji ¹⁵⁴, E. Kajomovitz ¹⁵¹, N. Kakati ¹⁷⁰, I. Kalaitzidou ⁵⁴, C.W. Kalderon ²⁹, N.J. Kang ¹³⁷, D. Kar ^{33g}, K. Karava ¹²⁷, M.J. Kareem ^{157b}, E. Karentzos ⁵⁴, I. Karkanas ¹⁵³, O. Karkout ¹¹⁵, S.N. Karpov ³⁸, Z.M. Karpova ³⁸, V. Kartvelishvili ⁹², A.N. Karyukhin ³⁷, E. Kasimi ¹⁵³, J. Katzy ⁴⁸, S. Kaur ³⁴, K. Kawade ¹⁴¹, M.P. Kawale ¹²¹, C. Kawamoto ⁸⁸, T. Kawamoto ^{62a}, E.F. Kay ³⁶, F.I. Kaya ¹⁵⁹, S. Kazakos ¹⁰⁸, V.F. Kazanin ³⁷, Y. Ke ¹⁴⁶, J.M. Keaveney ^{33a}, R. Keeler ¹⁶⁶, G.V. Kehris ⁶¹, J.S. Keller ³⁴, A.S. Kelly ⁹⁷,

J.J. Kempster ¹⁴⁷, P.D. Kennedy ¹⁰¹, O. Kepka ¹³², B.P. Kerridge ¹³⁵, S. Kersten ¹⁷²,
B.P. Kerševan ⁹⁴, L. Keszezhova ^{28a}, S. Ketabchi Haghighat ¹⁵⁶, R.A. Khan ¹³⁰, A. Khanov ¹²²,
A.G. Kharlamov ³⁷, T. Kharlamova ³⁷, E.E. Khoda ¹³⁹, M. Kholodenko ³⁷, T.J. Khoo ¹⁸,
G. Khoriauli ¹⁶⁷, J. Khubua ^{150b,*}, Y.A.R. Khwaira ⁶⁶, B. Kibirige ^{33g}, A. Kilgallon ¹²⁴,
D.W. Kim ^{47a,47b}, Y.K. Kim ³⁹, N. Kimura ⁹⁷, M.K. Kingston ⁵⁵, A. Kirchhoff ⁵⁵, C. Kirfel ²⁴,
F. Kirfel ²⁴, J. Kirk ¹³⁵, A.E. Kiryunin ¹¹¹, C. Kitsaki ¹⁰, O. Kivernyk ²⁴, M. Klassen ¹⁵⁹,
C. Klein ³⁴, L. Klein ¹⁶⁷, M.H. Klein ⁴⁴, S.B. Klein ⁵⁶, U. Klein ⁹³, P. Klimek ³⁶,
A. Klimentov ²⁹, T. Klioutchnikova ³⁶, P. Kluit ¹¹⁵, S. Kluth ¹¹¹, E. Kneringer ⁷⁹,
T.M. Knight ¹⁵⁶, A. Knue ⁴⁹, R. Kobayashi ⁸⁸, D. Kobylanski ¹⁷⁰, S.F. Koch ¹²⁷,
M. Kocian ¹⁴⁴, P. Kodyš ¹³⁴, D.M. Koeck ¹²⁴, P.T. Koenig ²⁴, T. Koffas ³⁴, O. Kolay ⁵⁰,
I. Koletsou ⁴, T. Komarek ¹²³, K. Köneke ⁵⁴, A.X.Y. Kong ¹, T. Kono ¹¹⁹, N. Konstantinidis ⁹⁷,
P. Kontaxakis ⁵⁶, B. Konya ⁹⁹, R. Kopeliansky ⁴¹, S. Koperny ^{86a}, K. Korcyl ⁸⁷, K. Kordas ^{153,e},
A. Korn ⁹⁷, S. Korn ⁵⁵, I. Korolkov ¹³, N. Korotkova ³⁷, B. Kortman ¹¹⁵, O. Kortner ¹¹¹,
S. Kortner ¹¹¹, W.H. Kostecka ¹¹⁶, V.V. Kostyukhin ¹⁴², A. Kotsokechagia ¹³⁶, A. Kotwal ⁵¹,
A. Koulouris ³⁶, A. Kourkoumeli-Charalampidi ^{73a,73b}, C. Kourkoumelis ⁹, E. Kourlitis ^{111,ac},
O. Kovanda ¹²⁴, R. Kowalewski ¹⁶⁶, W. Kozanecki ¹³⁶, A.S. Kozhin ³⁷, V.A. Kramarenko ³⁷,
G. Kramberger ⁹⁴, P. Kramer ¹⁰¹, M.W. Krasny ¹²⁸, A. Krasznahorkay ³⁶, J.W. Kraus ¹⁷²,
J.A. Kremer ⁴⁸, T. Kresse ⁵⁰, J. Kretschmar ⁹³, K. Kreul ¹⁸, P. Krieger ¹⁵⁶,
S. Krishnamurthy ¹⁰⁴, M. Krivos ¹³⁴, K. Krizka ²⁰, K. Kroeninger ⁴⁹, H. Kroha ¹¹¹, J. Kroll ¹³²,
J. Kroll ¹²⁹, K.S. Krowpman ¹⁰⁸, U. Kruchonak ³⁸, H. Krüger ²⁴, N. Krumnack ⁸¹, M.C. Kruse ⁵¹,
O. Kuchinskaia ³⁷, S. Kудay ^{3a}, S. Kuehn ³⁶, R. Kuesters ⁵⁴, T. Kuhl ⁴⁸, V. Kukhtin ³⁸,
Y. Kulchitsky ^{37,a}, S. Kuleshov ^{138d,138b}, M. Kumar ^{33g}, N. Kumari ⁴⁸, P. Kumari ^{157b},
A. Kupco ¹³², T. Kupfer ⁴⁹, A. Kupich ³⁷, O. Kuprash ⁵⁴, H. Kurashige ⁸⁵, L.L. Kurchaninov ^{157a},
O. Kurdysh ⁶⁶, Y.A. Kurochkin ³⁷, A. Kurova ³⁷, M. Kuze ¹⁵⁵, A.K. Kvam ¹⁰⁴, J. Kvita ¹²³,
T. Kwan ¹⁰⁵, N.G. Kyriacou ¹⁰⁷, L.A.O. Laatu ¹⁰³, C. Lacasta ¹⁶⁴, F. Lacava ^{75a,75b},
H. Lacker ¹⁸, D. Lacour ¹²⁸, N.N. Lad ⁹⁷, E. Ladygin ³⁸, A. Lafarge ⁴⁰, B. Laforge ¹²⁸,
T. Lagouri ¹⁷³, F.Z. Lahbabi ^{35a}, S. Lai ⁵⁵, I.K. Lakomiec ^{86a}, J.E. Lambert ¹⁶⁶, S. Lammers ⁶⁸,
W. Lampl ⁷, C. Lampoudis ^{153,e}, G. Lamprinoudis ¹⁰¹, A.N. Lancaster ¹¹⁶, E. Lançon ²⁹,
U. Landgraf ⁵⁴, M.P.J. Landon ⁹⁵, V.S. Lang ⁵⁴, O.K.B. Langrekken ¹²⁶, A.J. Lankford ¹⁶⁰,
F. Lanni ³⁶, K. Lantzsch ²⁴, A. Lanza ^{73a}, A. Lapertosa ^{57b,57a}, J.F. Laporte ¹³⁶, T. Lari ^{71a},
F. Lasagni Manghi ^{23b}, M. Lassnig ³⁶, V. Latonova ¹³², A. Laudrain ¹⁰¹, A. Laurier ¹⁵¹,
S.D. Lawlor ¹⁴⁰, Z. Lawrence ¹⁰², R. Lazaridou ¹⁶⁸, M. Lazzaroni ^{71a,71b}, B. Le ¹⁰²,
E.M. Le Boulicaut ⁵¹, L.T. Le Pottier ^{17a}, B. Leban ^{23b,23a}, A. Lebedev ⁸¹, M. LeBlanc ¹⁰²,
F. Ledroit-Guillon ⁶⁰, S.C. Lee ¹⁴⁹, S. Lee ^{47a,47b}, T.F. Lee ⁹³, L.L. Leeuw ^{33c}, H.P. Lefebvre ⁹⁶,
M. Lefebvre ¹⁶⁶, C. Leggett ^{17a}, G. Lehmann Miotto ³⁶, M. Leigh ⁵⁶, W.A. Leight ¹⁰⁴,
W. Leinonen ¹¹⁴, A. Leisos ^{153,r}, M.A.L. Leite ^{83c}, C.E. Leitgeb ¹⁸, R. Leitner ¹³⁴,
K.J.C. Leney ⁴⁴, T. Lenz ²⁴, S. Leone ^{74a}, C. Leonidopoulos ⁵², A. Leopold ¹⁴⁵, C. Leroy ¹⁰⁹,
R. Les ¹⁰⁸, C.G. Lester ³², M. Levchenko ³⁷, J. Levêque ⁴, L.J. Levinson ¹⁷⁰, G. Levrini ^{23b,23a},
M.P. Lewicki ⁸⁷, C. Lewis ¹³⁹, D.J. Lewis ⁴, A. Li ⁵, B. Li ^{62b}, C. Li ^{62a}, C-Q. Li ¹¹¹, H. Li ^{62a},
H. Li ^{62b}, H. Li ^{14c}, H. Li ^{14b}, H. Li ^{62b}, J. Li ^{62c}, K. Li ¹³⁹, L. Li ^{62c}, M. Li ^{14a,14e},
Q.Y. Li ^{62a}, S. Li ^{14a,14e}, S. Li ^{62d,62c,d}, T. Li ⁵, X. Li ¹⁰⁵, Z. Li ¹²⁷, Z. Li ¹⁵⁴, Z. Li ^{14a,14e},
S. Liang ^{14a,14e}, Z. Liang ^{14a}, M. Liberatore ¹³⁶, B. Liberti ^{76a}, K. Lie ^{64c}, J. Lieber Marin ^{83e},
H. Lien ⁶⁸, K. Lin ¹⁰⁸, R.E. Lindley ⁷, J.H. Lindon ², E. Lipeles ¹²⁹, A. Lipniacka ¹⁶,
A. Lister ¹⁶⁵, J.D. Little ⁴, B. Liu ^{14a}, B.X. Liu ¹⁴³, D. Liu ^{62d,62c}, E.H.L. Liu ²⁰, J.B. Liu ^{62a},
J.K.K. Liu ³², K. Liu ^{62d}, K. Liu ^{62d,62c}, M. Liu ^{62a}, M.Y. Liu ^{62a}, P. Liu ^{14a}, Q. Liu ^{62d,139,62c},
X. Liu ^{62a}, X. Liu ^{62b}, Y. Liu ^{14d,14e}, Y.L. Liu ^{62b}, Y.W. Liu ^{62a}, J. Llorente Merino ¹⁴³,
S.L. Lloyd ⁹⁵, E.M. Lobodzinska ⁴⁸, P. Loch ⁷, T. Lohse ¹⁸, K. Lohwasser ¹⁴⁰, E. Loiacono ⁴⁸,














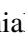

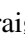

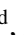


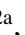
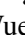






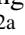


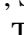

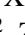
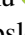
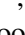


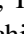
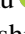
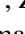
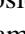
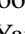





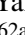






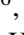

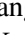


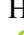

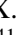






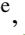

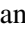








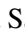

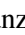


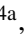



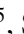


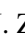

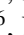
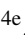

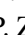



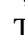

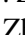
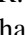


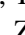
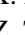
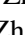


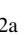
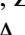

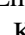




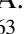

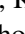



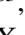

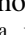



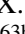
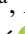









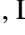

M. Lokajicek [id](#)^{132,*}, J.D. Lomas [id](#)²⁰, J.D. Long [id](#)¹⁶³, I. Longarini [id](#)¹⁶⁰, L. Longo [id](#)^{70a,70b},
R. Longo [id](#)¹⁶³, I. Lopez Paz [id](#)⁶⁷, A. Lopez Solis [id](#)⁴⁸, N. Lorenzo Martinez [id](#)⁴, A.M. Lory [id](#)¹¹⁰,
G. Löschcke Centeno [id](#)¹⁴⁷, O. Loseva [id](#)³⁷, X. Lou [id](#)^{47a,47b}, X. Lou [id](#)^{14a,14e}, A. Lounis [id](#)⁶⁶,
P.A. Love [id](#)⁹², G. Lu [id](#)^{14a,14e}, M. Lu [id](#)⁶⁶, S. Lu [id](#)¹²⁹, Y.J. Lu [id](#)⁶⁵, H.J. Lubatti [id](#)¹³⁹, C. Luci [id](#)^{75a,75b},
F.L. Lucio Alves [id](#)^{14c}, F. Luehring [id](#)⁶⁸, I. Luise [id](#)¹⁴⁶, O. Lukianchuk [id](#)⁶⁶, O. Lundberg [id](#)¹⁴⁵,
B. Lund-Jensen [id](#)^{145,*}, N.A. Luongo [id](#)⁶, M.S. Lutz [id](#)³⁶, A.B. Lux [id](#)²⁵, D. Lynn [id](#)²⁹, R. Lysak [id](#)¹³²,
E. Lytken [id](#)⁹⁹, V. Lyubushkin [id](#)³⁸, T. Lyubushkina [id](#)³⁸, M.M. Lyukova [id](#)¹⁴⁶, M.Firdaus M. Soberi [id](#)⁵²,
H. Ma [id](#)²⁹, K. Ma [id](#)^{62a}, L.L. Ma [id](#)^{62b}, W. Ma [id](#)^{62a}, Y. Ma [id](#)¹²², D.M. Mac Donell [id](#)¹⁶⁶,
G. Maccarrone [id](#)⁵³, J.C. MacDonald [id](#)¹⁰¹, P.C. Machado De Abreu Farias [id](#)^{83e}, R. Madar [id](#)⁴⁰,
T. Madula [id](#)⁹⁷, J. Maeda [id](#)⁸⁵, T. Maeno [id](#)²⁹, H. Maguire [id](#)¹⁴⁰, V. Maiboroda [id](#)¹³⁶,
A. Maio [id](#)^{131a,131b,131d}, K. Maj [id](#)^{86a}, O. Majersky [id](#)⁴⁸, S. Majewski [id](#)¹²⁴, N. Makovec [id](#)⁶⁶,
V. Maksimovic [id](#)¹⁵, B. Malaescu [id](#)¹²⁸, Pa. Malecki [id](#)⁸⁷, V.P. Maleev [id](#)³⁷, F. Malek [id](#)^{60,n}, M. Mali [id](#)⁹⁴,
D. Malito [id](#)⁹⁶, U. Mallik [id](#)⁸⁰, S. Maltezos¹⁰, S. Malyukov³⁸, J. Mamuzic [id](#)¹³, G. Mancini [id](#)⁵³,
M.N. Mancini [id](#)²⁶, G. Manco [id](#)^{73a,73b}, J.P. Mandalia [id](#)⁹⁵, I. Mandić [id](#)⁹⁴,
L. Manhaes de Andrade Filho [id](#)^{83a}, I.M. Maniatis [id](#)¹⁷⁰, J. Manjarres Ramos [id](#)⁹⁰, D.C. Mankad [id](#)¹⁷⁰,
A. Mann [id](#)¹¹⁰, S. Manzoni [id](#)³⁶, L. Mao [id](#)^{62c}, X. Mapekula [id](#)^{33c}, A. Marantis [id](#)^{153,r}, G. Marchiori [id](#)⁵,
M. Marcisovsky [id](#)¹³², C. Marcon [id](#)^{71a}, M. Marinescu [id](#)²⁰, S. Marium [id](#)⁴⁸, M. Marjanovic [id](#)¹²¹,
A. Markhoos [id](#)⁵⁴, M. Markovitch [id](#)⁶⁶, E.J. Marshall [id](#)⁹², Z. Marshall [id](#)^{17a}, S. Marti-Garcia [id](#)¹⁶⁴,
T.A. Martin [id](#)¹⁶⁸, V.J. Martin [id](#)⁵², B. Martin dit Latour [id](#)¹⁶, L. Martinelli [id](#)^{75a,75b}, M. Martinez [id](#)^{13,s},
P. Martinez Agullo [id](#)¹⁶⁴, V.I. Martinez Outschoorn [id](#)¹⁰⁴, P. Martinez Suarez [id](#)¹³, S. Martin-Haugh [id](#)¹³⁵,
G. Martinovicova [id](#)¹³⁴, V.S. Martoiu [id](#)^{27b}, A.C. Martyniuk [id](#)⁹⁷, A. Marzin [id](#)³⁶, D. Mascione [id](#)^{78a,78b},
L. Masetti [id](#)¹⁰¹, T. Mashimo [id](#)¹⁵⁴, J. Masik [id](#)¹⁰², A.L. Maslennikov [id](#)³⁷, P. Massarotti [id](#)^{72a,72b},
P. Mastrandrea [id](#)^{74a,74b}, A. Mastroberardino [id](#)^{43b,43a}, T. Masubuchi [id](#)¹⁵⁴, T. Mathisen [id](#)¹⁶²,
J. Matousek [id](#)¹³⁴, N. Matsuzawa¹⁵⁴, J. Maurer [id](#)^{27b}, A.J. Maury [id](#)⁶⁶, B. Maček [id](#)⁹⁴, D.A. Maximov [id](#)³⁷,
A.E. May [id](#)¹⁰², R. Mazini [id](#)¹⁴⁹, I. Maznas [id](#)¹¹⁶, M. Mazza [id](#)¹⁰⁸, S.M. Mazza [id](#)¹³⁷, E. Mazzeo [id](#)^{71a,71b},
C. Mc Ginn [id](#)²⁹, J.P. Mc Gowan [id](#)¹⁶⁶, S.P. Mc Kee [id](#)¹⁰⁷, C.C. McCracken [id](#)¹⁶⁵, E.F. McDonald [id](#)¹⁰⁶,
A.E. McDougall [id](#)¹¹⁵, J.A. Mcfayden [id](#)¹⁴⁷, R.P. McGovern [id](#)¹²⁹, G. Mchedlidze [id](#)^{150b},
R.P. Mckenzie [id](#)^{33g}, T.C. Mclachlan [id](#)⁴⁸, D.J. Mclaughlin [id](#)⁹⁷, S.J. McMahon [id](#)¹³⁵,
C.M. Mcpartland [id](#)⁹³, R.A. McPherson [id](#)^{166,w}, S. Mehlhase [id](#)¹¹⁰, A. Mehta [id](#)⁹³, D. Melini [id](#)¹⁶⁴,
B.R. Mellado Garcia [id](#)^{33g}, A.H. Melo [id](#)⁵⁵, F. Meloni [id](#)⁴⁸, A.M. Mendes Jacques Da Costa [id](#)¹⁰²,
H.Y. Meng [id](#)¹⁵⁶, L. Meng [id](#)⁹², S. Menke [id](#)¹¹¹, M. Mentink [id](#)³⁶, E. Meoni [id](#)^{43b,43a}, G. Mercado [id](#)¹¹⁶,
C. Merlassino [id](#)^{69a,69c}, L. Merola [id](#)^{72a,72b}, C. Meroni [id](#)^{71a,71b}, J. Metcalfe [id](#)⁶, A.S. Mete [id](#)⁶,
C. Meyer [id](#)⁶⁸, J-P. Meyer [id](#)¹³⁶, R.P. Middleton [id](#)¹³⁵, L. Mijović [id](#)⁵², G. Mikenberg [id](#)¹⁷⁰,
M. Mikestikova [id](#)¹³², M. Mikuž [id](#)⁹⁴, H. Mildner [id](#)¹⁰¹, A. Milic [id](#)³⁶, D.W. Miller [id](#)³⁹, E.H. Miller [id](#)¹⁴⁴,
L.S. Miller [id](#)³⁴, A. Milov [id](#)¹⁷⁰, D.A. Milstead^{47a,47b}, T. Min^{14c}, A.A. Minaenko [id](#)³⁷,
I.A. Minashvili [id](#)^{150b}, L. Mince [id](#)⁵⁹, A.I. Mincer [id](#)¹¹⁸, B. Mindur [id](#)^{86a}, M. Mineev [id](#)³⁸, Y. Mino [id](#)⁸⁸,
L.M. Mir [id](#)¹³, M. Miralles Lopez [id](#)⁵⁹, M. Mironova [id](#)^{17a}, A. Mishima¹⁵⁴, M.C. Missio [id](#)¹¹⁴,
A. Mitra [id](#)¹⁶⁸, V.A. Mitsou [id](#)¹⁶⁴, Y. Mitsumori [id](#)¹¹², O. Miu [id](#)¹⁵⁶, P.S. Miyagawa [id](#)⁹⁵,
T. Mkrtchyan [id](#)^{63a}, M. Mlinarevic [id](#)⁹⁷, T. Mlinarevic [id](#)⁹⁷, M. Mlynarikova [id](#)³⁶, S. Mobius [id](#)¹⁹,
P. Mogg [id](#)¹¹⁰, M.H. Mohamed Farook [id](#)¹¹³, A.F. Mohammed [id](#)^{14a,14e}, S. Mohapatra [id](#)⁴¹,
G. Mokgatitswane [id](#)^{33g}, L. Moleri [id](#)¹⁷⁰, B. Mondal [id](#)¹⁴², S. Mondal [id](#)¹³³, K. Mönig [id](#)⁴⁸,
E. Monnier [id](#)¹⁰³, L. Monsonis Romero¹⁶⁴, J. Montejo Berlingen [id](#)¹³, M. Montella [id](#)¹²⁰,
F. Montekali [id](#)^{77a,77b}, F. Monticelli [id](#)⁹¹, S. Monzani [id](#)^{69a,69c}, N. Morange [id](#)⁶⁶,
A.L. Moreira De Carvalho [id](#)⁴⁸, M. Moreno Llácer [id](#)¹⁶⁴, C. Moreno Martinez [id](#)⁵⁶, P. Morettini [id](#)^{57b},
S. Morgenstern [id](#)³⁶, M. Morii [id](#)⁶¹, M. Morinaga [id](#)¹⁵⁴, F. Morodei [id](#)^{75a,75b}, L. Morvaj [id](#)³⁶,
P. Moschovakos [id](#)³⁶, B. Moser [id](#)³⁶, M. Mosidze [id](#)^{150b}, T. Moskalets [id](#)⁵⁴, P. Moskvitina [id](#)¹¹⁴,
J. Moss [id](#)^{31,k}, P. Moszkowicz [id](#)^{86a}, A. Moussa [id](#)^{35d}, E.J.W. Moyse [id](#)¹⁰⁴, O. Mtintsilana [id](#)^{33g},

S. Muanza ¹⁰³, J. Mueller ¹³⁰, D. Muenstermann ⁹², R. Müller ¹⁹, G.A. Mullier ¹⁶²,
 A.J. Mullin ³², J.J. Mullin ¹²⁹, D.P. Mungo ¹⁵⁶, D. Munoz Perez ¹⁶⁴, F.J. Munoz Sanchez ¹⁰²,
 M. Murin ¹⁰², W.J. Murray ^{168,135}, M. Muškinja ⁹⁴, C. Mwewa ²⁹, A.G. Myagkov ^{37,a},
 A.J. Myers ⁸, G. Myers ¹⁰⁷, M. Myska ¹³³, B.P. Nachman ^{17a}, O. Nackenhorst ⁴⁹, K. Nagai ¹²⁷,
 K. Nagano ⁸⁴, J.L. Nagle ^{29,ag}, E. Nagy ¹⁰³, A.M. Nairz ³⁶, Y. Nakahama ⁸⁴, K. Nakamura ⁸⁴,
 K. Nakkalil ⁵, H. Nanjo ¹²⁵, R. Narayan ⁴⁴, E.A. Narayanan ¹¹³, I. Naryshkin ³⁷, M. Naseri ³⁴,
 S. Nasri ^{117b}, C. Nass ²⁴, G. Navarro ^{22a}, J. Navarro-Gonzalez ¹⁶⁴, R. Nayak ¹⁵², A. Nayaz ¹⁸,
 P.Y. Nechaeva ³⁷, S. Nechaeva ^{23b,23a}, F. Nechansky ⁴⁸, L. Nedic ¹²⁷, T.J. Neep ²⁰,
 A. Negri ^{73a,73b}, M. Negrini ^{23b}, C. Nellist ¹¹⁵, C. Nelson ¹⁰⁵, K. Nelson ¹⁰⁷, S. Nemecek ¹³²,
 M. Nessi ^{36,h}, M.S. Neubauer ¹⁶³, F. Neuhaus ¹⁰¹, J. Neundorf ⁴⁸, R. Newhouse ¹⁶⁵,
 P.R. Newman ²⁰, C.W. Ng ¹³⁰, Y.W.Y. Ng ⁴⁸, B. Ngair ^{117a}, H.D.N. Nguyen ¹⁰⁹,
 R.B. Nickerson ¹²⁷, R. Nicolaidou ¹³⁶, J. Nielsen ¹³⁷, M. Niemeyer ⁵⁵, J. Niermann ⁵⁵,
 N. Nikiporou ³⁶, V. Nikolaenko ^{37,a}, I. Nikolic-Audit ¹²⁸, K. Nikolopoulos ²⁰, P. Nilsson ²⁹,
 I. Ninca ⁴⁸, H.R. Nindhito ⁵⁶, G. Ninio ¹⁵², A. Nisati ^{75a}, N. Nishu ², R. Nisius ¹¹¹,
 J-E. Nitschke ⁵⁰, E.K. Nkadimeng ^{33g}, T. Nobe ¹⁵⁴, D.L. Noel ³², T. Nommensen ¹⁴⁸,
 M.B. Norfolk ¹⁴⁰, R.R.B. Norisam ⁹⁷, B.J. Norman ³⁴, M. Noury ^{35a}, J. Novak ⁹⁴, T. Novak ⁴⁸,
 L. Novotny ¹³³, R. Novotny ¹¹³, L. Nozka ¹²³, K. Ntekas ¹⁶⁰, N.M.J. Nunes De Moura Junior ^{83b},
 J. Ocariz ¹²⁸, A. Ochi ⁸⁵, I. Ochoa ^{131a}, S. Oerdek ^{48,t}, J.T. Offermann ³⁹, A. Ogrodnik ¹³⁴,
 A. Oh ¹⁰², C.C. Ohm ¹⁴⁵, H. Oide ⁸⁴, R. Oishi ¹⁵⁴, M.L. Ojeda ⁴⁸, Y. Okumura ¹⁵⁴,
 L.F. Oleiro Seabra ^{131a}, S.A. Olivares Pino ^{138d}, G. Oliveira Correa ¹³, D. Oliveira Damazio ²⁹,
 D. Oliveira Goncalves ^{83a}, J.L. Oliver ¹⁶⁰, Ö.O. Öncel ⁵⁴, A.P. O'Neill ¹⁹, A. Onofre ^{131a,131e},
 P.U.E. Onyisi ¹¹, M.J. Oreglia ³⁹, G.E. Orellana ⁹¹, D. Orestano ^{77a,77b}, N. Orlando ¹³,
 R.S. Orr ¹⁵⁶, V. O'Shea ⁵⁹, L.M. Osojnak ¹²⁹, R. Ospanov ^{62a}, G. Otero y Garzon ³⁰,
 H. Otono ⁸⁹, P.S. Ott ^{63a}, G.J. Ottino ^{17a}, M. Ouchrif ^{35d}, F. Ould-Saada ¹²⁶,
 T. Ovsiannikova ¹³⁹, M. Owen ⁵⁹, R.E. Owen ¹³⁵, K.Y. Oyulmaz ^{21a}, V.E. Ozcan ^{21a},
 F. Ozturk ⁸⁷, N. Ozturk ⁸, S. Ozturk ⁸², H.A. Pacey ¹²⁷, A. Pacheco Pages ¹³,
 C. Padilla Aranda ¹³, G. Padovano ^{75a,75b}, S. Pagan Griso ^{17a}, G. Palacino ⁶⁸, A. Palazzo ^{70a,70b},
 J. Pampel ²⁴, J. Pan ¹⁷³, T. Pan ^{64a}, D.K. Panchal ¹¹, C.E. Pandini ¹¹⁵, J.G. Panduro Vazquez ⁹⁶,
 H.D. Pandya ¹, H. Pang ^{14b}, P. Pani ⁴⁸, G. Panizzo ^{69a,69c}, L. Panwar ¹²⁸, L. Paolozzi ⁵⁶,
 S. Parajuli ¹⁶³, A. Paramonov ⁵, C. Paraskevopoulos ⁵³, D. Paredes Hernandez ^{64b},
 A. Pareti ^{73a,73b}, K.R. Park ⁴¹, T.H. Park ¹⁵⁶, M.A. Parker ³², F. Parodi ^{57b,57a}, E.W. Parrish ¹¹⁶,
 V.A. Parrish ⁵², J.A. Parsons ⁴¹, U. Parzefall ⁵⁴, B. Pascual Dias ¹⁰⁹, L. Pascual Dominguez ¹⁵²,
 E. Pasqualucci ^{75a}, S. Passaggio ^{57b}, F. Pastore ⁹⁶, P. Patel ⁸⁷, U.M. Patel ⁵¹, J.R. Pater ¹⁰²,
 T. Pauly ³⁶, C.I. Pazos ¹⁵⁹, J. Pearkes ¹⁴⁴, M. Pedersen ¹²⁶, R. Pedro ^{131a}, S.V. Peleganchuk ³⁷,
 O. Penc ³⁶, E.A. Pender ⁵², G.D. Penn ¹⁷³, K.E. Penski ¹¹⁰, M. Penzin ³⁷, B.S. Peralva ^{83d},
 A.P. Pereira Peixoto ¹³⁹, L. Pereira Sanchez ¹⁴⁴, D.V. Perepelitsa ^{29,ag}, E. Perez Codina ^{157a},
 M. Perganti ¹⁰, H. Pernegger ³⁶, O. Perrin ⁴⁰, K. Peters ⁴⁸, R.F.Y. Peters ¹⁰², B.A. Petersen ³⁶,
 T.C. Petersen ⁴², E. Petit ¹⁰³, V. Petousis ¹³³, C. Petridou ^{153,e}, T. Petru ¹³⁴, A. Petrukhin ¹⁴²,
 M. Pettee ^{17a}, N.E. Pettersson ³⁶, A. Petukhov ³⁷, K. Petukhova ¹³⁴, R. Pezoa ^{138f},
 L. Pezzotti ³⁶, G. Pezzullo ¹⁷³, T.M. Pham ¹⁷¹, T. Pham ¹⁰⁶, P.W. Phillips ¹³⁵, G. Piacquadio ¹⁴⁶,
 E. Pianori ^{17a}, F. Piazza ¹²⁴, R. Piegai ³⁰, D. Pietreanu ^{27b}, A.D. Pilkington ¹⁰²,
 M. Pinamonti ^{69a,69c}, J.L. Pinfeld ², B.C. Pinheiro Pereira ^{131a}, A.E. Pinto Pinoargote ^{101,136},
 L. Pintucci ^{69a,69c}, K.M. Piper ¹⁴⁷, A. Pirttikoski ⁵⁶, D.A. Pizzi ³⁴, L. Pizzimento ^{64b},
 A. Pizzini ¹¹⁵, M.-A. Pleier ²⁹, V. Plesanovs ⁵⁴, V. Pleskot ¹³⁴, E. Plotnikova ³⁸, G. Poddar ⁹⁵,
 R. Poettgen ⁹⁹, L. Poggioli ¹²⁸, I. Pokharel ⁵⁵, S. Polacek ¹³⁴, G. Polesello ^{73a}, A. Poley ^{143,157a},
 A. Polini ^{23b}, C.S. Pollard ¹⁶⁸, Z.B. Pollock ¹²⁰, E. Pompa Pacchi ^{75a,75b}, D. Ponomarenko ¹¹⁴,
 L. Pontecorvo ³⁶, S. Popa ^{27a}, G.A. Popeneciu ^{27d}, A. Poreba ³⁶, D.M. Portillo Quintero ^{157a},

S. Pospisil ¹³³, M.A. Postill ¹⁴⁰, P. Postolache ^{27c}, K. Potamianos ¹⁶⁸, P.A. Potepa ^{86a},
 I.N. Potrap ³⁸, C.J. Potter ³², H. Potti ¹, J. Poveda ¹⁶⁴, M.E. Pozo Astigarraga ³⁶,
 A. Prades Ibanez ¹⁶⁴, J. Pretel ⁵⁴, D. Price ¹⁰², M. Primavera ^{70a}, M.A. Principe Martin ¹⁰⁰,
 R. Privara ¹²³, T. Procter ⁵⁹, M.L. Proffitt ¹³⁹, N. Proklova ¹²⁹, K. Prokofiev ^{64c}, G. Proto ¹¹¹,
 J. Proudfoot ⁶, M. Przybycien ^{86a}, W.W. Przygoda ^{86b}, A. Psallidas ⁴⁶, J.E. Puddefoot ¹⁴⁰,
 D. Pudzha ³⁷, D. Pyatiizbyantseva ³⁷, J. Qian ¹⁰⁷, D. Qichen ¹⁰², Y. Qin ¹³, T. Qiu ⁵²,
 A. Quadt ⁵⁵, M. Queitsch-Maitland ¹⁰², G. Quetant ⁵⁶, R.P. Quinn ¹⁶⁵, G. Rabanal Bolanos ⁶¹,
 D. Rafanoharana ⁵⁴, F. Ragusa ^{71a,71b}, J.L. Rainbolt ³⁹, J.A. Raine ⁵⁶, S. Rajagopalan ²⁹,
 E. Ramakoti ³⁷, I.A. Ramirez-Berend ³⁴, K. Ran ^{48,14e}, N.P. Rapheeha ^{33g}, H. Rasheed ^{27b},
 V. Raskina ¹²⁸, D.F. Rassloff ^{63a}, A. Rastogi ^{17a}, S. Rave ¹⁰¹, B. Ravina ⁵⁵, I. Ravinovich ¹⁷⁰,
 M. Raymond ³⁶, A.L. Read ¹²⁶, N.P. Readioff ¹⁴⁰, D.M. Rebutzi ^{73a,73b}, G. Redlinger ²⁹,
 A.S. Reed ¹¹¹, K. Reeves ²⁶, J.A. Reidelsturz ¹⁷², D. Reikher ¹⁵², A. Rej ⁴⁹, C. Rembser ³⁶,
 M. Renda ^{27b}, M.B. Rendel ¹¹¹, F. Renner ⁴⁸, A.G. Rennie ¹⁶⁰, A.L. Rescia ⁴⁸, S. Resconi ^{71a},
 M. Ressegotti ^{57b,57a}, S. Rettie ³⁶, J.G. Reyes Rivera ¹⁰⁸, E. Reynolds ^{17a}, O.L. Rezanova ³⁷,
 P. Reznicek ¹³⁴, H. Riani ^{35d}, N. Ribaric ⁹², E. Ricci ^{78a,78b}, R. Richter ¹¹¹, S. Richter ^{47a,47b},
 E. Richter-Was ^{86b}, M. Ridel ¹²⁸, S. Ridouani ^{35d}, P. Rieck ¹¹⁸, P. Riedler ³⁶, E.M. Riefel ^{47a,47b},
 J.O. Rieger ¹¹⁵, M. Rijssenbeek ¹⁴⁶, M. Rimoldi ³⁶, L. Rinaldi ^{23b,23a}, T.T. Rinn ²⁹,
 M.P. Rinnagel ¹¹⁰, G. Ripellino ¹⁶², I. Riu ¹³, J.C. Rivera Vergara ¹⁶⁶, F. Rizatdinova ¹²²,
 E. Rizvi ⁹⁵, B.R. Roberts ^{17a}, S.H. Robertson ^{105,w}, D. Robinson ³², C.M. Robles Gajardo ^{138f},
 M. Robles Manzano ¹⁰¹, A. Robson ⁵⁹, A. Rocchi ^{76a,76b}, C. Roda ^{74a,74b}, S. Rodriguez Bosca ³⁶,
 Y. Rodriguez Garcia ^{22a}, A. Rodriguez Rodriguez ⁵⁴, A.M. Rodríguez Vera ¹¹⁶, S. Roe ³⁶,
 J.T. Roemer ¹⁶⁰, A.R. Roepe-Gier ¹³⁷, J. Roggel ¹⁷², O. Røhne ¹²⁶, R.A. Rojas ¹⁰⁴,
 C.P.A. Roland ¹²⁸, J. Roloff ²⁹, A. Romaniouk ³⁷, E. Romano ^{73a,73b}, M. Romano ^{23b},
 A.C. Romero Hernandez ¹⁶³, N. Rompotis ⁹³, L. Roos ¹²⁸, S. Rosati ^{75a}, B.J. Rosser ³⁹,
 E. Rossi ¹²⁷, E. Rossi ^{72a,72b}, L.P. Rossi ⁶¹, L. Rossini ⁵⁴, R. Rosten ¹²⁰, M. Rotaru ^{27b},
 B. Rottler ⁵⁴, C. Rougier ⁹⁰, D. Rousseau ⁶⁶, D. Rouso ⁴⁸, A. Roy ¹⁶³, S. Roy-Garand ¹⁵⁶,
 A. Rozanov ¹⁰³, Z.M.A. Rozario ⁵⁹, Y. Rozen ¹⁵¹, A. Rubio Jimenez ¹⁶⁴, A.J. Ruby ⁹³,
 V.H. Ruelas Rivera ¹⁸, T.A. Ruggeri ¹, A. Ruggiero ¹²⁷, A. Ruiz-Martinez ¹⁶⁴, A. Rummler ³⁶,
 Z. Rurikova ⁵⁴, N.A. Rusakovich ³⁸, H.L. Russell ¹⁶⁶, G. Russo ^{75a,75b}, J.P. Rutherford ⁷,
 S. Rutherford Colmenares ³², K. Rybacki ⁹², M. Rybar ¹³⁴, E.B. Rye ¹²⁶, A. Ryzhov ⁴⁴,
 J.A. Sabater Iglesias ⁵⁶, P. Sabatini ¹⁶⁴, H.F.W. Sadrozinski ¹³⁷, F. Safai Tehrani ^{75a},
 B. Safarzadeh Samani ¹³⁵, S. Saha ¹, M. Sahinsoy ¹¹¹, A. Saibel ¹⁶⁴, M. Saimpert ¹³⁶,
 M. Saito ¹⁵⁴, T. Saito ¹⁵⁴, A. Sala ^{71a,71b}, D. Salamani ³⁶, A. Salnikov ¹⁴⁴, J. Salt ¹⁶⁴,
 A. Salvador Salas ¹⁵², D. Salvatore ^{43b,43a}, F. Salvatore ¹⁴⁷, A. Salzburger ³⁶, D. Sammel ⁵⁴,
 E. Sampson ⁹², D. Sampsonidis ^{153,e}, D. Sampsonidou ¹²⁴, J. Sánchez ¹⁶⁴,
 V. Sanchez Sebastian ¹⁶⁴, H. Sandaker ¹²⁶, C.O. Sander ⁴⁸, J.A. Sandesara ¹⁰⁴, M. Sandhoff ¹⁷²,
 C. Sandoval ^{22b}, D.P.C. Sankey ¹³⁵, T. Sano ⁸⁸, A. Sansoni ⁵³, L. Santi ^{75a,75b}, C. Santoni ⁴⁰,
 H. Santos ^{131a,131b}, A. Santra ¹⁷⁰, E. Sanzani ^{23b,23a}, K.A. Saoucha ¹⁶¹, J.G. Saraiva ^{131a,131d},
 J. Sardain ⁷, O. Sasaki ⁸⁴, K. Sato ¹⁵⁸, C. Sauer ^{63b}, F. Sauerburger ⁵⁴, E. Sauvan ⁴,
 P. Savard ^{156,ae}, R. Sawada ¹⁵⁴, C. Sawyer ¹³⁵, L. Sawyer ⁹⁸, I. Sayago Galvan ¹⁶⁴, C. Sbarra ^{23b},
 A. Sbrizzi ^{23b,23a}, T. Scanlon ⁹⁷, J. Schaarschmidt ¹³⁹, U. Schäfer ¹⁰¹, A.C. Schaffer ^{66,44},
 D. Schaile ¹¹⁰, R.D. Schamberger ¹⁴⁶, C. Scharf ¹⁸, M.M. Schefer ¹⁹, V.A. Schegelsky ³⁷,
 D. Scheirich ¹³⁴, F. Schenck ¹⁸, M. Schernau ¹⁶⁰, C. Scheulen ⁵⁵, C. Schiavi ^{57b,57a},
 M. Schioppa ^{43b,43a}, B. Schlag ^{144,m}, K.E. Schleicher ⁵⁴, S. Schlenker ³⁶, J. Schmeing ¹⁷²,
 M.A. Schmidt ¹⁷², K. Schmieden ¹⁰¹, C. Schmitt ¹⁰¹, N. Schmitt ¹⁰¹, S. Schmitt ⁴⁸,
 L. Schoeffel ¹³⁶, A. Schoening ^{63b}, P.G. Scholer ³⁴, E. Schopf ¹²⁷, M. Schott ¹⁰¹,
 J. Schovancova ³⁶, S. Schramm ⁵⁶, T. Schroer ⁵⁶, H-C. Schultz-Coulon ^{63a}, M. Schumacher ⁵⁴,

B.A. Schumm ¹³⁷, Ph. Schune ¹³⁶, A.J. Schuy ¹³⁹, H.R. Schwartz ¹³⁷, A. Schwartzman ¹⁴⁴,
 T.A. Schwarz ¹⁰⁷, Ph. Schwemling ¹³⁶, R. Schwienhorst ¹⁰⁸, A. Sciandra ²⁹, G. Sciolla ²⁶,
 F. Scuri ^{74a}, C.D. Sebastiani ⁹³, K. Sedlaczek ¹¹⁶, P. Seema ¹⁸, S.C. Seidel ¹¹³, A. Seiden ¹³⁷,
 B.D. Seidlitz ⁴¹, C. Seitz ⁴⁸, J.M. Seixas ^{83b}, G. Sekhniaidze ^{72a}, L. Selem ⁶⁰,
 N. Semprini-Cesari ^{23b,23a}, D. Sengupta ⁵⁶, V. Senthilkumar ¹⁶⁴, L. Serin ⁶⁶, L. Serkin ^{69a,69b},
 M. Sessa ^{76a,76b}, H. Severini ¹²¹, F. Sforza ^{57b,57a}, A. Sfyrla ⁵⁶, Q. Sha ^{14a}, E. Shabalina ⁵⁵,
 A.H. Shah ³², R. Shaheen ¹⁴⁵, J.D. Shahinian ¹²⁹, D. Shaked Renous ¹⁷⁰, L.Y. Shan ^{14a},
 M. Shapiro ^{17a}, A. Sharma ³⁶, A.S. Sharma ¹⁶⁵, P. Sharma ⁸⁰, P.B. Shatalov ³⁷, K. Shaw ¹⁴⁷,
 S.M. Shaw ¹⁰², A. Shcherbakova ³⁷, Q. Shen ^{62c,5}, D.J. Sheppard ¹⁴³, P. Sherwood ⁹⁷, L. Shi ⁹⁷,
 X. Shi ^{14a}, C.O. Shimmin ¹⁷³, J.D. Shinner ⁹⁶, I.P.J. Shipsey ¹²⁷, S. Shirabe ⁸⁹,
 M. Shiyakova ^{38,u}, J. Shlomi ¹⁷⁰, M.J. Shochet ³⁹, J. Shojaii ¹⁰⁶, D.R. Shope ¹²⁶,
 B. Shrestha ¹²¹, S. Shrestha ^{120,ah}, E.M. Shrif ^{33g}, M.J. Shroff ¹⁶⁶, P. Sicho ¹³², A.M. Sickles ¹⁶³,
 E. Sideras Haddad ^{33g}, A.C. Sidley ¹¹⁵, A. Sidoti ^{23b}, F. Siegert ⁵⁰, Dj. Sijacki ¹⁵, F. Sili ⁹¹,
 J.M. Silva ⁵², M.V. Silva Oliveira ²⁹, S.B. Silverstein ^{47a}, S. Simion ⁶⁶, R. Simoniello ³⁶,
 E.L. Simpson ¹⁰², H. Simpson ¹⁴⁷, L.R. Simpson ¹⁰⁷, N.D. Simpson ⁹⁹, S. Simsek ⁸²,
 S. Sindhu ⁵⁵, P. Sinervo ¹⁵⁶, S. Singh ¹⁵⁶, S. Sinha ⁴⁸, S. Sinha ¹⁰², M. Sioli ^{23b,23a}, I. Siral ³⁶,
 E. Sitnikova ⁴⁸, J. Sjölin ^{47a,47b}, A. Skaf ⁵⁵, E. Skorda ²⁰, P. Skubic ¹²¹, M. Slawinska ⁸⁷,
 V. Smakhtin ¹⁷⁰, B.H. Smart ¹³⁵, S.Yu. Smirnov ³⁷, Y. Smirnov ³⁷, L.N. Smirnova ^{37,a},
 O. Smirnova ⁹⁹, A.C. Smith ⁴¹, D.R. Smith ¹⁶⁰, E.A. Smith ³⁹, H.A. Smith ¹²⁷, J.L. Smith ¹⁰²,
 R. Smith ¹⁴⁴, M. Smizanska ⁹², K. Smolek ¹³³, A.A. Snesarev ³⁷, S.R. Snider ¹⁵⁶, H.L. Snoek ¹¹⁵,
 S. Snyder ²⁹, R. Sobie ^{166,w}, A. Soffer ¹⁵², C.A. Solans Sanchez ³⁶, E.Yu. Soldatov ³⁷,
 U. Soldevila ¹⁶⁴, A.A. Solodkov ³⁷, S. Solomon ²⁶, A. Soloshenko ³⁸, K. Solovieva ⁵⁴,
 O.V. Solovyanov ⁴⁰, P. Sommer ³⁶, A. Sonay ¹³, W.Y. Song ^{157b}, A. Sopczak ¹³³, A.L. Soppio ⁹⁷,
 F. Sopkova ^{28b}, J.D. Sorenson ¹¹³, I.R. Sotarriva Alvarez ¹⁵⁵, V. Sothilingam ^{63a},
 O.J. Soto Sandoval ^{138c,138b}, S. Sottocornola ⁶⁸, R. Soualah ¹⁶¹, Z. Soumami ^{35e}, D. South ⁴⁸,
 N. Soybelman ¹⁷⁰, S. Spagnolo ^{70a,70b}, M. Spalla ¹¹¹, D. Sperlich ⁵⁴, G. Spigo ³⁶, S. Spinali ⁹²,
 D.P. Spiteri ⁵⁹, M. Spousta ¹³⁴, E.J. Staats ³⁴, R. Stamen ^{63a}, A. Stampekis ²⁰, M. Standke ²⁴,
 E. Stanecka ⁸⁷, W. Stanek-Maslouska ⁴⁸, M.V. Stange ⁵⁰, B. Stanislaus ^{17a}, M.M. Stanitzki ⁴⁸,
 B. Stapf ⁴⁸, E.A. Starchenko ³⁷, G.H. Stark ¹³⁷, J. Stark ⁹⁰, P. Staroba ¹³², P. Starovoitov ^{63a},
 S. Stärz ¹⁰⁵, R. Staszewski ⁸⁷, G. Stavropoulos ⁴⁶, J. Steentoft ¹⁶², P. Steinberg ²⁹,
 B. Stelzer ^{143,157a}, H.J. Stelzer ¹³⁰, O. Stelzer-Chilton ^{157a}, H. Stenzel ⁵⁸, T.J. Stevenson ¹⁴⁷,
 G.A. Stewart ³⁶, J.R. Stewart ¹²², M.C. Stockton ³⁶, G. Stoicea ^{27b}, M. Stolarski ^{131a},
 S. Stonjek ¹¹¹, A. Straessner ⁵⁰, J. Strandberg ¹⁴⁵, S. Strandberg ^{47a,47b}, M. Stratmann ¹⁷²,
 M. Strauss ¹²¹, T. Strebler ¹⁰³, P. Strizenc ^{28b}, R. Ströhmer ¹⁶⁷, D.M. Strom ¹²⁴,
 R. Stroynowski ⁴⁴, A. Strubig ^{47a,47b}, S.A. Stucci ²⁹, B. Stugu ¹⁶, J. Stupak ¹²¹, N.A. Styles ⁴⁸,
 D. Su ¹⁴⁴, S. Su ^{62a}, W. Su ^{62d}, X. Su ^{62a}, D. Suchy ^{28a}, K. Sugizaki ¹⁵⁴, V.V. Sulin ³⁷,
 M.J. Sullivan ⁹³, D.M.S. Sultan ¹²⁷, L. Sultanaliyeva ³⁷, S. Sultansoy ^{3b}, T. Sumida ⁸⁸,
 S. Sun ¹⁰⁷, S. Sun ¹⁷¹, O. Sunneborn Gudnadottir ¹⁶², N. Sur ¹⁰³, M.R. Sutton ¹⁴⁷,
 H. Suzuki ¹⁵⁸, M. Svatos ¹³², M. Swiatlowski ^{157a}, T. Swirski ¹⁶⁷, I. Sykora ^{28a}, M. Sykora ¹³⁴,
 T. Sykora ¹³⁴, D. Ta ¹⁰¹, K. Tackmann ^{48,t}, A. Taffard ¹⁶⁰, R. Tafirout ^{157a}, J.S. Tafuya Vargas ⁶⁶,
 Y. Takubo ⁸⁴, M. Talby ¹⁰³, A.A. Talyshev ³⁷, K.C. Tam ^{64b}, N.M. Tamir ¹⁵², A. Tanaka ¹⁵⁴,
 J. Tanaka ¹⁵⁴, R. Tanaka ⁶⁶, M. Tanasini ¹⁴⁶, Z. Tao ¹⁶⁵, S. Tapia Araya ^{138f}, S. Tapprogge ¹⁰¹,
 A. Tarek Abouelfadl Mohamed ¹⁰⁸, S. Tarem ¹⁵¹, K. Tariq ^{14a}, G. Tarna ^{27b}, G.F. Tartarelli ^{71a},
 M.J. Tartarin ⁹⁰, P. Tas ¹³⁴, M. Tasevsky ¹³², E. Tassi ^{43b,43a}, A.C. Tate ¹⁶³, G. Tateno ¹⁵⁴,
 Y. Tayalati ^{35e,v}, G.N. Taylor ¹⁰⁶, W. Taylor ^{157b}, A.S. Tee ¹⁷¹, R. Teixeira De Lima ¹⁴⁴,
 P. Teixeira-Dias ⁹⁶, J.J. Teoh ¹⁵⁶, K. Terashi ¹⁵⁴, J. Terron ¹⁰⁰, S. Terzo ¹³, M. Testa ⁵³,
 R.J. Teuscher ^{156,w}, A. Thaler ⁷⁹, O. Theiner ⁵⁶, N. Themistokleous ⁵², T. Theveneaux-Pelzer ¹⁰³,

O. Thielmann ¹⁷², D.W. Thomas ⁹⁶, J.P. Thomas ²⁰, E.A. Thompson ^{17a}, P.D. Thompson ²⁰, E. Thomson ¹²⁹, R.E. Thornberry ⁴⁴, Y. Tian ⁵⁵, V. Tikhomirov ^{37,a}, Yu.A. Tikhonov ³⁷, S. Timoshenko ³⁷, D. Timoshyn ¹³⁴, E.X.L. Ting ¹, P. Tipton ¹⁷³, S.H. Tlou ^{33g}, K. Todome ¹⁵⁵, S. Todorova-Nova ¹³⁴, S. Todt ⁵⁰, L. Toffolin ^{69a,69c}, M. Togawa ⁸⁴, J. Tojo ⁸⁹, S. Tokár ^{28a}, K. Tokushuku ⁸⁴, O. Toldaiev ⁶⁸, R. Tombs ³², M. Tomoto ^{84,112}, L. Tompkins ^{144,m}, K.W. Topolnicki ^{86b}, E. Torrence ¹²⁴, H. Torres ⁹⁰, E. Torró Pastor ¹⁶⁴, M. Toscani ³⁰, C. Toscirci ³⁹, M. Tost ¹¹, D.R. Tovey ¹⁴⁰, A. Traeet ¹⁶, I.S. Trandafir ^{27b}, T. Trefzger ¹⁶⁷, A. Tricoli ²⁹, I.M. Trigger ^{157a}, S. Trincaz-Duvoid ¹²⁸, D.A. Trischuk ²⁶, B. Trocmé ⁶⁰, L. Truong ^{33c}, M. Trzebinski ⁸⁷, A. Trzupek ⁸⁷, F. Tsai ¹⁴⁶, M. Tsai ¹⁰⁷, A. Tsiamis ^{153,e}, P.V. Tsiarehka ³⁷, S. Tsigaridas ^{157a}, A. Tsirigotis ^{153,r}, V. Tsiskaridze ¹⁵⁶, E.G. Tskhadadze ^{150a}, M. Tsopoulou ¹⁵³, Y. Tsujikawa ⁸⁸, I.I. Tsukerman ³⁷, V. Tsulaia ^{17a}, S. Tsuno ⁸⁴, K. Tsurii ¹¹⁹, D. Tsybychev ¹⁴⁶, Y. Tu ^{64b}, A. Tudorache ^{27b}, V. Tudorache ^{27b}, A.N. Tuna ⁶¹, S. Turchikhin ^{57b,57a}, I. Turk Cakir ^{3a}, R. Turra ^{71a}, T. Turtuvshin ^{38,x}, P.M. Tuts ⁴¹, S. Tzamarias ^{153,e}, E. Tzovara ¹⁰¹, F. Ukegawa ¹⁵⁸, P.A. Ulloa Poblete ^{138c,138b}, E.N. Umaka ²⁹, G. Unal ³⁶, A. Undrus ²⁹, G. Unel ¹⁶⁰, J. Urban ^{28b}, P. Urquijo ¹⁰⁶, P. Urrejola ^{138a}, G. Usai ⁸, R. Ushioda ¹⁵⁵, M. Usman ¹⁰⁹, Z. Uysal ⁸², V. Vacek ¹³³, B. Vachon ¹⁰⁵, T. Vafeiadis ³⁶, A. Vaitkus ⁹⁷, C. Valderanis ¹¹⁰, E. Valdes Santurio ^{47a,47b}, M. Valente ^{157a}, S. Valentinetti ^{23b,23a}, A. Valero ¹⁶⁴, E. Valiente Moreno ¹⁶⁴, A. Vallier ⁹⁰, J.A. Valls Ferrer ¹⁶⁴, D.R. Van Arneman ¹¹⁵, T.R. Van Daalen ¹³⁹, A. Van Der Graaf ⁴⁹, P. Van Gemmeren ⁶, M. Van Rijnbach ¹²⁶, S. Van Stroud ⁹⁷, I. Van Vulpen ¹¹⁵, P. Vana ¹³⁴, M. Vanadia ^{76a,76b}, W. Vandelli ³⁶, E.R. Vandewall ¹²², D. Vannicola ¹⁵², L. Vannoli ⁵³, R. Vari ^{75a}, E.W. Varnes ⁷, C. Varni ^{17b}, T. Varol ¹⁴⁹, D. Varouchas ⁶⁶, L. Varriale ¹⁶⁴, K.E. Varvell ¹⁴⁸, M.E. Vasile ^{27b}, L. Vaslin ⁸⁴, G.A. Vasquez ¹⁶⁶, A. Vasyukov ³⁸, R. Vavricka ¹⁰¹, F. Vazeille ⁴⁰, T. Vazquez Schroeder ³⁶, J. Veatch ³¹, V. Vecchio ¹⁰², M.J. Veen ¹⁰⁴, I. Veliscek ²⁹, L.M. Veloce ¹⁵⁶, F. Veloso ^{131a,131c}, S. Veneziano ^{75a}, A. Ventura ^{70a,70b}, S. Ventura Gonzalez ¹³⁶, A. Verbytskyi ¹¹¹, M. Verducci ^{74a,74b}, C. Vergis ⁹⁵, M. Verissimo De Araujo ^{83b}, W. Verkerke ¹¹⁵, J.C. Vermeulen ¹¹⁵, C. Vernieri ¹⁴⁴, M. Vessella ¹⁰⁴, M.C. Vetterli ^{143,ae}, A. Vgenopoulos ^{153,e}, N. Viaux Maira ^{138f}, T. Vickey ¹⁴⁰, O.E. Vickey Boeriu ¹⁴⁰, G.H.A. Viehhauser ¹²⁷, L. Vigani ^{63b}, M. Villa ^{23b,23a}, M. Villaplana Perez ¹⁶⁴, E.M. Villhauer ⁵², E. Vilucchi ⁵³, M.G. Vincter ³⁴, A. Visible ¹¹⁵, C. Vittori ³⁶, I. Vivarelli ^{23b,23a}, E. Voevodina ¹¹¹, F. Vogel ¹¹⁰, J.C. Voigt ⁵⁰, P. Vokac ¹³³, Yu. Volkotrub ^{86b}, J. Von Ahnen ⁴⁸, E. Von Toerne ²⁴, B. Vormwald ³⁶, V. Vorobel ¹³⁴, K. Vorobev ³⁷, M. Vos ¹⁶⁴, K. Voss ¹⁴², M. Vozak ¹¹⁵, L. Vozdecky ¹²¹, N. Vranjes ¹⁵, M. Vranjes Milosavljevic ¹⁵, M. Vreeswijk ¹¹⁵, N.K. Vu ^{62d,62c}, R. Vuillermet ³⁶, O. Vujinovic ¹⁰¹, I. Vukotic ³⁹, S. Wada ¹⁵⁸, C. Wagner ¹⁰⁴, J.M. Wagner ^{17a}, W. Wagner ¹⁷², S. Wahdan ¹⁷², H. Wahlberg ⁹¹, M. Wakida ¹¹², J. Walder ¹³⁵, R. Walker ¹¹⁰, W. Walkowiak ¹⁴², A. Wall ¹²⁹, E.J. Wallin ⁹⁹, T. Wamorkar ⁶, A.Z. Wang ¹³⁷, C. Wang ¹⁰¹, C. Wang ¹¹, H. Wang ^{17a}, J. Wang ^{64c}, R.-J. Wang ¹⁰¹, R. Wang ⁶¹, R. Wang ⁶, S.M. Wang ¹⁴⁹, S. Wang ^{62b}, S. Wang ^{14a}, T. Wang ^{62a}, W.T. Wang ⁸⁰, W. Wang ^{14a}, X. Wang ^{14c}, X. Wang ¹⁶³, X. Wang ^{62c}, Y. Wang ^{62d}, Y. Wang ^{14c}, Z. Wang ¹⁰⁷, Z. Wang ^{62d,51,62c}, Z. Wang ¹⁰⁷, A. Warburton ¹⁰⁵, R.J. Ward ²⁰, N. Warrack ⁵⁹, S. Waterhouse ⁹⁶, A.T. Watson ²⁰, H. Watson ⁵⁹, M.F. Watson ²⁰, E. Watton ^{59,135}, G. Watts ¹³⁹, B.M. Waugh ⁹⁷, J.M. Webb ⁵⁴, C. Weber ²⁹, H.A. Weber ¹⁸, M.S. Weber ¹⁹, S.M. Weber ^{63a}, C. Wei ^{62a}, Y. Wei ⁵⁴, A.R. Weidberg ¹²⁷, E.J. Weik ¹¹⁸, J. Weingarten ⁴⁹, M. Weirich ¹⁰¹, C. Weiser ⁵⁴, C.J. Wells ⁴⁸, T. Wenaus ²⁹, B. Wendland ⁴⁹, T. Wengler ³⁶, N.S. Wenke ¹¹¹, N. Wermes ²⁴, M. Wessels ^{63a}, A.M. Wharton ⁹², A.S. White ⁶¹, A. White ⁸, M.J. White ¹, D. Whiteson ¹⁶⁰, L. Wickremasinghe ¹²⁵, W. Wiedenmann ¹⁷¹, M. Wielers ¹³⁵, C. Wiglesworth ⁴², D.J. Wilbern ¹²¹, H.G. Wilkens ³⁶, J.J.H. Wilkinson ³², D.M. Williams ⁴¹, H.H. Williams ¹²⁹, S. Williams ³²,

S. Willocq ¹⁰⁴, B.J. Wilson ¹⁰², P.J. Windischhofer ³⁹, F.I. Winkel ³⁰, F. Winklmeier ¹²⁴, B.T. Winter ⁵⁴, J.K. Winter ¹⁰², M. Wittgen¹⁴⁴, M. Wobisch ⁹⁸, T. Wojtkowski⁶⁰, Z. Wolffs ¹¹⁵, J. Wollrath¹⁶⁰, M.W. Wolter ⁸⁷, H. Wolters ^{131a,131c}, M.C. Wong¹³⁷, E.L. Woodward ⁴¹, S.D. Worm ⁴⁸, B.K. Wosiek ⁸⁷, K.W. Woźniak ⁸⁷, S. Wozniowski ⁵⁵, K. Wraight ⁵⁹, C. Wu ²⁰, M. Wu ^{14d}, M. Wu ¹¹⁴, S.L. Wu ¹⁷¹, X. Wu ⁵⁶, Y. Wu ^{62a}, Z. Wu ⁴, J. Wuerzinger ^{111,ac}, T.R. Wyatt ¹⁰², B.M. Wynne ⁵², S. Xella ⁴², L. Xia ^{14c}, M. Xia ^{14b}, J. Xiang ^{64c}, M. Xie ^{62a}, X. Xie ^{62a}, S. Xin ^{14a,14e}, A. Xiong ¹²⁴, J. Xiong ^{17a}, D. Xu ^{14a}, H. Xu ^{62a}, L. Xu ^{62a}, R. Xu ¹²⁹, T. Xu ¹⁰⁷, Y. Xu ^{14b}, Z. Xu ⁵², Z. Xu^{14c}, B. Yabsley ¹⁴⁸, S. Yacoob ^{33a}, Y. Yamaguchi ¹⁵⁵, E. Yamashita ¹⁵⁴, H. Yamauchi ¹⁵⁸, T. Yamazaki ^{17a}, Y. Yamazaki ⁸⁵, J. Yan^{62c}, S. Yan ⁵⁹, Z. Yan ¹⁰⁴, H.J. Yang ^{62c,62d}, H.T. Yang ^{62a}, S. Yang ^{62a}, T. Yang ^{64c}, X. Yang ³⁶, X. Yang ^{14a}, Y. Yang ⁴⁴, Y. Yang^{62a}, Y. Yang ¹⁰⁵, Z. Yang ^{62a}, W-M. Yao ^{17a}, H. Ye ^{14c}, H. Ye ⁵⁵, J. Ye ^{14a}, S. Ye ²⁹, X. Ye ^{62a}, Y. Yeh ⁹⁷, I. Yeletsikh ³⁸, B.K. Yeo ^{17b}, M.R. Yexley ⁹⁷, T.P. Yildirim ¹²⁷, P. Yin ⁴¹, K. Yorita ¹⁶⁹, S. Younas ^{27b}, C.J.S. Young ³⁶, C. Young ¹⁴⁴, C. Yu ^{14a,14e}, Y. Yu ^{62a}, M. Yuan ¹⁰⁷, R. Yuan ^{62d,62c}, L. Yue ⁹⁷, M. Zaazoua ^{62a}, B. Zabinski ⁸⁷, E. Zaid⁵², Z.K. Zak ⁸⁷, T. Zakareishvili ¹⁶⁴, N. Zakharchuk ³⁴, S. Zambito ⁵⁶, J.A. Zamora Saa ^{138d,138b}, J. Zang ¹⁵⁴, D. Zanzi ⁵⁴, O. Zaplatilek ¹³³, C. Zeitnitz ¹⁷², H. Zeng ^{14a}, J.C. Zeng ¹⁶³, D.T. Zenger Jr ²⁶, O. Zenin ³⁷, T. Ženiš ^{28a}, S. Zenz ⁹⁵, S. Zerradi ^{35a}, D. Zerwas ⁶⁶, M. Zhai ^{14a,14e}, D.F. Zhang ¹⁴⁰, J. Zhang ^{62b}, J. Zhang ⁶, K. Zhang ^{14a,14e}, L. Zhang ^{62a}, L. Zhang ^{14c}, P. Zhang ^{14a,14e}, R. Zhang ¹⁷¹, S. Zhang ¹⁰⁷, S. Zhang ⁴⁴, T. Zhang ¹⁵⁴, X. Zhang ^{62c}, X. Zhang ^{62b}, Y. Zhang ^{62c,5}, Y. Zhang ⁹⁷, Y. Zhang ^{14c}, Z. Zhang ^{17a}, Z. Zhang ⁶⁶, H. Zhao ¹³⁹, T. Zhao ^{62b}, Y. Zhao ¹³⁷, Z. Zhao ^{62a}, Z. Zhao ^{62a}, A. Zhemchugov ³⁸, J. Zheng ^{14c}, K. Zheng ¹⁶³, X. Zheng ^{62a}, Z. Zheng ¹⁴⁴, D. Zhong ¹⁶³, B. Zhou ¹⁰⁷, H. Zhou ⁷, N. Zhou ^{62c}, Y. Zhou ^{14c}, Y. Zhou⁷, C.G. Zhu ^{62b}, J. Zhu ¹⁰⁷, X. Zhu^{62d}, Y. Zhu ^{62c}, Y. Zhu ^{62a}, X. Zhuang ^{14a}, K. Zhukov ³⁷, N.I. Zimine ³⁸, J. Zinsser ^{63b}, M. Ziolkowski ¹⁴², L. Živković ¹⁵, A. Zoccoli ^{23b,23a}, K. Zoch ⁶¹, T.G. Zorbas ¹⁴⁰, O. Zormpa ⁴⁶, W. Zou ⁴¹, L. Zwalinski ³⁶.

¹Department of Physics, University of Adelaide, Adelaide; Australia.

²Department of Physics, University of Alberta, Edmonton AB; Canada.

³(^a)Department of Physics, Ankara University, Ankara; (^b)Division of Physics, TOBB University of Economics and Technology, Ankara; Türkiye.

⁴LAPP, Université Savoie Mont Blanc, CNRS/IN2P3, Annecy; France.

⁵APC, Université Paris Cité, CNRS/IN2P3, Paris; France.

⁶High Energy Physics Division, Argonne National Laboratory, Argonne IL; United States of America.

⁷Department of Physics, University of Arizona, Tucson AZ; United States of America.

⁸Department of Physics, University of Texas at Arlington, Arlington TX; United States of America.

⁹Physics Department, National and Kapodistrian University of Athens, Athens; Greece.

¹⁰Physics Department, National Technical University of Athens, Zografou; Greece.

¹¹Department of Physics, University of Texas at Austin, Austin TX; United States of America.

¹²Institute of Physics, Azerbaijan Academy of Sciences, Baku; Azerbaijan.

¹³Institut de Física d'Altes Energies (IFAE), Barcelona Institute of Science and Technology, Barcelona; Spain.

¹⁴(^a)Institute of High Energy Physics, Chinese Academy of Sciences, Beijing; (^b)Physics Department, Tsinghua University, Beijing; (^c)Department of Physics, Nanjing University, Nanjing; (^d)School of Science, Shenzhen Campus of Sun Yat-sen University; (^e)University of Chinese Academy of Science (UCAS), Beijing; China.

¹⁵Institute of Physics, University of Belgrade, Belgrade; Serbia.

- ¹⁶Department for Physics and Technology, University of Bergen, Bergen; Norway.
- ¹⁷(^a)Physics Division, Lawrence Berkeley National Laboratory, Berkeley CA; (^b)University of California, Berkeley CA; United States of America.
- ¹⁸Institut für Physik, Humboldt Universität zu Berlin, Berlin; Germany.
- ¹⁹Albert Einstein Center for Fundamental Physics and Laboratory for High Energy Physics, University of Bern, Bern; Switzerland.
- ²⁰School of Physics and Astronomy, University of Birmingham, Birmingham; United Kingdom.
- ²¹(^a)Department of Physics, Bogazici University, Istanbul; (^b)Department of Physics Engineering, Gaziantep University, Gaziantep; (^c)Department of Physics, Istanbul University, Istanbul; Türkiye.
- ²²(^a)Facultad de Ciencias y Centro de Investigaciones, Universidad Antonio Nariño, Bogotá; (^b)Departamento de Física, Universidad Nacional de Colombia, Bogotá; Colombia.
- ²³(^a)Dipartimento di Fisica e Astronomia A. Righi, Università di Bologna, Bologna; (^b)INFN Sezione di Bologna; Italy.
- ²⁴Physikalisches Institut, Universität Bonn, Bonn; Germany.
- ²⁵Department of Physics, Boston University, Boston MA; United States of America.
- ²⁶Department of Physics, Brandeis University, Waltham MA; United States of America.
- ²⁷(^a)Transilvania University of Brasov, Brasov; (^b)Horia Hulubei National Institute of Physics and Nuclear Engineering, Bucharest; (^c)Department of Physics, Alexandru Ioan Cuza University of Iasi, Iasi; (^d)National Institute for Research and Development of Isotopic and Molecular Technologies, Physics Department, Cluj-Napoca; (^e)National University of Science and Technology Politehnica, Bucharest; (^f)West University in Timisoara, Timisoara; (^g)Faculty of Physics, University of Bucharest, Bucharest; Romania.
- ²⁸(^a)Faculty of Mathematics, Physics and Informatics, Comenius University, Bratislava; (^b)Department of Subnuclear Physics, Institute of Experimental Physics of the Slovak Academy of Sciences, Kosice; Slovak Republic.
- ²⁹Physics Department, Brookhaven National Laboratory, Upton NY; United States of America.
- ³⁰Universidad de Buenos Aires, Facultad de Ciencias Exactas y Naturales, Departamento de Física, y CONICET, Instituto de Física de Buenos Aires (IFIBA), Buenos Aires; Argentina.
- ³¹California State University, CA; United States of America.
- ³²Cavendish Laboratory, University of Cambridge, Cambridge; United Kingdom.
- ³³(^a)Department of Physics, University of Cape Town, Cape Town; (^b)iThemba Labs, Western Cape; (^c)Department of Mechanical Engineering Science, University of Johannesburg, Johannesburg; (^d)National Institute of Physics, University of the Philippines Diliman (Philippines); (^e)University of South Africa, Department of Physics, Pretoria; (^f)University of Zululand, KwaDlangezwa; (^g)School of Physics, University of the Witwatersrand, Johannesburg; South Africa.
- ³⁴Department of Physics, Carleton University, Ottawa ON; Canada.
- ³⁵(^a)Faculté des Sciences Ain Chock, Université Hassan II de Casablanca; (^b)Faculté des Sciences, Université Ibn-Tofail, Kénitra; (^c)Faculté des Sciences Semlalia, Université Cadi Ayyad, LPHEA-Marrakech; (^d)LPMR, Faculté des Sciences, Université Mohamed Premier, Oujda; (^e)Faculté des sciences, Université Mohammed V, Rabat; (^f)Institute of Applied Physics, Mohammed VI Polytechnic University, Ben Guerir; Morocco.
- ³⁶CERN, Geneva; Switzerland.
- ³⁷Affiliated with an institute covered by a cooperation agreement with CERN.
- ³⁸Affiliated with an international laboratory covered by a cooperation agreement with CERN.
- ³⁹Enrico Fermi Institute, University of Chicago, Chicago IL; United States of America.
- ⁴⁰LPC, Université Clermont Auvergne, CNRS/IN2P3, Clermont-Ferrand; France.
- ⁴¹Nevis Laboratory, Columbia University, Irvington NY; United States of America.
- ⁴²Niels Bohr Institute, University of Copenhagen, Copenhagen; Denmark.

- ^{43(a)}Dipartimento di Fisica, Università della Calabria, Rende; ^(b)INFN Gruppo Collegato di Cosenza, Laboratori Nazionali di Frascati; Italy.
- ⁴⁴Physics Department, Southern Methodist University, Dallas TX; United States of America.
- ⁴⁵Physics Department, University of Texas at Dallas, Richardson TX; United States of America.
- ⁴⁶National Centre for Scientific Research "Demokritos", Agia Paraskevi; Greece.
- ^{47(a)}Department of Physics, Stockholm University; ^(b)Oskar Klein Centre, Stockholm; Sweden.
- ⁴⁸Deutsches Elektronen-Synchrotron DESY, Hamburg and Zeuthen; Germany.
- ⁴⁹Fakultät Physik, Technische Universität Dortmund, Dortmund; Germany.
- ⁵⁰Institut für Kern- und Teilchenphysik, Technische Universität Dresden, Dresden; Germany.
- ⁵¹Department of Physics, Duke University, Durham NC; United States of America.
- ⁵²SUPA - School of Physics and Astronomy, University of Edinburgh, Edinburgh; United Kingdom.
- ⁵³INFN e Laboratori Nazionali di Frascati, Frascati; Italy.
- ⁵⁴Physikalisches Institut, Albert-Ludwigs-Universität Freiburg, Freiburg; Germany.
- ⁵⁵II. Physikalisches Institut, Georg-August-Universität Göttingen, Göttingen; Germany.
- ⁵⁶Département de Physique Nucléaire et Corpusculaire, Université de Genève, Genève; Switzerland.
- ^{57(a)}Dipartimento di Fisica, Università di Genova, Genova; ^(b)INFN Sezione di Genova; Italy.
- ⁵⁸II. Physikalisches Institut, Justus-Liebig-Universität Giessen, Giessen; Germany.
- ⁵⁹SUPA - School of Physics and Astronomy, University of Glasgow, Glasgow; United Kingdom.
- ⁶⁰LPSC, Université Grenoble Alpes, CNRS/IN2P3, Grenoble INP, Grenoble; France.
- ⁶¹Laboratory for Particle Physics and Cosmology, Harvard University, Cambridge MA; United States of America.
- ^{62(a)}Department of Modern Physics and State Key Laboratory of Particle Detection and Electronics, University of Science and Technology of China, Hefei; ^(b)Institute of Frontier and Interdisciplinary Science and Key Laboratory of Particle Physics and Particle Irradiation (MOE), Shandong University, Qingdao; ^(c)School of Physics and Astronomy, Shanghai Jiao Tong University, Key Laboratory for Particle Astrophysics and Cosmology (MOE), SKLPPC, Shanghai; ^(d)Tsung-Dao Lee Institute, Shanghai; ^(e)School of Physics and Microelectronics, Zhengzhou University; China.
- ^{63(a)}Kirchhoff-Institut für Physik, Ruprecht-Karls-Universität Heidelberg, Heidelberg; ^(b)Physikalisches Institut, Ruprecht-Karls-Universität Heidelberg, Heidelberg; Germany.
- ^{64(a)}Department of Physics, Chinese University of Hong Kong, Shatin, N.T., Hong Kong; ^(b)Department of Physics, University of Hong Kong, Hong Kong; ^(c)Department of Physics and Institute for Advanced Study, Hong Kong University of Science and Technology, Clear Water Bay, Kowloon, Hong Kong; China.
- ⁶⁵Department of Physics, National Tsing Hua University, Hsinchu; Taiwan.
- ⁶⁶IJCLab, Université Paris-Saclay, CNRS/IN2P3, 91405, Orsay; France.
- ⁶⁷Centro Nacional de Microelectrónica (IMB-CNM-CSIC), Barcelona; Spain.
- ⁶⁸Department of Physics, Indiana University, Bloomington IN; United States of America.
- ^{69(a)}INFN Gruppo Collegato di Udine, Sezione di Trieste, Udine; ^(b)ICTP, Trieste; ^(c)Dipartimento Politecnico di Ingegneria e Architettura, Università di Udine, Udine; Italy.
- ^{70(a)}INFN Sezione di Lecce; ^(b)Dipartimento di Matematica e Fisica, Università del Salento, Lecce; Italy.
- ^{71(a)}INFN Sezione di Milano; ^(b)Dipartimento di Fisica, Università di Milano, Milano; Italy.
- ^{72(a)}INFN Sezione di Napoli; ^(b)Dipartimento di Fisica, Università di Napoli, Napoli; Italy.
- ^{73(a)}INFN Sezione di Pavia; ^(b)Dipartimento di Fisica, Università di Pavia, Pavia; Italy.
- ^{74(a)}INFN Sezione di Pisa; ^(b)Dipartimento di Fisica E. Fermi, Università di Pisa, Pisa; Italy.
- ^{75(a)}INFN Sezione di Roma; ^(b)Dipartimento di Fisica, Sapienza Università di Roma, Roma; Italy.
- ^{76(a)}INFN Sezione di Roma Tor Vergata; ^(b)Dipartimento di Fisica, Università di Roma Tor Vergata, Roma; Italy.
- ^{77(a)}INFN Sezione di Roma Tre; ^(b)Dipartimento di Matematica e Fisica, Università Roma Tre, Roma;

Italy.

^{78(a)}INFN-TIFPA; ^(b)Università degli Studi di Trento, Trento; Italy.

⁷⁹Universität Innsbruck, Department of Astro and Particle Physics, Innsbruck; Austria.

⁸⁰University of Iowa, Iowa City IA; United States of America.

⁸¹Department of Physics and Astronomy, Iowa State University, Ames IA; United States of America.

⁸²Istinye University, Sariyer, Istanbul; Türkiye.

^{83(a)}Departamento de Engenharia Elétrica, Universidade Federal de Juiz de Fora (UFJF), Juiz de Fora; ^(b)Universidade Federal do Rio De Janeiro COPPE/EE/IF, Rio de Janeiro; ^(c)Instituto de Física, Universidade de São Paulo, São Paulo; ^(d)Rio de Janeiro State University, Rio de Janeiro; ^(e)Federal University of Bahia, Bahia; Brazil.

⁸⁴KEK, High Energy Accelerator Research Organization, Tsukuba; Japan.

⁸⁵Graduate School of Science, Kobe University, Kobe; Japan.

^{86(a)}AGH University of Krakow, Faculty of Physics and Applied Computer Science, Krakow; ^(b)Marian Smoluchowski Institute of Physics, Jagiellonian University, Krakow; Poland.

⁸⁷Institute of Nuclear Physics Polish Academy of Sciences, Krakow; Poland.

⁸⁸Faculty of Science, Kyoto University, Kyoto; Japan.

⁸⁹Research Center for Advanced Particle Physics and Department of Physics, Kyushu University, Fukuoka ; Japan.

⁹⁰L2IT, Université de Toulouse, CNRS/IN2P3, UPS, Toulouse; France.

⁹¹Instituto de Física La Plata, Universidad Nacional de La Plata and CONICET, La Plata; Argentina.

⁹²Physics Department, Lancaster University, Lancaster; United Kingdom.

⁹³Oliver Lodge Laboratory, University of Liverpool, Liverpool; United Kingdom.

⁹⁴Department of Experimental Particle Physics, Jožef Stefan Institute and Department of Physics, University of Ljubljana, Ljubljana; Slovenia.

⁹⁵School of Physics and Astronomy, Queen Mary University of London, London; United Kingdom.

⁹⁶Department of Physics, Royal Holloway University of London, Egham; United Kingdom.

⁹⁷Department of Physics and Astronomy, University College London, London; United Kingdom.

⁹⁸Louisiana Tech University, Ruston LA; United States of America.

⁹⁹Fysiska institutionen, Lunds universitet, Lund; Sweden.

¹⁰⁰Departamento de Física Teórica C-15 and CIAFF, Universidad Autónoma de Madrid, Madrid; Spain.

¹⁰¹Institut für Physik, Universität Mainz, Mainz; Germany.

¹⁰²School of Physics and Astronomy, University of Manchester, Manchester; United Kingdom.

¹⁰³CPPM, Aix-Marseille Université, CNRS/IN2P3, Marseille; France.

¹⁰⁴Department of Physics, University of Massachusetts, Amherst MA; United States of America.

¹⁰⁵Department of Physics, McGill University, Montreal QC; Canada.

¹⁰⁶School of Physics, University of Melbourne, Victoria; Australia.

¹⁰⁷Department of Physics, University of Michigan, Ann Arbor MI; United States of America.

¹⁰⁸Department of Physics and Astronomy, Michigan State University, East Lansing MI; United States of America.

¹⁰⁹Group of Particle Physics, University of Montreal, Montreal QC; Canada.

¹¹⁰Fakultät für Physik, Ludwig-Maximilians-Universität München, München; Germany.

¹¹¹Max-Planck-Institut für Physik (Werner-Heisenberg-Institut), München; Germany.

¹¹²Graduate School of Science and Kobayashi-Maskawa Institute, Nagoya University, Nagoya; Japan.

¹¹³Department of Physics and Astronomy, University of New Mexico, Albuquerque NM; United States of America.

¹¹⁴Institute for Mathematics, Astrophysics and Particle Physics, Radboud University/Nikhef, Nijmegen; Netherlands.

- ¹¹⁵Nikhef National Institute for Subatomic Physics and University of Amsterdam, Amsterdam; Netherlands.
- ¹¹⁶Department of Physics, Northern Illinois University, DeKalb IL; United States of America.
- ¹¹⁷(^a)New York University Abu Dhabi, Abu Dhabi;(^b)United Arab Emirates University, Al Ain; United Arab Emirates.
- ¹¹⁸Department of Physics, New York University, New York NY; United States of America.
- ¹¹⁹Ochanomizu University, Otsuka, Bunkyo-ku, Tokyo; Japan.
- ¹²⁰Ohio State University, Columbus OH; United States of America.
- ¹²¹Homer L. Dodge Department of Physics and Astronomy, University of Oklahoma, Norman OK; United States of America.
- ¹²²Department of Physics, Oklahoma State University, Stillwater OK; United States of America.
- ¹²³Palacký University, Joint Laboratory of Optics, Olomouc; Czech Republic.
- ¹²⁴Institute for Fundamental Science, University of Oregon, Eugene, OR; United States of America.
- ¹²⁵Graduate School of Science, Osaka University, Osaka; Japan.
- ¹²⁶Department of Physics, University of Oslo, Oslo; Norway.
- ¹²⁷Department of Physics, Oxford University, Oxford; United Kingdom.
- ¹²⁸LPNHE, Sorbonne Université, Université Paris Cité, CNRS/IN2P3, Paris; France.
- ¹²⁹Department of Physics, University of Pennsylvania, Philadelphia PA; United States of America.
- ¹³⁰Department of Physics and Astronomy, University of Pittsburgh, Pittsburgh PA; United States of America.
- ¹³¹(^a)Laboratório de Instrumentação e Física Experimental de Partículas - LIP, Lisboa;(^b)Departamento de Física, Faculdade de Ciências, Universidade de Lisboa, Lisboa;(^c)Departamento de Física, Universidade de Coimbra, Coimbra;(^d)Centro de Física Nuclear da Universidade de Lisboa, Lisboa;(^e)Departamento de Física, Universidade do Minho, Braga;(^f)Departamento de Física Teórica y del Cosmos, Universidad de Granada, Granada (Spain);(^g)Departamento de Física, Instituto Superior Técnico, Universidade de Lisboa, Lisboa; Portugal.
- ¹³²Institute of Physics of the Czech Academy of Sciences, Prague; Czech Republic.
- ¹³³Czech Technical University in Prague, Prague; Czech Republic.
- ¹³⁴Charles University, Faculty of Mathematics and Physics, Prague; Czech Republic.
- ¹³⁵Particle Physics Department, Rutherford Appleton Laboratory, Didcot; United Kingdom.
- ¹³⁶IRFU, CEA, Université Paris-Saclay, Gif-sur-Yvette; France.
- ¹³⁷Santa Cruz Institute for Particle Physics, University of California Santa Cruz, Santa Cruz CA; United States of America.
- ¹³⁸(^a)Departamento de Física, Pontificia Universidad Católica de Chile, Santiago;(^b)Millennium Institute for Subatomic physics at high energy frontier (SAPHIR), Santiago;(^c)Instituto de Investigación Multidisciplinario en Ciencia y Tecnología, y Departamento de Física, Universidad de La Serena;(^d)Universidad Andres Bello, Department of Physics, Santiago;(^e)Instituto de Alta Investigación, Universidad de Tarapacá, Arica;(^f)Departamento de Física, Universidad Técnica Federico Santa María, Valparaíso; Chile.
- ¹³⁹Department of Physics, University of Washington, Seattle WA; United States of America.
- ¹⁴⁰Department of Physics and Astronomy, University of Sheffield, Sheffield; United Kingdom.
- ¹⁴¹Department of Physics, Shinshu University, Nagano; Japan.
- ¹⁴²Department Physik, Universität Siegen, Siegen; Germany.
- ¹⁴³Department of Physics, Simon Fraser University, Burnaby BC; Canada.
- ¹⁴⁴SLAC National Accelerator Laboratory, Stanford CA; United States of America.
- ¹⁴⁵Department of Physics, Royal Institute of Technology, Stockholm; Sweden.
- ¹⁴⁶Departments of Physics and Astronomy, Stony Brook University, Stony Brook NY; United States of

America.

¹⁴⁷Department of Physics and Astronomy, University of Sussex, Brighton; United Kingdom.

¹⁴⁸School of Physics, University of Sydney, Sydney; Australia.

¹⁴⁹Institute of Physics, Academia Sinica, Taipei; Taiwan.

¹⁵⁰(^a) E. Andronikashvili Institute of Physics, Iv. Javakhishvili Tbilisi State University, Tbilisi; (^b) High Energy Physics Institute, Tbilisi State University, Tbilisi; (^c) University of Georgia, Tbilisi; Georgia.

¹⁵¹Department of Physics, Technion, Israel Institute of Technology, Haifa; Israel.

¹⁵²Raymond and Beverly Sackler School of Physics and Astronomy, Tel Aviv University, Tel Aviv; Israel.

¹⁵³Department of Physics, Aristotle University of Thessaloniki, Thessaloniki; Greece.

¹⁵⁴International Center for Elementary Particle Physics and Department of Physics, University of Tokyo, Tokyo; Japan.

¹⁵⁵Department of Physics, Tokyo Institute of Technology, Tokyo; Japan.

¹⁵⁶Department of Physics, University of Toronto, Toronto ON; Canada.

¹⁵⁷(^a) TRIUMF, Vancouver BC; (^b) Department of Physics and Astronomy, York University, Toronto ON; Canada.

¹⁵⁸Division of Physics and Tomonaga Center for the History of the Universe, Faculty of Pure and Applied Sciences, University of Tsukuba, Tsukuba; Japan.

¹⁵⁹Department of Physics and Astronomy, Tufts University, Medford MA; United States of America.

¹⁶⁰Department of Physics and Astronomy, University of California Irvine, Irvine CA; United States of America.

¹⁶¹University of Sharjah, Sharjah; United Arab Emirates.

¹⁶²Department of Physics and Astronomy, University of Uppsala, Uppsala; Sweden.

¹⁶³Department of Physics, University of Illinois, Urbana IL; United States of America.

¹⁶⁴Instituto de Física Corpuscular (IFIC), Centro Mixto Universidad de Valencia - CSIC, Valencia; Spain.

¹⁶⁵Department of Physics, University of British Columbia, Vancouver BC; Canada.

¹⁶⁶Department of Physics and Astronomy, University of Victoria, Victoria BC; Canada.

¹⁶⁷Fakultät für Physik und Astronomie, Julius-Maximilians-Universität Würzburg, Würzburg; Germany.

¹⁶⁸Department of Physics, University of Warwick, Coventry; United Kingdom.

¹⁶⁹Waseda University, Tokyo; Japan.

¹⁷⁰Department of Particle Physics and Astrophysics, Weizmann Institute of Science, Rehovot; Israel.

¹⁷¹Department of Physics, University of Wisconsin, Madison WI; United States of America.

¹⁷²Fakultät für Mathematik und Naturwissenschaften, Fachgruppe Physik, Bergische Universität Wuppertal, Wuppertal; Germany.

¹⁷³Department of Physics, Yale University, New Haven CT; United States of America.

^a Also Affiliated with an institute covered by a cooperation agreement with CERN.

^b Also at An-Najah National University, Nablus; Palestine.

^c Also at Borough of Manhattan Community College, City University of New York, New York NY; United States of America.

^d Also at Center for High Energy Physics, Peking University; China.

^e Also at Center for Interdisciplinary Research and Innovation (CIRI-AUTH), Thessaloniki; Greece.

^f Also at Centro Studi e Ricerche Enrico Fermi; Italy.

^g Also at CERN, Geneva; Switzerland.

^h Also at Département de Physique Nucléaire et Corpusculaire, Université de Genève, Genève; Switzerland.

ⁱ Also at Departament de Física de la Universitat Autònoma de Barcelona, Barcelona; Spain.

^j Also at Department of Financial and Management Engineering, University of the Aegean, Chios; Greece.

^k Also at Department of Physics, California State University, Sacramento; United States of America.

- l* Also at Department of Physics, King's College London, London; United Kingdom.
- m* Also at Department of Physics, Stanford University, Stanford CA; United States of America.
- n* Also at Department of Physics, Stellenbosch University; South Africa.
- o* Also at Department of Physics, University of Fribourg, Fribourg; Switzerland.
- p* Also at Department of Physics, University of Thessaly; Greece.
- q* Also at Department of Physics, Westmont College, Santa Barbara; United States of America.
- r* Also at Hellenic Open University, Patras; Greece.
- s* Also at Institutio Catalana de Recerca i Estudis Avancats, ICREA, Barcelona; Spain.
- t* Also at Institut für Experimentalphysik, Universität Hamburg, Hamburg; Germany.
- u* Also at Institute for Nuclear Research and Nuclear Energy (INRNE) of the Bulgarian Academy of Sciences, Sofia; Bulgaria.
- v* Also at Institute of Applied Physics, Mohammed VI Polytechnic University, Ben Guerir; Morocco.
- w* Also at Institute of Particle Physics (IPP); Canada.
- x* Also at Institute of Physics and Technology, Mongolian Academy of Sciences, Ulaanbaatar; Mongolia.
- y* Also at Institute of Physics, Azerbaijan Academy of Sciences, Baku; Azerbaijan.
- z* Also at Institute of Theoretical Physics, Ilia State University, Tbilisi; Georgia.
- aa* Also at Lawrence Livermore National Laboratory, Livermore; United States of America.
- ab* Also at National Institute of Physics, University of the Philippines Diliman (Philippines); Philippines.
- ac* Also at Technical University of Munich, Munich; Germany.
- ad* Also at The Collaborative Innovation Center of Quantum Matter (CICQM), Beijing; China.
- ae* Also at TRIUMF, Vancouver BC; Canada.
- af* Also at Università di Napoli Parthenope, Napoli; Italy.
- ag* Also at University of Colorado Boulder, Department of Physics, Colorado; United States of America.
- ah* Also at Washington College, Chestertown, MD; United States of America.
- ai* Also at Yeditepe University, Physics Department, Istanbul; Türkiye.
- * Deceased